Immobilized catalysts for the oxidation of hydrocarbons based on triazole complexes of ruthenium

by

Laura Leckie

Thesis presented in fulfilment of the requirements for the degree of MSc in Chemistry in the Faculty of Natural Sciences at Stellenbosch University

Supervisor: Prof. S. F. Mapolie

March 2017

Declaration

By submitting this thesis electronically, I declare that the entirety of the work contained therein is my own, original work, that I am the sole author thereof (save to the extent explicitly otherwise stated), that reproduction and publication thereof by Stellenbosch University will not infringe any third party rights and that I have not previously in its entirety or in part submitted it for obtaining any qualification.

March 2017

Abstract

The synthesis of model and siloxane functionalized ruthenium complexes and the subsequent immobilization of the latter onto mesoporous silica, as well as the application of the prepared substances in the oxidation of hydrocarbons, is described in this thesis.

Model and siloxane functionalized pyridine triazole (**ML1** and **SL1**), pyridine N-oxide triazole (**ML2** and **SL2**) and quinoline triazole (**ML3** and **SL3**) ligands were successfully synthesized utilising a copper mediated click-type cycloaddition reactions. These ligands were reacted with the ruthenium arene dimer, $[RuCl_2(p\text{-cymene})]_2$, to produce mononuclear cationic complexes (**MC1-MC3**) which were stabilized with tetraphenylborate as counterion. The ligands together with the model and siloxane functionalized complexes, **MC1-MC3** and **SC1-SC3**, were fully characterized using FT-IR spectroscopy, NMR (^{1}H and ^{13}C) spectroscopy, ESI-MS analysis and microanalysis.

The siloxane functionalized complexes, **SC1-SC3**, were immobilized onto mesoporous silica supports, MCM-41 and SBA-15, to afford the immobilized catalysts **IC1-IC6**. The immobilization is effected by a condensation reaction between the siloxane functionality of the complexes and the surface silanols on the MCM-41 and SBA-15 supports, thereby affording a ruthenium complex that is covalently immobilized onto the support. Furthermore the model complex, **MC1**, was physically adsorbed onto MCM-41 and SBA-15 to afford the adsorbed catalysts **AC1** and **AC2**. The native silicas as well as the supported catalysts were fully characterized using a variety of solid state characterization techniques including infrared spectroscopy, nitrogen adsorption/desorption (Brunauer–Emmett–Teller, BET) surface analysis, low-angle powder X-ray diffraction, transmission electron microscopy (TEM), scanning electron microscopy (SEM), thermal gravimetric analysis (TGA) and ICP-OES. ICP-OES was used to determine the ruthenium loading on the silica supports, thereby facilitating an accurate and direct comparison between the model, adsorbed and immobilized systems during catalysis.

The model (**MC1-MC3**) and immobilized (**IC1-IC6**) ruthenium catalysts were employed in the oxidative cleavage of 1-octene. The catalysts were successful in transforming 1-octene to heptaldehyde and subsequently to heptanoic acid at extended reaction times. The immobilized N,N (pyridine triazole and quinoline triazole) catalysts were significantly more active than their model counterparts at a low catalyst loading of 0.1 mol%. At this same catalyst loading the N,O (pyridine N-oxide triazole) complexes gave similar results when

comparing the model and immobilized systems. The N,O catalyst systems performed better in the oxidative cleavage of 1-octene than the N,N systems. The role of the mesoporous silica supports in the oxidative cleavage reaction was investigated using various catalytic systems including: model complex **MC1**, model complex **MC1** in the presence of either MCM-41 or SBA-15 and model complex **MC1** adsorbed on MCM-41 and SBA-15 (**AC1** and **AC2**, respectively). From the results of this investigation it was noted that the immobilized catalysts employed appear to be hydrophilic in nature. This was deduced from the fact that in these biphasic systems, the silica material was found closely associated with the water layer. Thus the immobilization of the ruthenium complex on the silica support facilitates the transfer of the ruthenium pre-catalyst from the organic phase into the aqueous phase which contains the oxidant. This promotes the oxidation of the precursor to RuO_4 which is the actual active species. This phase transfer allows thus the proposed active species, RuO_4, to form at a faster rate and leads to enhanced reaction rates for the immobilized catalysts compared to their model analogues in the oxidative cleavage of 1-octene. The presence of RuO_4 as an important intermediate in the oxidative cleavage reaction was confirmed using UV-Vis studies.

The ruthenium model complexes (**MC1-MC3**) and their immobilized counterparts (**IC1-IC6**) were also applied in the oxidation of *n*-octane. The catalysts were successful in transforming *n*-octane into octanones and octanols in the presence of *tert*-Butyl hydroperoxide (TBHP), with a catalyst loading of only 0.01 mol% being required for the catalytic oxidation. Reaction mixtures were reduced with an excess of triphenylphosphine after the oxidation reaction, from this an estimate of the selectivity for octyl hydroperoxides could be obtained. Hydrogen peroxide was found to be ineffective as terminal oxidant for these reactions.

The immobilized catalysts **IC4** and **IC5** could be recycled once, while **IC3** could be recycled twice. Very little drop in product yield was observed in the recycling of the immobilized catalysts.

Opsomming

In hierdie tesis word die sintese van model en siloksaan gefunksioneerde ruteniumkomplekse, die daaropvolgende immobilisering van die laasgenoemde komplekse op mesoporiëuse silika, sowel as die toepassing van die komplekse in die oksidasie van koolwaterstowwe beskryf.

Model en siloksaan gefunksioneerde piridien-triasool (**ML1** en **SL1**), piridien N-oksied triasool (**ML2** en **SL2**) en kinolien triasool (**ML3** en **SL3**) ligande is sukselvol gesintetiseer deur van koper-bemiddelde klik-tipe sikloaddisiereaksies gebruik te maak. Hierdie ligande is gereageer met die rutenium areen dimeer, $[RuCl_2(p\text{-simeen})]_2$, gereageer om mononukluêre kationiese komplekse wat met tetrafenielboraat as teenioon gestabiliseer is, te lewer. Die ligande sowel as die model en siloksaan gefunsioneerde komplekse **MC1-MC3** en **SC1-SC3** is volledig gekarakteriseer deur van FT-IR spektroskopie, KMR (^{1}H en ^{13}C) spektroskopie, ESI massaspektrometrie en mikroanalise gebruik te maak.

Die siloksaan gefunksioneerde komplekse, **SC1-SC3**, is op die mesoporiëuse silica, MCM-41 en SBA-15, geïmmobiliseer om die geïmmobiliseerde komplekse **IC1-IC6** te lewer. Die immobilisering vind plaas deur ‘n kondenseringsreaksie tussen die siloksaan funksionaliteit van die komplekse en die silanol groepe op die oppervlak van die MCM-41 and SBA-15 draers. Die ruteniumkomplekse is dus op kovalente wyse aan die draer gebind. Die modelkompleks **MC1** is verder fisies geabsorbeer op MCM-41 en SBA-15 om die geabsorbeerde katalisators **AC1** en **AC2** te lewer. Die natuurlike silikas sowel as die gedraagde katalisators is volledig gekarakteriseer deur van verskeie vastestof analise tegnieke gebruik te maak, insluitende infrarooi spektroskopie, stikstof adsorpsie/desorpsie (BET) oppervlakanalise, lae-hoek poeier X-straal diffraksie, transmissie elektron mikroskopie (TEM), skandeer elektron mikroskopie (SEM), termiese gravimetriese analisie (TGA) en IKP-OES. IKP-OES is gebruik om die hoeveelheid rutenium op die silika draers te bepaal om sodoende ‘n akkurate vergelyking tussen die model, geabsorbeerde en geïmmobiliseerde stelsels tydens katalise moontlik te maak.

Die model (**MC1-MC3**) en geïmmobiliseerde (**IC1-IC6**) rutenium katalisators is gebruik in die oksidatiewe splitsing van 1-okteen. Die katalisators kon 1-okteen suksesvol transformeer na heptaldehied en daarna, oor lang reaksietye, na heptanoësuur. Die geïmmobiliseerde N,N (piridien triasool en kinolien triasool) katalisators was aansienlik meer aktief as hulle model ewekniëe by ‘n lae katalisator-lading van 0.1 mol%. Die N,O (piridien N-oksied triasool)

komplekse het, by hierdie lading, vergelykbare resultate vir die model en geïmmobiliseerde stelsels getoon. Die N,O stelsels het oor die algemeen beter resultate as die N,N stelsel in die oksidatiewe splitsing van 1-okteen gelewer. Die rol van die mesoporiëuse silika draers in die oksidatiewe splytingsreaksie is ondersoek deur van ‘n verskeidenheid katalitise stelsels gebruik te maak. Dit sluit modelkompleks **MC1**, modelkompleks **MC1** in die teenwoondigheid van óf MCM-41 óf SBA-15, en modelkompleks **MC1** wat op MCM-41 en SBA-15 geabsorbeer is (**AC1** en **AC2** onderskeidelik) in. Daar is in hierdie ondersoek waargeneem dat die geïmmobiliseerde katalisators hidrofilies is. Hierdie insig is aflei vanaf die feit dat, in die tweefasige stelsels, die silikamateriaal in die waterlaag gevind is. Die immobilisering van die ruteniumkompleks op die silika draer bevorder dus die oordrag van die rutenium pre-katalisator vanaf die organise laag na die waterlaag – waarin die oksidant gevind word. Die oksidasie van die voorloper na RuO_4, die werklike aktiewe spesie, word dus bevorder. Die fase-oordrag veroorsaak dus dat die aktiewe spesie, RuO_4, vinniger vorm en dit lei tot hoër reaksietempos in die geval van die geïmmobiliseerde katalisators in vergelyking met dit van hul model ewekniëe in die oksidatiewe splitsing van 1-okteen. UV-Vis is gebruik om die teenwoordigheid van RuO_4, ‘n belangrike tussenspesie in die oksidatiewe splitsingsreaksie, te bevestig.

Die rutenium modelkomplekse (**MC1-MC3**) en hulle geïmmobiliseerde ewekniëe (**IC1-IC6**) is ook as katilisator voorganger in die oksidasie van *n*-oktaan gebruik. Die katalisators kon *n*-oktaan sukselvol omskep in oktanone en oktanole in die teenwoordigheid van TBHP. ‘n Katalisator-lading van slegs 0.01 mol% is gebruik vir die katalitiese *n*-oktaan oksidasie. Die reaksiemengsels is met ‘n oormaat van trifenielfosfien gereduseer na afloop van die oksidasiereaksie. Vanaf laasgenoemde reaksie kon ‘n skatting van die selektiwiteit vir oktiel waterperoksiede bepaal word. Daar is gevind dat waterstofperoksied nie ‘n effektiewe oksidant vir hierdie reaksies is nie.

Die geïmmobiliseerde katalisators **IC4** en **IC5** kon een keer herwin word, terwyl **IC3** twee keer herwin is. Daar is slegs ‘n baie klein vermindering in die opbrengs opgelet tydens die herwinning van die geïmmobiliseerde katalisators.

Acknowledgements

First and foremost I would like to thank our Heavenly Father. All things are made possible through Him.

To my family and friends; thank you for your patience, encouragement and support along the way.

A big thank you to my supervisor, Prof. Selwyn Mapolie, for his guidance, patience and discipline throughout.

To my colleagues, at the Organometallic Research Group, I would like to thank you for the day to day conversations and laughs, as well as your willingness to help in almost any situation.

I would like to thank the technical staff at the Inorganic Chemistry building for their assistance and the staff at the Central Analytical Facility (CAF), at Stellenbosch University, for their assistance with various analytical techniques.

I would like to acknowledge the National Research Foundation (NRF) and c*change for financial support.

Conference Contributions

Laura Leckie and Prof S.F. Mapolie

Poster presentation titled: *Development of immobilized ruthenium catalysts for the oxidation of alkanes*

Catalysis Society of South Africa (CATSA), Kleinmond (Arabella), South Africa, 2015.

Laura Leckie and Prof S.F. Mapolie

Poster presentation titled: *The oxidative transformation of hydrocarbons using immobilized ruthenium catalysts*

Catalysis Society of South Africa (CATSA), Drakensberg (Champagne Sports Resort), South Africa, 2016.

Table of Content

List of Figures

List of Schemes

List of Tables

List of Abbreviations

δ	chemical shift
Å	angstrom
ATR	attenuated total reflectance
BET	Brunauer Emmett Teller
BHT	2,6-di-*tert*-butyl-4-methylphenol
bipy	bipyridine
BJH	Barret-Joyner-Halenda
cm^{-1}	wavenumber
CTAB	cetyltrimethylammonium bromide
CWAO	catalytic wet air oxidation
d	doublet
DCM	dichloromethane
DFT	Density Functional Theory
dmp	2,9-dimethyl-1,10-phenanthroline
DMSO	dimethyl sulfoxide
DNA	deoxyribonucleic acid
ee	enantiomeric excess
ESI-MS	electrospray ionization mass spectrometry
FT-IR	Fourier Transform infrared spectroscopy
GC	gas chromatography
HAP	hydroxyapatite
Hz	Hertz
ICP-OES	inductively coupled plasma optical emission spectroscopy
m	multiplet
m/z	mass-to-charge ratio
MCM	Mobil crystalline material
MHz	Megahertz
ml	milliliters
min	minute(s)
mol	mole
mmol	millimole
MOF	metal–organic framework
NHC	N-heterocyclic carbene

nm	nanometer
NMR	nuclear magnetic resonance
ntb	tris(benzimidazol-2-ylmethyl)amine
P/Po	relative pressure
PEG	polyethylene glycol
ph	phenyl
PIB	polyisobutylene
PMO	periodic mesoporous organosilica
Por	porphyrin
PPG	polypropylene glycol
ppm	chemical shift
q	quartet
RCDA	radical cation Diels-Alder
s	singlet
SBA	Santa Barbara amorphous
SEM	scanning electron microscopy
t	triplet
tacn	triazacyclononane
TBHP	tert-butyl hydroperoxide
TEM	transmission electron microscopy
TEOS	tetraethylorthosilicate
TFA	trifluoroacetic acid
TGA	thermal gravimetric analysis
THF	tetrahydrofuran
TMP	2,2,6,6-tetramethylpiperidine
TON	turn-over number
TPA	tris(2-pyridylmethyl)amine
UV-Vis	ultraviolet-visible
XRD	X-ray diffraction

Chapter 1: Ruthenium in the catalytic oxidation of hydrocarbons

1.1 Introduction

Ruthenium is one of the most versatile and useful metals applied in catalytic processes, with applications extending from reactions such as hydrogenations, isomerizations, metathesis and oxidations.[1–6] Successful application of this metal in such a wide variety of catalytic organic transformations is proof of its significant contribution to catalysis research, in both academia and industry, in the 21st century. Ruthenium based catalysts, which are capable of oxidizing various hydrocarbons, are especially promising in light of the current global necessity for functionalization of abundant and cheap hydrocarbon substrates.

The ability of ruthenium to assume a wide range of oxidation states (from -2 to +8) allows this metal to be used catalytically for reactions such as nucleophilic addition to C-C multiple bonds and also for C-C bond formation carried out by ruthenacycle intermediates and ruthenium carbene complexes.[1] Interesting to note is that ruthenium has been found to activate C-H bonds, this includes both aromatic as well as aliphatic C-H bond activation.[7–10] Ruthenium has commonly been applied in cleavage reactions, including the cleavage of C-N bonds[11], C-C bonds[12], as well as the cleavage of DNA[13].

When looking at the application of ruthenium in catalytic oxidation reactions, it has been found to be successful in the oxidation of water[14,15] and various alcohols.[16–18] However more importantly, which by the way is relevant to the subject of this thesis, is the ability of ruthenium to oxidize various hydrocarbons.[19–21] Ruthenium oxo species are usually responsible for carrying out oxidation reactions. The type of oxidizing species formed largely depends on the terminal oxidant as well as the catalyst precursor, which could be a metal salt or a discrete metal complex. For ruthenium complexes the types of ligand scaffolds or inorganic supports present can have a distinct effect on the type of active species formed. The most common active species for hydrocarbon cleavage reactions is RuO_4[2,5], followed by $RuO_2(L_2)$[8,9,22] while for other oxidations such as alkane oxidations Ru=O, Ru-OH or Ru-OOH species have been implicated.[21,23,24]

Homogeneous systems are essential for catalysis and are very versatile due to complexation of different ligands giving rise to catalysts that can be used for various applications. The

development of environmentally sustainable industrial chemical processes has become increasingly important. Homogeneous catalysts have difficulty being implemented industrially due to catalyst separation issues, leading to the loss of expensive metals and ligands causing the process to not be economically feasible. It is therefore necessary to develop effective multiphase catalyst systems to combine the selectivity of homogeneous catalysts with the simple separation techniques normally associated with heterogeneous systems. Currently there exist both homogeneous and heterogeneous ruthenium catalysts capable of hydrocarbon functionalization.[3,5] The success of each of these types of systems varies, but does not directly depend on whether the catalyst is homogeneous or heterogeneous. It is desirable to design heterogeneous ruthenium catalysts demonstrating the same optimum activity and/or selectivity as homogeneous catalysts which can be recycled. Ruthenium was valued at $41.75 on average between January-November 2016, significantly cheaper than the other platinum group metals which were valued between $566-$999 on average over the same time period.[25] This precious metal is however still very costly and it therefore goes without saying as to why development of recyclable catalytic systems using ruthenium has been the topic of much research over the past few decades.[17,26–31]

An effective means of developing a heterogeneous catalytic system would be to covalently anchor a homogeneous complex on an inorganic support such as mesoporous silica.[17] Previous research has demonstrated systems where this type of approach has been successful in the development of catalysts for hydrocarbon oxidations.[17,32,33] Extensive research has been carried out with regards to the synthesis and characterization of mesoporous materials, such as the mesoporous silica MCM-41, which consists of cylindrical pores arranged in a hexagonal array.[34] In some cases these supported homogeneous catalysts are not necessarily recyclable, due to the nature of the actual catalytically active species formed during the reaction. However synergistic effects that arise between the metal species and the support can result in a catalyst with better activity and/or selectivity. A prime example of this is work reported by Kotze, where it was found that the immobilized ruthenium catalysts were significantly more active than their homogeneous counterparts at a tenfold lower catalyst loading.[32]

The efficient oxidation of hydrocarbon substrates, using ruthenium based catalysts, requires careful catalyst design. With regards to supported catalysts it is necessary to incorporate appropriate ligand structures and combine these with desirable supports which can give rise to a catalyst system that exhibits optimum activity and/or selectivity in the various oxidation processes. An overview of the different ruthenium based catalytic systems employed for the oxidation of hydrocarbons such as aromatics, alkynes, alkenes and alkanes is given below.

1.2 Ruthenium catalyzed oxidation of aromatic compounds

Ruthenium tetroxide for hydrocarbon oxidation has been successfully employed in the oxidation of various aromatic compounds.[35–38] Caputo and Fuchs employed RuO_4 for the oxidation of aromatic compounds with specific stereochemistries. The catalytically active species was generated *in-situ* from $RuCl_3$ or RuO_2, using $NaIO_4$ with CCl_4 as solvent. It was shown that retention of stereochemistry occurs during the oxidation of the aromatic fragments in the substrates.[36] Sharpless and co-workers subsequently made a significant discovery which led to greater insight into ruthenium tetroxide catalysed oxidations. It was found that the use of a co-ordinating solvent, acetonitrile, in a biphasic CCl_4/H_2O system resulted in a catalyst system which was capable of oxidizing aromatic compounds as well as other compounds such as olefins, alcohols and ethers with high conversions and good selectivity towards oxidized products.[39]

The development was also used by Stock et al. who adapted the Sharpless system for the oxidation of the aromatic components of coal, which until that point had only been achieved under rather harsh conditions employing hydrogen peroxide and trifluoroacetic acid under reflux. Catalytic amounts of $RuCl_3{\cdot}xH_2O$ (1 mol%), in $MeCN/CCl_4/H_2O$, were employed using sodium bromate/periodate/hypochlorite or periodic acid as oxidant to generate RuO_4. Model reactions included the oxidation of aliphatic molecules, namely decane, and various carboxylic acids which showed 0-5% conversions. The authors then continued with various aromatic compounds and they observed that aromatic compounds bearing an activating hydroxy or methoxy group are oxidised rapidly to acetic acid, and that alkyl aromatics are converted predominantly to the corresponding alkanoic acids with some of the alkylbenzoic acids being formed.[40]

The biphasic solvent system, $CCl_4/MeCN/H_2O$, with periodic acid as oxidant proved to be a simple means by which pheromones could be synthesized from the selective oxidation of aromatic components in the substrate as demonstrated by Martin and Nufiez.[37]

In 1995, Hirobe and co-workers showed that a ruthenium porphyrin (Ru(TMP)CO) is capable of selectively oxidizing various aromatic compounds, to their corresponding quinones, in the presence of an acid additive (HBr or HCl) with 2,6-dichloropyridine N-oxide (Cl_2pyNO) as oxidant (Scheme 1.1). The authors observed that the addition of the acid was necessary for the reaction to proceed, and they propose that an oxoruthenium species is responsible for the oxidation.[41]

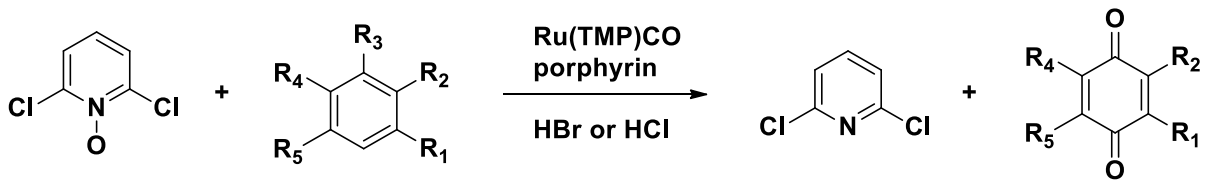

Scheme 1.1: Oxidation of substituted aromatic compounds with ruthenium porphyrin.[41]

Che and co-workers later demonstrated the use of a D4-symmetric chiral ruthenium porphyrin catalyst, [RuII(D4-Por*)(CO)(MeOH)] (D4-H2Por* = tetrakis[(1S,4R,5R,8S)-1,2,3,4,5,6,7,8-octahydro-1,4:5,8-dimethanoanthracen-9-yl]porphyrin), for the enantioselective hydroxylation of aromatic hydrocarbons (Figure 1.1). For the asymmetric hydroxylation of 4-ethyltoluene, 1,1 diethylindan and benzylcyclopropane up to 76% ee was achieved with Cl_2pyNO as oxidant. Mechanistic investigations lead the authors to conclude that hydrogen atom abstraction is involved in the oxidation, and they proposed that an oxoruthenium species is responsible for the rate-limiting hydrogen atom abstraction.[42]

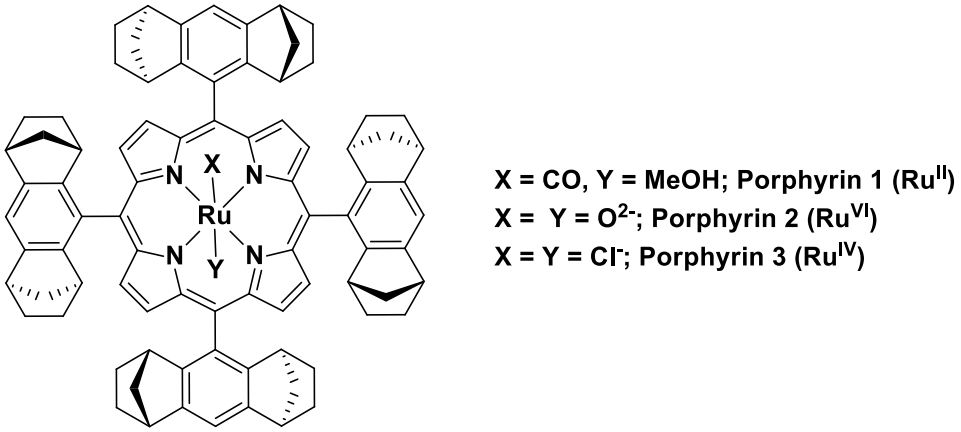

Figure 1.1: D4-symmetric chiral ruthenium porphyrin catalyst for enantioselective hydroxylation of aromatic hydrocarbons. [42]

Guerrero-Ruiz and co-workers evaluated ruthenium catalysts supported on ZrO_2, graphite and activated carbon for the catalytic wet air oxidation (CWAO) of the model aromatic compounds, aniline and phenol. Their aim was to develop a CWAO system which potentially could efficiently oxidize highly toxic and non-biodegradable industrial effluents under mild conditions. These types of CWAO systems are capable of mineralizing aromatic pollutants into CO_2, N_2 and H_2O or transforming these toxic hydrocarbons into more desirable and biodegradable carboxylic acids. Their system used molecular oxygen (2 MPa) at a

temperature of 413 K and after as little as 3 hours 78% conversion and 17% mineralization of aniline was achieved, whereas 100% of phenol was converted and up to 70% was mineralized. The authors found that Ru supported on activated carbon produced the best catalyst, most likely due to the microporous nature of the support material. They also found that $RuCl_3$ was the best ruthenium precursor for their catalytic mineralization.[43] In the same year Tran et al. used a titanium expanded mesh anode covered with ruthenium oxide (Ti/RuO_2) to anodically oxidize toxic polycyclic aromatic hydrocarbons (PAH's) present in creosote solution. Their electrochemical oxidation is capable of reducing 80–82% of PAH concentrations and 90% of the toxicity of synthetic creosote-oily solutions.[44]

Tabatabaeian & co-workers developed a catalytic system for the oxidation of aromatic and hetero aromatic compounds. The method involved the formation of RuO_4 *in-situ* from catalytic amounts of $RuCl_3.xH_2O$ (5 mol%) with a $MeCN/CH_2Cl_2/H_2O$ solvent mixture and $NaIO_4$ as the oxidant. This system incorporates the use of ultrasonic irradiation during the reaction process, thereby accelerating the rate of the reaction. The authors reported that predominantly ketones and aldehydes were obtained as products in the oxidation of arenes, with the exceptions being the oxidation of biphenyl and *trans*-stilbene where benzoic acid was observed to be the major product. The irradiation results in comparable yields of oxygenates, varying from 36-98%, after a reaction time of only 2 hours as opposed to a 12 hour reaction time in the absence of irradiation. The oxidation of chrysene, when irradiated, resulted in the products chrysene-5,6-dione and 2-(2-formylphenyl)-1-naphthaldehyde (Scheme 1.2; **1a** & **1b**; 8:2 mol ratio). The authors propose that the mechanism for the oxidation of chrysene involves the formation of a ruthenium cyclo-diester, resulting from the reaction of RuO_4 with a C=C double bond within the aromatic ring. The ruthenium cyclo-diester can then rearrange following two pathways, the pathway with a RuO_2 intermediate gives rise to the major compound **1a** and the pathway with a $Ru(OH)_2$ intermediate produces the minor compound **1b**. In the case of pyrene the oxidation was carried out in different conditions, irradiation room temperature yielded pyrene-4,5-dione (Scheme 1.2; **2a**) whereas irradiation at 50 °C yielded pyrene-4,5,9,10-tetraone (Scheme 1.2; **2b**).[45]

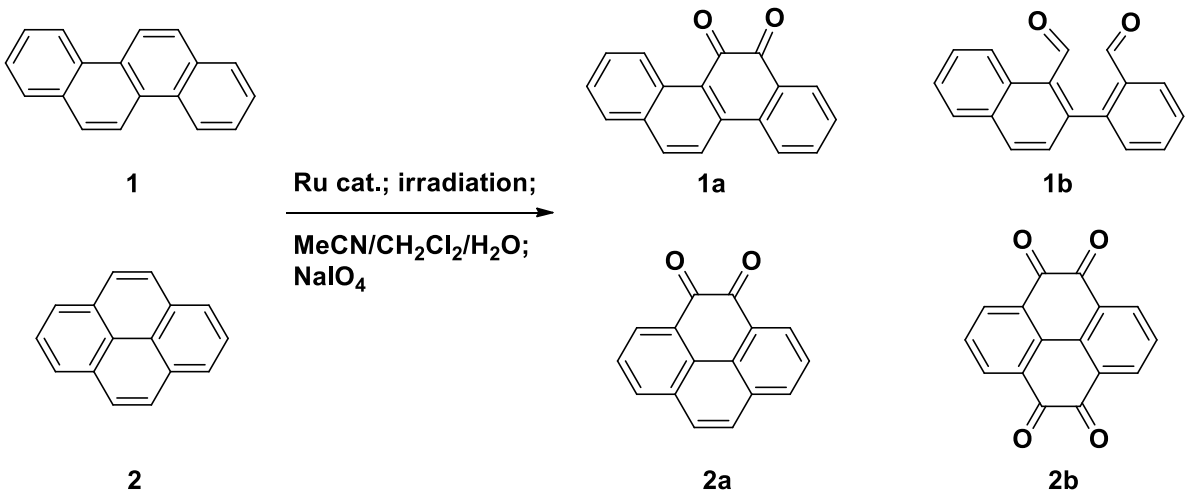

Scheme 1.2: Ultrasonic assisted ruthenium catalyzed oxidation of arenes.[45]

More recently Tabatabaeian & co-workers published a paper on the catalytic oxidation of aromatic and hetero aromatic compounds using a cationic $Ru(N,N)(CO)_4$ Schiff base complex anchored onto a microporous metal-organic framework IRMOF-3, with yields up to 76% of oxygenated products. This heterogeneous catalyst was capable of mediating hydrocarbon oxidation using ultrasonic irradiation in a $MeCN/CH_2Cl_2/H_2O$ solvent mixture, with $NaIO_4$ as the oxidant. In the oxidation of arenes, chrysene was selectively oxidized to chrysene-5,6-dione (Scheme 1.2; **1a**) and pyrene was oxidized to a mixture of pyrene-4,5-dione & pyrene-4,5,9,10-tetraone (Scheme 1.2; **2a** & **2b**). In the case of hetero aromatic compounds, sulfoxides and sulfones could be obtained from the oxidation of sulphides. The authors propose that a RuO_2 species, which is still co-ordinated to the Schiff base moiety, is responsible for the oxidation. They conclude that this system therefore offers the opportunity for recycling of the catalyst, however they did not confirm this property experimentally.[8]

In the same year Taylor and co-workers used RuO_4 for the oxidation of alkyl substituted aromatics. The oxidation of alkyl aromatics, to the corresponding carboxylic acid, is a method which has previously been used to determine what type of alkyl chains are present in complex aromatic structures. The production of these carboxylic acids is assumed to be due to the overoxidation of the aromatic rings, producing carbon dioxide and water, while the alkyl fragment is still intact bearing the carboxylic acid functionality. It was observed that the oxidation of 2-ethylnaphthalene, using $RuCl_3{\cdot}xH_2O$ and $NaIO_4$ as oxidant, in either a biphasic (CH_2Cl_2/MeCN/H_2O) or monophasic (MeCN/H_2O) solvent system gave similar reaction rates and product selectivity. According to GC-MS analysis various oxygenated products were obtained for the oxidation of 1-ethylnapthalene including phthalaldehyde, isobenzofuran

ketone derivatives and 6-ethylnaphthalene-1,4-dione. Overall, the authors found that the aromatic components are only partially oxidized and that the alkyl substituents are fairly resistant to oxidation.[46]

Very recently Miura and co-workers used a ruthenium complex, [Ru(*p*-cymene)Cl_2]$_2$, for the acetoxylation of carbazole and indole aromatic frameworks (Scheme 1.3). Using ruthenium catalysis the system is capable of regioselectively cleaving the C-H bond, followed by the formation of the C-O bond. Reactions were carried out at elevated temperatures (140 °C) in chlorobenzene, with acetic acid additive and Ag_2CO_3 as oxidant. At a catalyst loading of 5 mol%, 9-(pyridin-2-yl)carbazole could be acetoxylated with a maximum yield of 75%.[47]

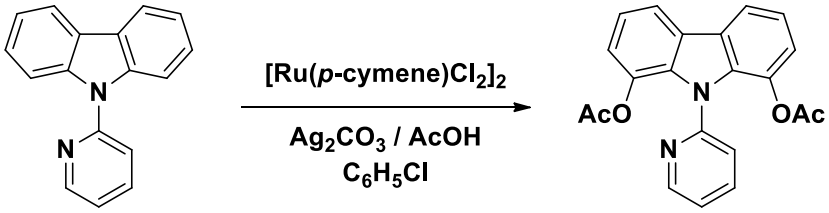

Scheme 1.3: Acetoxylation of aromatic frameworks using [Ru(*p*-cymene)Cl_2]$_2$. [47]

Supported ruthenium nanoparticles have also been shown to be useful for hydrocarbon oxidations, as demonstrated by Khorshidi and co-workers. The authors make use of ruthenium nanoparticles supported on mesoporous silica, MCM-41, in the ultrasound-assisted oxidation of arenes. The system is capable of oxidizing naphtalene to phtalaldehyde, chrysene to chrysene-5,6-dione (Scheme 1.2; **1a**) and pyrene to pyrene-4,5-dione & pyrene-4,5,9,10-tetraone (Scheme 1.2; **2a** & **2b**). Benzoic acid was obtained after the respective oxidations of biphenyl and *trans*-stilbene. The supported nanoparticles (~5 nm) give rise to a selective and recyclable catalyst (re-used for several runs), and ultrasound irradiation improved the yields of oxidation products of various arenes in the presence of $KBrO_3$ as terminal oxidant.[20]

1.3 Ruthenium catalyzed oxidative cleavage of C-C bonds in alkenes and alkynes

1.3.1 Introduction to ruthenium catalyzed oxidative cleavage of C-C bonds

In general oxidative cleavage of alkenes involves scission of the carbon-carbon double bond and simultaneously the incorporation of oxygen to afford the oxygenated products. When an α,β-disubstituted alkene is oxidatively cleaved it initially affords the aldehyde product and subsequently carboxylic acids due to over-oxidation (Scheme 1.4a). Alternatively the oxidative cleavage of tri-substituted alkenes afford oxygenated products such as ketones as depicted below (Scheme 1.4b).[5]

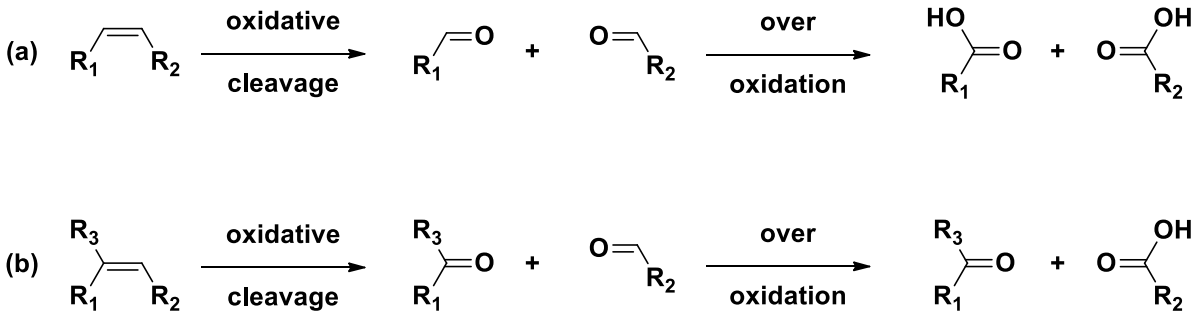

Scheme 1.4: Oxidative cleavage of substituted alkenes.[5]

Ruthenium based catalysts are of particular interest due the versatility of the metal oxide, RuO_4, which is known to be the active species in oxidative cleavage reactions. Ruthenium tetroxide can be used stoichiometrically to oxidise alkenes to aldehydes.[5] There are various systems where ruthenium trichloride can be used catalytically to convert alkenes into carboxylic acids[48,49] in the presence of an oxidant such as sodium hypochlorite or sodium periodate.[12,39] Ruthenium trichloride in the presence of periodic acid, $IO(OH)_5$, is known to convert alkenes to carboxylic acids however in this case the reduction product HIO is very soluble in water preventing issues with regards to work-up of the reaction.[5] Studies have shown that RuO_4 exhibits high selectivity towards the oxygenated cleavage products. This is due to the fact that neither dihydroxylated nor epoxidized intermediates are involved in the reaction mechanism.[50] Therefore after the alkene coordinates the metal it produces a metal diester, which is formed as a result of a pericyclic reaction. The rearrangement of the metal diester affords aldehydes (Pathway **a**, Scheme 1.5), in the case of ruthenium tetroxide the mechanism does not follow the hydrolysis of the metal diester to produce diols (Pathway **b**, Scheme 1.5). Carboxylic acid products result from overoxidation of the aldehyde.[5]

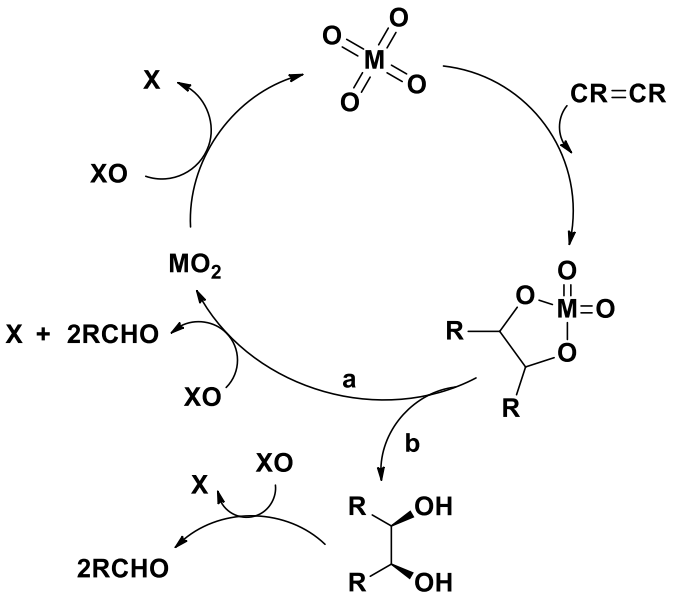

Scheme 1.5: Mechanism for oxidative cleavage of alkenes using MO_4 (where M = Ru; OX = oxidant).[5]

1.3.2 Oxidative cleavage of C-C bonds using ruthenium coordination complexes

Neumann and Abu-Gnim synthesised a ruthenium-substituted heteropolyanion, $[SiRu(H_2O)W_{11}O_{39}]((C_6H_{13})_4N)_5$, for the catalytic oxidation of alkenes. Reactions were carried out using different oxidants, namely tert-butyl hydroperoxide, potassium persulfate, iodosobenzene, and sodium periodate. The different oxidants resulted in different types of oxidations taking place including oxidative cleavage, allylic oxidation and epoxidation. The oxidative cleavage of alkenes could be induced when sodium periodate was used as oxidant, to selectively produce the corresponding aldehydes. These authors conducted a thorough mechanistic study of the oxidative cleavage of styrene derivatives. They conclude that the catalyst and styrene substrate interact to form a metallocyclooxetane, which then rearranges to form a cyclodiester, followed by rearrangement of the cyclodiester to afford the aldehyde product.[51]

Kogan and co-workers used the known complex, $[cis\text{-}Ru(II)(dmp)_2(H_2O)_2]^{2+}$ (dmp = 2,9-dimethylphenanthroline), for the regioselective cleavage of alkenes to aldehydes in the presence of hydrogen peroxide. This cleavage reaction is carried out by $[cis\text{-}Ru(II)(dmp)_2(O)_2]^{2+}$ which has a sterically hindered active site due to the bulky nature of the dmp ligands. Reactions were carried out with a 1 mol% catalyst loading, in acetonitrile at 55 °C with H_2O_2 as oxidant (10 equiv. of 30% H_2O_2 solution, added in 10 portions over 8 h). Primary alkenes, such as 1-octene, were oxidized to their corresponding aldehydes with excellent selectivity and 80-95% product yields. Secondary alkenes, such as 2-Me-1-

heptene (2-heptanone, 73% yield) and 2-Me-2-heptene (no oxygenated products), were much less reactive.[22]

Che and co-workers used $[(Me_3tacn)(CF_3CO_2)_2Ru^{III}(OH_2)]CF_3CO_2$ (Me_3tacn = 1,4,7-trimethyl-1,4,7-triazacyclononane) as a catalyst for the oxidative cleavage of alkenes and alkynes to produce the corresponding carboxylic acids in the presence of aqueous hydrogen peroxide. The cleavage of alkenes and alkynes gave 100% conversion of substrates under reflux, after 12 hrs and 4 hrs respectively. The corresponding acids were obtained with selectivity between 75-89% under aerobic conditions, with 1 mol% catalyst, in aqueous *tert*-butanol.[52]

Shoair and co-workers found that a ruthenium bipyridine complex, *cis*-$[RuCl_2$-$(bipy)_2]\cdot 2H_2O$, in the presence of $IO(OH)_5$ was capable of selectively oxidizing both terminal and internal alkenes to terminal carboxylic acids. Reactions were carried out at room temperature in a biphasic solvent system, $CH_3CN/CCl_4/H_2O$ (1:1:2 v/v), with a substrate to oxidant mol ratio of 1:5 and 70-92% conversion of the substrate could be achieved after as little as 2 hrs. Cyclic alkenes are converted to bifunctional carboxylic acids. In the case of 1-olefins, the carboxylic acid product has one carbon less than the parent alkene. The mechanism for oxidative cleavage carried out by the Ru-bipy complex with $IO(OH)_5$ as an oxidant involves oxidation of the Ru(II) complex to a Ru(VIII) species. Subsequently the produced RuO_4 (active species) then cleaves the cyclic alkene into dicarboxylic acid and is itself converted into RuO_2, which can be reoxidized to RuO_4 by an excess of $IO(OH)_5$, depicted in Scheme 1.6 below.[12]

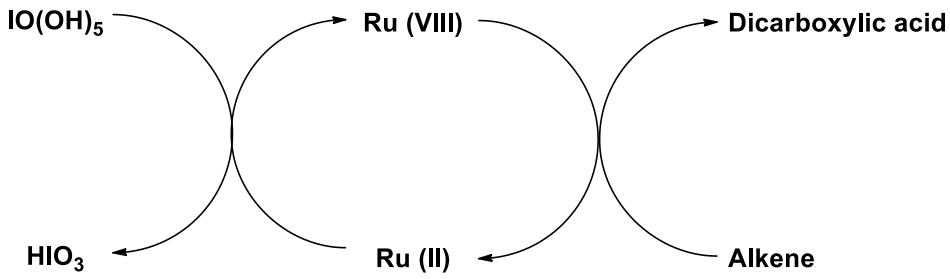

Scheme 1.6: Catalytic cycle for the oxidative cleavage of a cyclic alkene involving Ruthenium and periodic acid.[12]

Xia and co-workers published a paper on the oxidative C-C cleavage of aldehydes using a $[Ru(bipy)_3Cl_2]$ (bipy = 2,20-bipyridine) as photoredox catalyst in the presence of visible light (Scheme 1.7). The cleavage reaction proceeded with good yields of between 60-96%, for

the cleavage of both aromatic and aliphatic aldehydes, after a 6-24 hour time period. Reactions were carried out with a 5 mol% catalyst loading, piperidine as co-catalyst in a 3 eqiv. excess to the substrate, air as the oxidant, at 25 °C and irradiation with a 15 W fluorescent light bulb. The mild conditions employed and the ability to apply the cleavage reaction to a wide range of substrates causes this system to be an improvement on previously reported procedures.[53]

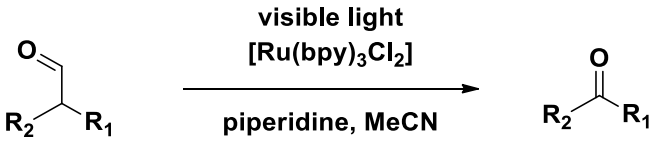

Scheme 1.7: Photocatalytic oxidative cleavage of aldehydes using ruthenium. [53]

Bera *et al.* synthesised a sterically bulky Ru NHC complex, [Ru(COD)(L1)Br_2] (L1 = imidazo[1,2-a][1,8]naphthyridine-based abnormal N-heterocyclic carbene ligand), found this to selectively cleave C=C bonds to aldehydes C-C triple bonds to α-diketones. N-Heterocyclic carbene (NHC) ligands are desirable due to the formation of robust metal−C bonds which increases the stability of their metal complexes. These ligands possess strong sigma donation ability, which in turn increases the oxidation potential of the resulting NHC metal complexes. The oxidative cleavage of alkenes and alkynes was performed with 1 mol % [Ru(COD)(NHC)Br_2], a 2.1 equiv. excess of $NaIO_4$ as oxidant, at 25 °C in a MeCN/EtOAc/H_2O solvent mixture. Reactions proceeded with good yields (72-100%) after only half an hour. Their system could even be applied in the cleavage of C-C bonds present in highly functionalized sugar- and amino acid-derived compounds, with cleavage yields between 76-91%. After mechanistic studies the authors concluded that a *cis*-RuO_2 species, still bearing the abnormal NHC ligand, is the active catalyst in these oxidative cleavage reactions (Figure 1.2).[9]

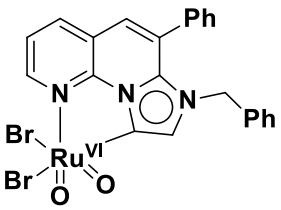

Figure 1.2: Ru NHC dioxo active species in the oxidative cleavage of alkenes[9]

Brasholz and co-workers used the red dyes tris(bipyridine)-ruthenium(II), $[Ru(bipy)_3]^{2+}$ and tris(bipyrazine)ruthenium(II), $[Ru(bpz)_3]^{2+}$ as photoredox catalysts for tandem photoredox/oxidation processes. These complexes are converted to RuO_4 in the presence of visible light and an oxidant, such as $NaIO_4$ or H_5IO_6, via photoassisted ligand field labilisation (Scheme 1.8).[54]

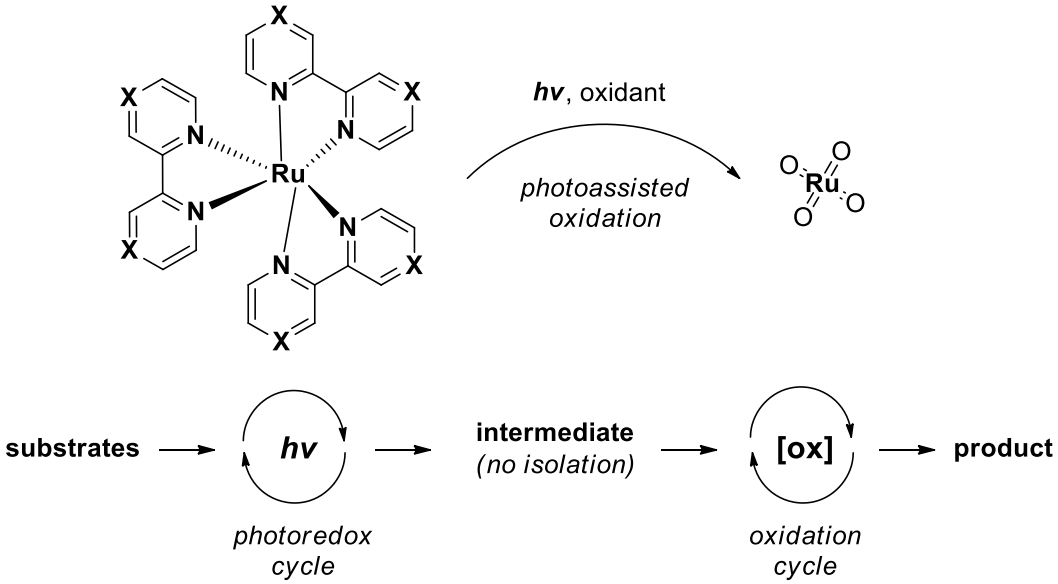

Scheme 1.8: Orthogonal tandem photoredox and oxidation catalysis through photoassisted *in-situ* oxidation of ruthenium complexes to RuO_4 (X = H or N).[54]

This system could therefore be applied in a tandem catalytic process where a photoredox radical cation Diels–Alder (RCDA)/1,5-diene cyclisation reaction occurs followed by RuO_4 mediated oxidative cleavage. This one pot reaction utilises 1 mol% $[Ru(bpz)_3](PF_6)_2$ under blue LED irradiation for the 1,5-diene cyclisation. Once the intermediates of the cyclisation are observed the solvent is changed from CH_3NO_2 to a mixture of EtOAc/H_2O (1:2, v/v), along with the addition of 3-8 eqiv. of $NaIO_4$. The mixture is then stirred for a further 3 hrs under blue LED irradiation until the C=C oxidative cleavage products are observed. The system afforded the cleavage products in yields between 55–59%.[54]

Liu and co-workers synthesized a $Ca[Ru_2(dcnp)(\mu OAc)_3]_2$ complex which was found to be excellent for the oxidative cleavage of olefins (Scheme 1.9). The catalytic cleavage reactions were carried out under mild conditions (1 mol% Ru complex, 4 equiv. $NaIO_4$ in 1 ml H_2O, 45 °C, 16 h) and achieved yields between 33-99% of the corresponding carboxylic acids.[55]

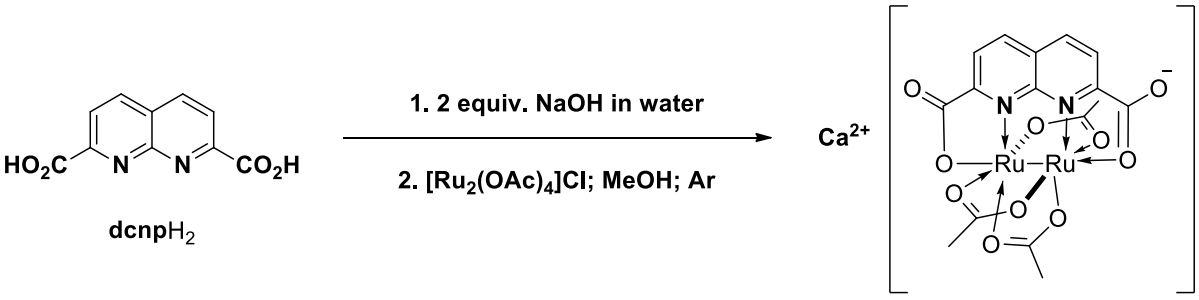

Scheme 1.9: Synthesis of a $Ca[Ru_2(dcnp)(\mu OAc)_3]_2$ for the oxidative cleavage of olefins.[55]

1.3.3 Oxidative cleavage of C-C bonds using heterogeneous ruthenium catalysts

Che and co-workers used ruthenium nanoparticles supported on hydroxyapatite (nano-RuHAP) as a catalyst for the *cis*-hydroxylation and oxidative cleavage of alkenes. The catalyst could be recycled with no significant drop in activity for the oxidation reactions and a TON of 298 was obtained over four consecutive runs. Oxidative cleavage was performed with nano-RuHAP (4 mol% Ru) in a 1,2-dichloroethane-H_2O (5:1 v/v) solvent mixture and $NaIO_4$ as oxidant at room temperature. The cleavage could also be carried out using oxone and $NaHCO_3$ under similar conditions to the $NaIO_4$ reaction conditions, instead with a MeCN-H_2O (1.5:1 v/v) solvent mixture. The dihydroxylation reactions were conducted with only 1 mol% nano-RuHAP in the presence of $NaIO_4$, however a 20 mol% addition of H_2SO_4 and a solvent mixture of EtOAc/MeCN/H_2O (3:3:1 v/v) at 0° C afforded the dihydroxylated products with good yields (45-85%).[29]

Okumoto and co-workers used a composite $RuO_2/BaTi_4O_9$ material for the oxidative cleavage of alkenes. A catalyst loading of 1-3 mol% was required to yield 71-93% ketones and 12-98% aldehydes produced from internal and terminal alkenes respectively after 3-72 hrs. The double bonds of certain sugars were also oxidatively cleaved, depending on the time length of the reaction either the corresponding aldehyde or carboxylic acid was produced. Reactions were conducted with $NaIO_4$ as oxidant in an EtOAc–H_2O–buffer (pH 6.88) solution. The composite was also successfully recycled, with a slight drop in conversion, from 98% for the first run to 75% for the second and third runs.[56]

Rao et al developed an efficient and recyclable ruthenium catalyst for the oxidative cleavage of alkenes and alkynes to produce aldehydes and carboxylic acids respectively. Between 1-2.5 mol% of the Ru/C (ruthenium on carbon) catalyst was required to obtain 36-92% yields of aldehydes or 76-94% yields of carboxylic acids after 1.5-8 hrs. The alkyne (Scheme 1.10a) and alkene (Scheme 1.10b) oxidations were carried out with oxone and $NaIO_4$ as the terminal oxidant, respectively. The catalyst could be recycled up to 5 times for oxidation of

alkynes with no significant drop in activity (run 1: 89% to run 5: 87%) and could be recycled up to 3 times for alkenes. The authors propose that the reason for the catalysts recyclability is due to the formations of a catalytically active RuO_2 species, which is still adsorbed on the Charcoal. The RuO_2 interacts with the alkene or alkyne to form a metal cyclodiester which rearranges to provide the cleaved products.[30]

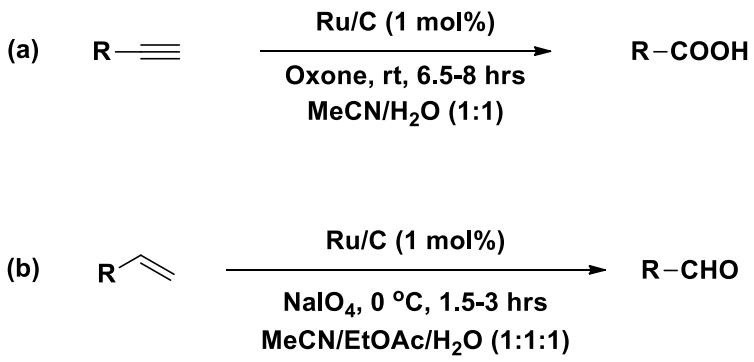

Scheme 1.10: Ruthenium on charcoal (Ru/C) catalysed oxidation of alkynes (a) and alkenes (b).[30]

In 2014 work done by Kotze demonstrated that Ru N,N complexes immobilized on mesoporous silica (Scheme 1.11) were more active than their homogeneous counterparts in the oxidative cleavage of 1-octene. It was found that RuO4 was formed in a biphasic solvent system CCl4/MeCN/H_2O (1:1:2, v/v) with $IO(OH)_5$ as the terminal oxidant at 23 °C in air. High conversions to the aldehyde could be achieved at short reaction times, and longer reaction times selectively afforded octanoic acid. Although the catalysts could not be recycled they proved to have a significantly higher activity than their model counterparts at a much lower catalyst loading (0.05 mol%).[32]

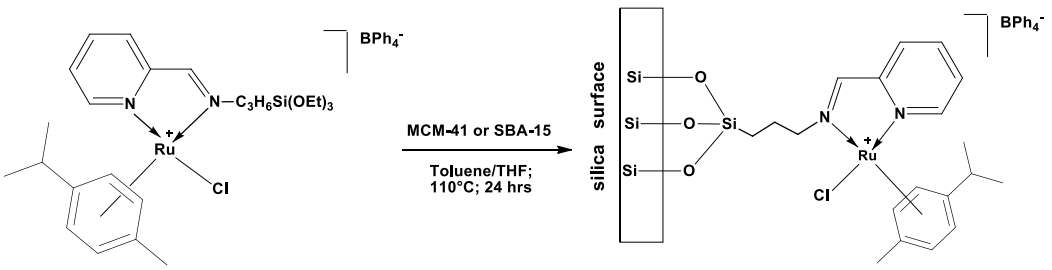

Scheme 1.11: Immobilization of Ru(N,N) complex on mesoporous silica.[32]

Most recently Liang and Bergbreiter prepared a polyisobutylene (PIB) bound, Ru(II)-bipyridine, recyclable, photoredox catalyst capable of performing both oxidative cleavage of C-C bonds in aldehydes (Scheme 1.12), as well as the [2 + 2] cycloaddition of bis-enones. The cleavage reactions were carried out in the presence of piperidine, under an oxygen atmosphere and irradiation from a 30 W household fluorescent bulb at ambient temperature, with a homogeneous CH_2Cl_2/CH_3CN (9:1, v/v) solvent mixture. The catalyst showed high conversions and could be recycled for 5 consecutive runs with no loss of catalytic activity.[28]

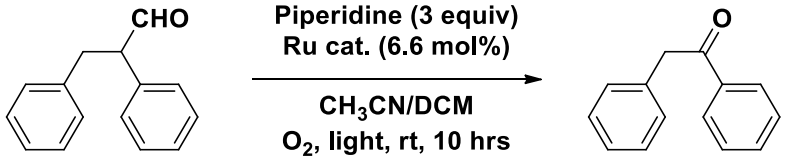

Scheme 1.12: Oxidative C-C bond cleavage catalysed by PIB-bound Ru(II)-bipyridine complex.[28]

1.4 Ruthenium catalyzed epoxidation of alkenes and alkynes

Goldstein and co-workers synthesised sterically hindered *cis*-$[Ru(dmp)_2(S)_2]$ $(PF_6)_2$ (S = H_2O; CH_3CN) complexes (dmp = 2,9-dimethyl-1,10-phenanthroline) capable of catalytically oxidizing norbornene with dioxygen under mild pressures and temperatures between 65-75 °C. The authors deduce that a *cis* ruthenium dioxo species, formed via a free radical reaction between the pre-catalyst $[Ru(dmp)_2(CH_3CN)_2](PF_6)_2$ and molecular oxygen, is responsible for oxidation to selectively produce 2,3-epoxynorbornane.[24]

Griffith and co-workers used various bis-bipy (2,2'-bipyridyl) and bis-phen (1,10-phenanthroline) ruthenium complexes for the catalytic epoxidation of alkenes in the presence of oxidants such as $NaIO_4$, or $[NBu_4]IO_4$. The yields obtained for the epoxidation of cyclooctene by various Ru(N,N) complexes were between 41-99%. The authors were able to isolate an orange ruthenium iodo complex, $[RuO_2(bipy) - \{IO_3(OH)_3\}]\sim1.5H_2O$, which was synthesized from RuO_4, $NaIO_4$ and bipy in water-acetone (Figure 1.3). This complex was found to be excellent for the stereospecific epoxidation of various cyclic and linear alkenes with yields of epoxide between 5-99%.[57]

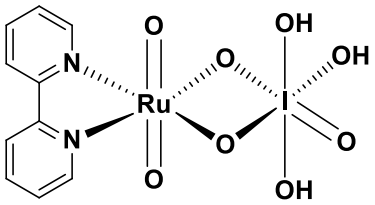

Figure 1.3: Structure of the complex $[RuO_2(bipy) - \{IO_3(OH)_3\}]\sim1.5H_2O$. [57]

Yin and co-workers recently made a significant discovery when they observed a synergistic effect between non-redox metal ions (as Lewis acids) and the catalytic oxygen atom transfer ability of a ruthenium bipyridine complex. In the absence of the non-redox metal ion the oxidation of $Ru(bipy)_2Cl_2$, to the Ru(IV)=O species, in the presence of $(PhI(OAc)_2$ is slow and the subsequent oxidation of cyclooctene converts only 21.2% of the substrate with 6.7% of the oxygenated products being 1,2-epoxycyclooctane. When a nonredox metal ion, such as Al(III), was added a significant improvement in the conversion (100% cyclooctene converted) and selectivity (89.9% 1,2-epoxycyclooctane obtained) could be observed. The authors propose that a Ru(IV)=O/Al(III) adduct is the active species in the epoxidation reactions, and that when reduced a Ru(III)–O–Ru(III) dimer is generated. The addition of the Lewis acid is apparently responsible for accelerating the rate of oxidation of the Ru(III)–O–Ru(III) dimer back to the catalytically active Ru(IV)=O/Al(III) species.[58]

1.5 Ruthenium catalyzed oxidation of Alkanes

1.5.1 Homogeneous ruthenium catalysts in alkane oxidation

Ruthenium has been applied in the oxidation of alkanes, to afford mostly ketones and alcohols as products. More than two decades ago Tenaglia and co-workers used RuO_4 for the oxidation of various bridged bicyclic and tricyclic alkanes. They were capable of hydroxylating substrates with yields between 29-90% using 2 mol% $RuCl_3$ in a CCl_4/MeCN/H_2O (2:2:3, v/v) solvent mixture, with $NaIO_4$ as oxidant and reaction temperatures varying between 25-90 °C. The authors found that the oxidation occurs preferentially at the tertiary position with retentions of configuration of the substrate. It was proposed that the mechanism involves the activation of the C-H bond by RuO_4 leading to the formation of a four centred transition state which then rearranges to afford the oxidized alkane and a reduced RuO_3 species which is then reoxidized by the $NaIO_4$ terminal oxidant (Scheme 1.13).[59]

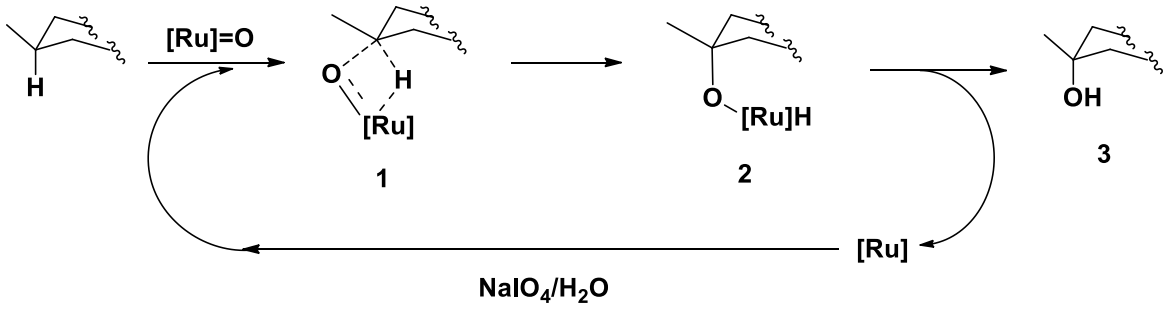

Scheme 1.13: Mechanism for activation of an alkane C-H bond by RuO_4, where [Ru] = RuO_3.[59]

Murahashi et al. have developed two systems using ruthenium for alkane oxidation. The first system involves the use of 1 mol% of a $RuCl_2(PPh_3)_3$ complex in the presence of *t*-BuOOH in dry benzene at room temperature. Linear (26-28%), cyclic (36-82%) and aromatic substituted (47-100%) alkanes were converted predominantly to their corresponding ketones and to a lesser extent conversion to their corresponding alcohols. The aromatic components of the alkyl substituted compounds were untouched during the oxidation process, with only the alkyl fragments being oxidized. In some cases the corresponding alkyl tert-butyl peroxide, *t*-BuOOR, was formed. The authors rationalized the mechanism by assuming a cytochrome P-450 type oxidation involving hydrogen atom abstraction by an oxoruthenium species, as depicted in Scheme 1.14 below. They propose that the complex interacts with *t*-BuOOH to form a Ru(IV)=O (**1**) species which then abstracts a proton from the alkane to form a radical pair (**2**). The radical pair can then react following two different pathways. Pathway A involves the transfer of the hydroxyl group from the metal to the alkyl radical to produce the alcohol and a Ru(II) species, the alcohols are then further oxidized via this pathway to afford ketones. Pathway B involves electron transfer from the caged alkyl radical to the metal to form an alkyl cation (**3**) which then reacts with *t*-BuOOH to afford the corresponding alkyl *tert*-butyl peroxide and a Ru(II) species to complete the catalytic cycle.[23]

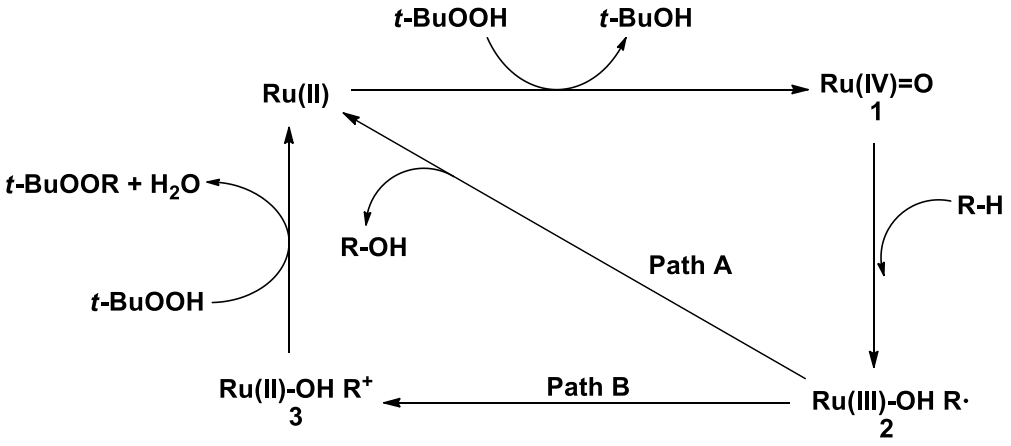

Scheme 1.14: Proposed cytochrome P-450 type oxidation involving hydrogen atom abstraction by an oxoruthenium species.[23]

An alternative system developed by Murahashi and co-workers involves the ruthenium-catalyzed oxidation of alkanes with peracids such as peracetic acid and m-chloroperbenzoic acid (mCPBA). Various metal complexes were tested for the oxidation of n-decane in ethyl acetate at room temperature for 1 h. Complexes such as $RuCl_2(PPh_3)_3$, $RuCl_2(bipy)_2$, RuO_2, and $Ru_3(CO)_{12}$ did not give satisfactory results, whereas ruthenium on charcoal and $RuCl_3 \cdot xH_2O$ showed appreciable catalytic activity. Linear (49%), cyclic (52-69%) and aromatic substituted (23-35%) alkanes were converted predominantly to their corresponding ketones and with a small amount of the corresponding alcohols being produced. As for the previous system, the aromatic components of the alkyl substituted compounds were untouched during the oxidation reaction, with only the alkyl fragments being oxidized. When the oxidant was changed to trifluoroacetic acid the corresponding alkyl trifluoroacetates were obtained. This seems to indicate that using this oxidant alcohols are formed as the primary oxidation products. The alcohols subsequently react with the TFA to form the acetates. The product distribution obtained after the oxidation of methylcyclohexane indicated that tertiary and secondary carbons were significantly more reactive in the oxidation as opposed to primary carbons. These authors once again assumed a cytochrome-P450 type mechanism involving hydrogen atom abstraction from the alkane by oxoruthenium species, however this assumption was not experimentally confirmed.[60]

Goldstein and co-workers synthesised sterically hindered complexes *cis*-$[Ru(dmp)_2(S)_2](PF_6)_2$ (S = H_2O; CH_3CN) (dmp = 2,9-dimethyl-1,10-phenanthroline) capable of oxidizing adamantane in the presence of excess H_2O_2. The authors deduced that a *cis* ruthenium dioxo species is responsible for the oxidation. It was concluded that the reaction proceeds via a radical mechanism (Scheme 1.15), this is due to inhibition of the oxidation reaction

when benzoquinone was added, as well as the occurrence of halogen scrambling when halogenated hydrocarbons were used in the catalytic reaction.[24]

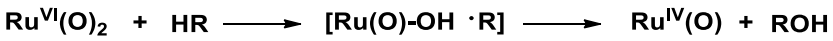

Scheme 1.15: Proposed free radical pathway for adamantane oxidation.[24]

Kinetic analysis gave insight into a possible mechanism (Scheme 1.15) which involves hydrogen atom abstraction by a RuO_2 species (still bearing the dmp ligand) followed by the formation of a ruthenium hydroxo alkyl radical cage. Radical recombination of the alkyl radical and Ru hydroxide followed by solvation of the Ru complex gives rise to the Ru mono-oxo species and an alcohol as product. The *cis* ruthenium dioxo active species can be regenerated from the mono-oxo species in the presence of excess hydrogen peroxide. The authors also state that they cannot exclude the participation of a metal peroxyl radical species, hydrocarbon peroxide or peroxyl radicals in their oxidation reactions.[24]

Hirobe and co-workers showed that a ruthenium porphyrin (Ru(TMP)CO) is capable of oxidizing unactivated alkanes, to afford high yields of alcohols and/or ketones, in the presence of and acid additive (HBr or HCl) with 2,6-dichloropyridine N-oxide (Cl_2pyNO) as oxidant. The authors observed that the addition of the acid was necessary for the reaction to proceed and to achieve high TON's, and they propose that an oxoruthenium species is responsible for the oxidation.[41]

Griffith and co-workers used various bis-bipy (2,2'-bipyridyl) and bis-phen (1,10-phenanthroline) ruthenium complexes for the catalytic oxidation of alkanes in the presence of oxidants such as $NaIO_4$, or $[NBu_4]IO_4$. The oxidation of alkanes was carried out with two different systems. The first system used $[Ru(H_2O)_2(bipy)_2]^{2+}$ with *t*-BuOOH as oxidant in benzene, while the second system employed a $[RuO_2(bipy) - \{IO_3(OH)_3\}]\sim1.5H_2O$ complex as catalyst with IO_4^- as oxidant at 80 °C in a biphasic CH_2Cl_2/H_2O solvent system. Both catalyst systems were active and their capabilities of oxidizing both linear and cyclic alkanes with high yields (between 3-98%) proved to be comparable.[57]

Patin and co-workers used $RuCl_3 \cdot 3H_2O$ in the presence of TBHP for the catalytic oxidation of cycloalkanes to their corresponding alcohols and ketones. Reactions were carried out in a biphasic mixture of the substrate (as the organic layer) and water and it was found that the yields of oxygenates could be increased by increasing the concentration of TBHP or by

introducing an oxygen atmosphere. The authors proposed that a colloidal ruthenium species is formed in-situ which is responsible for the oxidation and that the reaction proceeds via two pathways. The first oxidation pathway is a radical one which involves a Haber-Weiss decomposition of TBHP (Scheme 1.16, Equations 1-5), however results obtained after the addition of a radical scavenger such as dimethyl sulphide provided evidence that a second oxidation pathway exists which is most likely due to the presence of a high valent ruthenium oxo species (Scheme 1.16, Equations 6 & 7).[21]

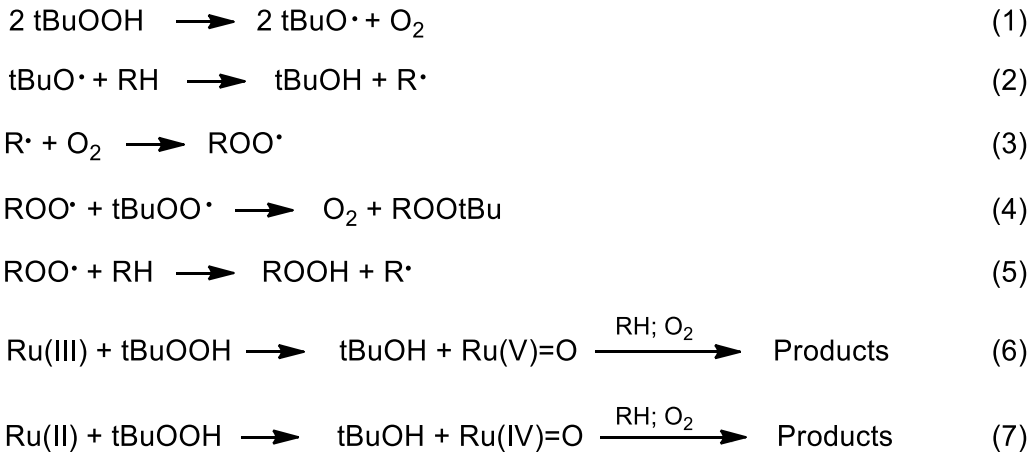

Scheme 1.16: Radical reactions and formation of oxo ruthenium species for alkane oxidation with TBHP (R = cyclooctyl).[21]

Kojima and co-workers developed two different systems for alkane oxidation. The first of which employed Ru(II) and Ru(III) complexes, bearing tris(2-pyridylmethyl)amine (TPA) and tris(5-methyl-2-pyridylmethyl)amine (5-Me_3-TPA) ligands, for the oxidation of alkanes in MeCN under N_2. It was found that the use of MCPBA as the cooxidant led to the formation of mononuclear high-valent Ru=O species during the oxidation reactions. Whereas when TBHP was employed as the oxidant the reaction proceeded via a redox-controlled free radical mechanism.[61] The second system made use of $[Ru^{II}Cl(L)]_2(ClO_4)_2$ dimers, where L=tris(2-pyridylmethyl)amine & tris(5-methyl-2-pyridylmethyl)amine, for catalytic alkane oxidation at 40 °C, using the oxidants TBHP (t-butyl hydroperoxide) or CHP (cumene hydroperoxide). It was found that reactions were mediated by alkoxo (RO.) and alkylperoxo (ROO.) radicals generated via Haber–Weiss-type electron-transfer reactions. Two factors regulate the reactivity of ruthenium in the oxidation. Firstly, the redox potentials of the complexes govern electron transfer between the metal and oxidant having an effect on the production of the reactive alkoxo and alkylperoxo radicals (Scheme 1.17, Equations 1 & 2).

Secondly, steric effects of bulky ligands around the metal centre affects the reactivity of the metal complex by somewhat preventing the approach of peroxides to the metal centre in turn decreasing the rate of electron transfer for the production of the active oxidizing species. It was concluded that the oxidation proceeds mainly via a series of radical chain reactions (Scheme 1.17, Equations 3-8). The production of molecular oxygen, generated from the decomposition of peroxides, plays a significant role in accelerating the rate of oxidation by acting as a radical chain carrier.[62]

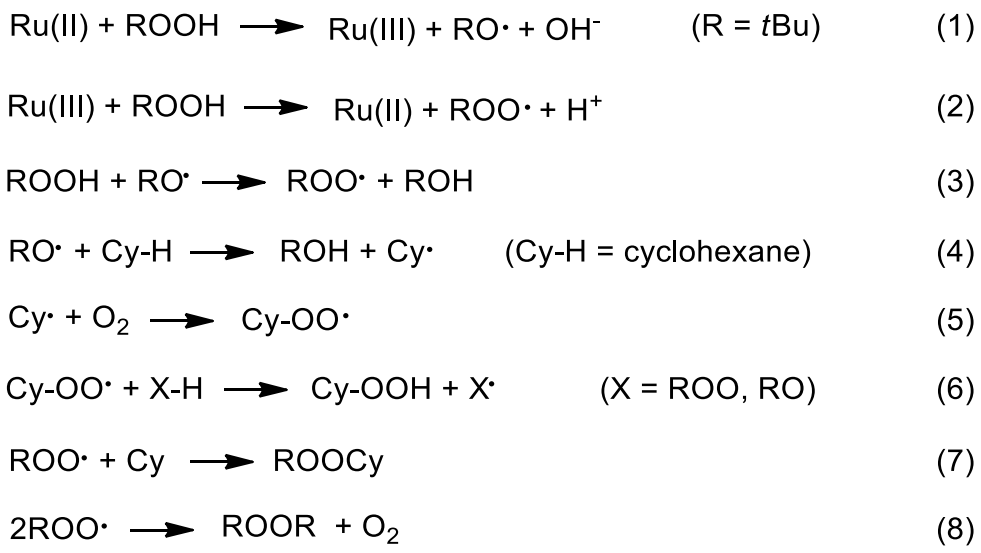

Scheme 1.17: Radical reactions initiated by ruthenium during alkane oxidation in the presence of TBHP.[62]

Britovsek and co-workers synthesized Ru(II) complexes containing bis(imino)pyridine or bis(amino)pyridine ligands, with weakly coordinating triflate (OTf^-) or non-coordinating SbF^{6-} anions. The complexes were tested as catalysts for the oxidation of cyclohexane with H_2O_2, however it was found that these complexes were inactive for the above-mentioned oxidation reaction.[63]

Che and co-workers demonstrated the use of a D_4-symmetric chiral ruthenium porphyrin catalyst, [Ru^{II}(D_4-Por*)(CO)(MeOH)] (D_4-H_2Por* = tetrakis[(1S,4R,5R,8S)-1,2,3,4,5,6,7,8-octahydro-1,4:5,8-dimethanoanthracen-9-yl]porphyrin), for the oxidation of alkanes. The alcohol products exhibited high stereoretention and moderate-to-good enantioselectivity. Mechanistic investigations led the authors to conclude that hydrogen atom abstraction is

involved in the oxidation, and they proposed that an oxoruthenium species is responsible for the rate-limiting hydrogen atom abstraction.[42]

Murali and co-workers synthesised Ru(III) complexes, $[Ru(ntb)Cl_2]Cl$ & $[Ru(ntb)Cl_2]ClO_4$ (ntb = tris-(benzimidazol-2-ylmethyl)amine) capable of cyclohexane, THF, ethylbenzene and toluene hydroxylation in the presence of TBHP.[64]

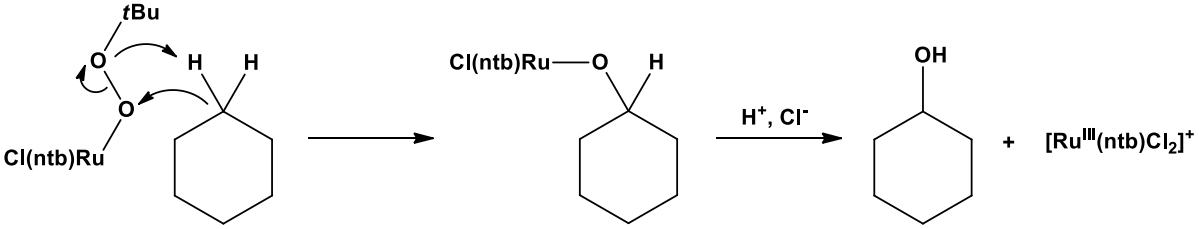

Scheme 1.18: Proposed mechanistic pathway for the catalytic oxidation of alkanes. [64]

The authors propose that the mechanistic pathway involves the formation of a ruthenium peroxide species $[Cl(ntb)Ru–O–O–tBu]^+$ which reacts with the C-H alkane bond directly. This is followed by heterolytic cleavage of the O–O bond to give rise to an alkoxido species, $[Cl(ntb)Ru–O–CH_2^-]^+$. This intermediate then reacts with H^+ and Cl^- to regenerate the catalyst and produce the hydroxylated product (Scheme 1.18). The addition of a radical trapping agent, 2,6-di-*tert*-butyl-4-methylphenol (BHT), to the cyclohexane oxidation reactions using TBHP yielded no BHT oxidation products which confirmed that a radical mechanism was not involved in the system.[64]

1.5.2 Heterogeneous ruthenium catalysts in alkane oxidation

Valodkar *et al.* synthesized ruthenium(III) complexes with N,O donor sites anchored on l-valine-bound styrene–divinyl benzene copolymer. The catalysts were effective in the oxidation of cyclohexane and toluene, using TBHP as oxidant. A homogeneous complex, $Ru(l\text{-valine})_2Cl_2$, was generated *in-situ* and tested in the oxidation of alkanes using TBHP. Using the optimized reaction conditions, higher yields were achieved compared to the heterogeneous catalyst, with yields of 11.2% and 30.1% for the oxidation of toluene and cyclohexane respectively. The authors proposed that mass transfer issues may be the reason for the decrease in activity. The catalyst could be recycled for up to four runs without degradation of the polymer, however a reduction in activity was observed for each recycle and catalyst leaching was determined to not be the cause of the observed trend.[65]

Balkus & coworkers developed a zeolite encapsulated ruthenium catalyst, which was 10 times more active than its homogeneous analogue, in the oxidation of cyclohexane. The authors conclude that the high conversions, up 70%, are as a result of site isolation.[66]

Hara et al synthesised a Ruthenium-Immobilized Periodic Mesoporous Organosilica (Ru-PMO) which was applied for the selective oxidation of alkanes such as adamantane and cis-decalin. The Ru complex, $[RuCl_2(CO)_3]_2$, was successfully co-ordinated to the 2,2'-bipyridine (bipy) units present in the PMO. This heterogeneous catalyst is capable of regioselectively oxidizing the tertiary bonds of adamantane much faster than the secondary bonds, to afford the corresponding alcohols, in ethyl acetate as solvent at 50 °C with NaClO as terminal oxidant. It was found that the catalyst could be recycled without loss of activity or selectivity. The catalyst exhibited capabilities for the oxidation of cis-decalin, predominantly to cis-9-decalol, with retention of substrate stereochemistry.[10]

1.6 Project Objectives

The project focused on homogeneous catalyst systems, synthesised using organometallic chemistry techniques. The catalysts are based on ruthenium triazole complexes, some of which were immobilized on mesoporous silica in an attempt to develop a heterogeneous catalytic system. Previous work carried out in our lab led to the discovery that RuCl(arene)(N,N) diimine complexes successfully immobilized on mesoporous silica (MCM-41 & SBA-15) were much more active in the oxidative cleavage of 1-octene than their homogeneous counterparts, and depending on the reaction time, very good selectivity for aldehydes versus carboxylic acids could be obtained. The catalysts could however not be

recycled as the active species was determined to be RuO_4, resulting in the metal leaching from the support into solution in its oxidized form. The ligands employed in the RuCl(arene)(N,N) complexes possessed an imine functionality and it was thought that hydrolysis of this functionality may be part of the reason for the metal leaching.[32] The above observations led to the need for further investigation into this phenomenon, resulting in the nature of this current study. For this reason the project aims to synthesise RuCl(arene)(N,N) and RuCl(arene)(N,O) complexes which possess a triazole moiety in order to possibly prevent any issues with hydrolysis and also to generate a catalyst which will be recyclable, selective and active in hydrocarbon oxidation. This oxidative transformation is particularly important due to the fact that it provides a means by which to obtain high value fine chemicals from cheaper and largely abundant hydrocarbon feedstocks.

1.7 Thesis outline

A review of the literature regarding ruthenium catalysts and their application in the oxidation of hydrocarbons is covered in **Chapter 1**.

Chapter 2 describes the synthesis and characterization of siloxane functionalized RuCl(*p*-cymene)(N,N) and RuCl(*p*-cymene)(N,O) complexes based on triazole ligands. The incorporation of the siloxane functionality into the obtained complexes is achieved through a copper catalyzed ‘click’ reaction of an appropriate alkyne and a siloxane functionalized azide resulting in the desired triazole ring. Ligands and complexes were characterized using several analytical techniques including IR and NMR spectroscopy, mass spectrometry and elemental analysis.

Synthesis of the native MCM-41 and SBA-15 mesoporous silica materials is described in **Chapter 3** along with immobilization of the siloxane functionalized complexes on the mesoporous silica. The complexes are covalently anchored to the silica via a reaction between the siloxane functionality of the complexes and the surface silanols on the silica surface. The immobilized catalysts were characterized by a wide range of solid state techniques including: infrared spectroscopy, nitrogen adsorption/desorption (BET) surface analysis, low-angle powder X-ray diffraction, transmission electron microscopy (TEM), scanning electron microscopy (SEM), thermal gravimetric analysis (TGA) and ICP-OES.

Evaluation of the model and immobilized complexes as catalysts in the oxidative cleavage of alkenes and the oxidation of alkanes is discussed in **Chapters 4** and **5**, respectively. A summary of the project and future work regarding this thesis is discussed in **Chapter 6**.

1.8 References

1 T. Naota, H. Takaya and S. Murahashi, *Chem. Rev.*, 1998, **98**, 2599–2660.

2 V. Piccialli, *Molecules*, 2014, **19**, 6534–6582.

3 L. Souillart and N. Cramer, *Chem. Rev.*, 2015, 9410–9464.

4 A. Rajagopalan, M. Lara and W. Kroutil, *Adv. Synth. Catal.*, 2013, 3321–3335.

5 P. Spannring, P. C. A. Bruijnincx, B. M. Weckhuysen and R. J. M. Klein Gebbink, *Catal. Sci. Technol.*, 2014, **4**, 2182-2209.

6 S. N. Dhuri, K. Cho, Y. Lee, S. Y. Shin, J. H. Kim, D. Mandal, S. Shaik and W. Nam, *J. Am. Chem. Soc.*, 2015, **137**, 8623–8632.

7 S. Dérien; F. Monnier; P. H. Dixneuf, *Top. Organomet Chem*, 2004, **11**, 1–44.

8 K. Tabatabaeian, M. A. Zanjanchi, N. O. Mahmoodi and T. Eftekhari, *RSC Adv.*, 2015, **5**, 101013–101022.

9 P. Daw, R. Petakamsetty, A. Sarbajna, S. Laha, R. Ramapanicker and J. K. Bera, *J. Am. Chem. Soc.*, 2014, 13987–13990.

10 N. Ishito, H. Kobayashi, K. Nakajima, Y. Maegawa, S. Inagaki, K. Hara and A. Fukuoka, *Chem. - A Eur. J.*, 2015, 15564–15569.

11 W. Man, J. Xie, Y. Pan, W. W. Y. Lam, H. Kwong, K. Ip, S. Yiu, K. Lau and T. Lau, *J. Am. Chem. Soc.*, 2013, **135**, 5533–5536.

12 A. G. F. Shoair and R. H. Mohamed, *Synth. Commun.*, 2006, **36**, 59–64.

13 G. Sathyaraj, M. Kiruthika, T. Weyhermüller and B. U. Nair, *Organometallics*, 2012, **31**, 6980–6987.

14 L. Bernet, R. Lalrempuia, W. Ghattas, H. Mueller-Bunz, L. Vigara, A. Llobet and M. Albrecht, *Chem. Commun. (Camb).*, 2011, **47**, 8058–8060.

15 W. Rabten, M. D. Kärkäs, T. Åkermark, H. Chen, R. Liao, F. Tinnis, J. Sun, P. E. M. Siegbahn, P. G. Andersson and B. Åkermark, *Inorg. Chem.*, 2015, **54**, 4611–4620.

16 F. Saleem, G. K. Rao, A. Kumar, G. Mukherjee and A. K. Singh, *Organometallics*, 2013, **32**, 3595–3603.

17 S. Ganesamoorthy, M. M. Tamizh, K. Shanmugasundaram and R. Karvembu, *Tetrahedron Lett.*, 2013, **54**, 7035–7039.

18 A. Bolje, S. Hohloch, D. Urankar, A. Pevec, M. Gazvoda, B. Sarkar and J. Košmrlj, *Organometallics*, 2014, **33**, 2588–2598.

19 H. Ziyat, M. A. Ali, A. Karim, C. Meliet, Y. Castanet and A. Mortreux, *Acta Chim. Slovaca*, 2004, **51**, 223–230.

20 A. Khorshidi, *Chinese J. Catal.*, 2016, **37**, 153–158.

21 F. Launay, A. Roucoux and H. Patin, *Tetrahedron Lett.*, 1998, **39**, 1353–1356.

22 V. Kogan, M. M. Quintal and R. Neumann, *Org. Lett.*, 2005, **7**, 5039–5042.

23 S. I. Murahashi, Y. Oda, T. Naota and T. Kuwabara, *Tetrahedron Lett.*, 1993, **34**, 1299–1302.

24 A. S. Goldstein, R. H. Beer and R. S. Drago, *J. Am. Chem. Soc.*, 1994, **116**, 2424–2429.

25 Johnson Matthey Precious Metals Management: Price Charts. Accessed at www.platinum.matthey.com/prices/price-charts# on November 29, 2016.

26 A. Jana, J. Mondal, P. Borah, S. Mondal, A. Bhaumik and Y. Zhao, *Chem. Commun.*, 2015, **51**, 10746–10749.

27 C. Hagelüken, *Platin. Met. Rev.*, 2012, **56**, 29–35.

28 Y. Liang and D. E. Bergbreiter, *Catal. Sci. Technol.*, 2016, **6**, 215–221.

29 C. Ho, W. Yu and C. Che, *Angew. Chem. Int. Ed.*, 2004, **43**, 3303–3307.

30 V. Kumar, V. P. Reddy, R. Sridhar, B. Srinivas and K. R. Rao, *Synlett*, 2009, **5**, 739–742.

31 R. A. Molla, A. S. Roy, K. Ghosh, N. Salam, M. A. Iqubal, K. Tuhina and S. M. Islam, *J. Organomet. Chem.*, 2015, **776**, 170–179.

32 H. Kotze, Immobilized Ru(II) Catalysts for Transfer Hydrogenation and Oxidative Alkene Cleavage Reactions, Stellenbosch University, 2015.

33 E. Ispir, *Phosphorus. Sulfur. Silicon Relat. Elem.*, 2014, **189**, 1644–1655.

34 J. Ying, C. Mehnert and M. Wong, *Angew. Chem. Int. Ed.*, 1999, **38**, 56–77.

35 D. M. Piatak, G. Herbst, J. Wicha and E. Caspi, *J. Org. Chem.*, 1969, **34**, 116–120.

36 J. A. Caputo and R. Fuchs, *Tetrahedron Lett.*, 1967, 4729–4731.

37 M. T. Nunez and V. S. Martin, *J. Org. Chem.*, 1990, **55**, 1928–1932.

38 M. Kasai and H. Ziffer, *J. Org. Chem.*, 1983, **48**, 2346–2349.

39 P. Carlsen, T. Katsuki, V. Martin and K. Sharpless, *J. Org. Chem.*, 1981, **46**, 3936–3938.

40 L. M. Stock and K. T. Tse, *Short Commun. - Fuel*, 1983, **62**, 974–976.

41 T. Higuchi, C. Satake and M. Hirobe, *J. Am. Chem. Soc.*, 1995, **117**, 8879–8880.

42 R. Zhang, W. Yu and C. Che, *Tetrahedron Asymmetry*, 2005, **16**, 3520–3526.

43 E. Castillejos-Lopez, A. Maroto-Valiente, D. M. Nevskaia, V. Munoz, I. Rodriguez-Ramos and A. Guerrero-Ruiz, *Catal. Today*, 2009, **143**, 355–363.

44 L. Tran, P. Drogui, G. Mercier and J. F. Blais, *J. Hazard. Mater.*, 2009, **164**, 1118–1129.

45 K. Tabatabaeian, M. Mamaghani, N. O. Mahmoodi and A. Khorshidi, *Catal. Commun.*, 2008, **9**, 416–420.

46 E. Nowicka, M. Sankar, R. L. Jenkins, D. W. Knight, D. J. Willock, G. J. Hutchings, M. Francisco and S. H. Taylor, *Chem. Eur. J.*, 2015, **21**, 4285–4293.

47 T. Okada, K. Nobushige, T. Satoh and M. Miura, *Org. Lett.*, 2016, **18**, 1150–1153.

48 R. Neumann and C. Abu-gnim, *Chem. Commun.*, 1989, 1324–1325.

49 W. P. Griffith, A. G. Shoair and M. Suriaatmaja, *Synth. Commun.*, 2000, **30**, 3091–3095.

50 L. Albarella, F. Giordano, M. Lasalvia, V. Piccialli and D. Sica, *Tetrahedron Lett.*, 1995, **36**, 5267–5270.

51 R. Neumann and C. Abu-gnim, *J. Am Chem. Soc.*, 1990, 6025–6031.

52 C. M. Che, W. P. Yip and W. Y. Yu, *Chem. - An Asian J.*, 2006, **1**, 453–458.

53 H. Sun, C. Yang, F. Gao, Z. Li and W. Xia, *Org. Lett.*, 2013, **15**, 624–627.

54 D. Alpers, M. Gallhof, C. B. W. Stark and M. Brasholz, *Chem. Commun.*, 2015, **52**, 1025–1028.

55 C. Lee, C. Wu, S. Hua, Y. Liu, S.-M. Peng and S.-T. Liu, *Eur. J. Inorg. Chem.*, 2015, **2015**, 1417–1423.

56 R. Bati, O. Solid, O. Cleavage, K. Ohtsuka and S. Banjoya, *Synlett*, 2007, **20**, 3201–3205.

57 A. J. Bailey, W. P. Griffith and P. D. Savage, *J. Chem. Soc. Dalton Trans.*, 1995, 3537–3542.

58 Z. Lv, W. Zheng, Z. Chen, Z. Tang, W. Mo and G. Yin, *Dalton Trans.*, 2016, **45**, 11369–11383.

59 A. Tenaglia, E. Terranova and B. Waegell, *Tetrahedron Lett.*, 1989, **30**, 5271–5274.

60 S. I. Murahashi, Y. Oda, N. Komiya and T. Naota, *Tetrahedron Lett.*, 1994, **35**, 7953–7956.

61 T. Kojima, T. Amano, Y. Ishii and Y. Matsuda, *J. Inorg. Biochem.*, 1996, **238**, 107.

62 T. Kojima, H. Matsuo and Y. Matsuda, *Inorganica Chim. Acta*, 2000, **300**, 661–667.

63 G. J. P. Britovsek, J. England, S. K. Spitzmesser, A. J. P. White and D. J. Williams, *Dalton Trans.*, 2005, 945–955.

64 M. Murali, R. Mayilmurugan and M. Palaniandavar, *Eur. J. Inorg. Chem.*, 2009, **2009**, 3238–3249.

65 V. B. Valodkar, G. L. Tembe, M. Ravindranathan and H. S. Rama, *J. Mol. Catal. A Chem.*, 2004, **223**, 31–38.

66 K. J. Balkus, M. Eissa and R. Levado, *J. Am. Chem. Soc.*, 1995, **117**, 10753–10754.

Chapter 2: Synthesis and characterization of model and siloxane functionalized RuCl(*p*-cymene) triazole complexes

2.1 Introduction

2.1.1 Ruthenium arene complexes

It has been found that ruthenium arene complexes of the type $[(\eta^6\text{-arene})Ru^{II}(N\text{-}N)Cl]^+$ (N-N = bidentate ligand; arene = benzene, *p*-cymene, tetrahydroanthracene, dihydroanthracene and biphenyl) adopt a pseudo-octahedral "piano-stool" structure. In this conformation the neutral arene ligand occupies three coordination positions (the "seat") with the chelating N-N ligand and the monodentate chloride in the other three coordination positions (the "legs"). A general example of this structure is shown in Figure 2.1 (where N-N is a chelating ligand). Within this structure the Ru-Cl bond is highly reactive, whereas the arene ligand stabilizes ruthenium in the +2 oxidation state and prevents oxidation of ruthenium to the +3 state.[1]

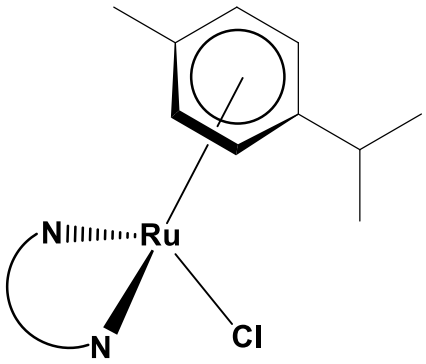

Figure 2.1: "Piano-stool" conformation of a RuCl(N,N)(*p*-cymene) complex.[1]

Ruthenium arene complexes have found application as catalyst precursors for various catalytic processes, such as the oxidation of alcohols[2] and water[3]. These types of complexes have also been found to have application in medicinal chemistry.[1]

2.1.2 Ruthenium triazole complexes

Ligands bearing triazole moieties have previously shown potential as versatile ligand scaffolds for various metal complexes which can be applied in optics, biomedicine, redox sensing and catalysis to name a few. There are several different ways in which 1,2,3-triazole ligands can coordinate to transition metal centres, which usually result in the formation of five- or six-membered metallocycles (Figure 2. 2). The first of these is through coordination of the nitrogen, for these systems, N3 has been found to be a better donor compared to N2 as determined from DFT calculations. The N3 nitrogen can either coordinate as a mono dentate ligand (type A) or when there are other donor sites nearby, it can form part of a bi- or poly-dentate chelator (type B). Furthermore coordination through N2 is possible when the additional donor site is adjacent to N, in this case a bi- or poly-dentate chelator (type C) is obtained. The triazole can also take on bridging coordination modes with two metal centres coordinating to two different nitrogen atoms (types D and E).[4]

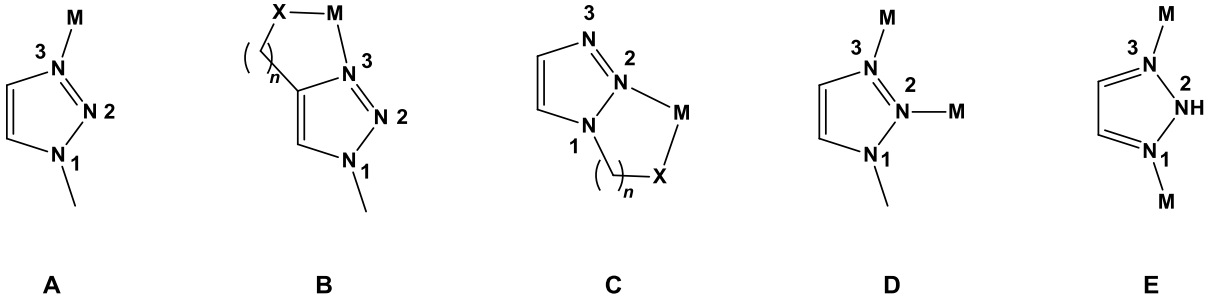

Figure 2. 2: Coordination modes of simple and chelating 1,2,3-triazoles to transition metal centres (X = N,P,S,C etc.; *n* = 1,2).[4]

Ruthenium N-coordinated 1,2,3-triazole complexes have mainly been synthesized in the relatively low oxidation state as of +2. These types of complexes have been applied in various catalytic transformations such as the oxidation of alcohols. It was found that the ruthenium N-coordinated 1,2,3-triazole complexes in which N2 is coordinated to the metal centre showed higher activity in the oxidation of various primary and secondary alcohols in the presence of N-methylmorpholine N-oxide compared to the complexes where N3 was coordinated.[4]

2.1.3 Ligand Scaffolds

Compounds bearing triazole functionalities have been used extensively since the early 2000's due to the breakthrough in triazole 'click' chemistry by Sharpless and co-workers. The ability to incorporate and link various functionalities using triazole formation has allowed the synthesis of a number of robust ligand scaffolds.[4] Bürglová *et al.* showed that triazole 'click' chemistry affords versatile reactions, allowing products to be synthesized in high yields, exhibiting excellent functional group tolerance. They exploited these properties to develop a microwave assisted method for the synthesis of trialkoxysilated molecules under anhydrous conditions. Various compounds possessing a preserved ethoxy siloxane functionality, were prepared and subsequently used as sol-gel prescursors.[6]

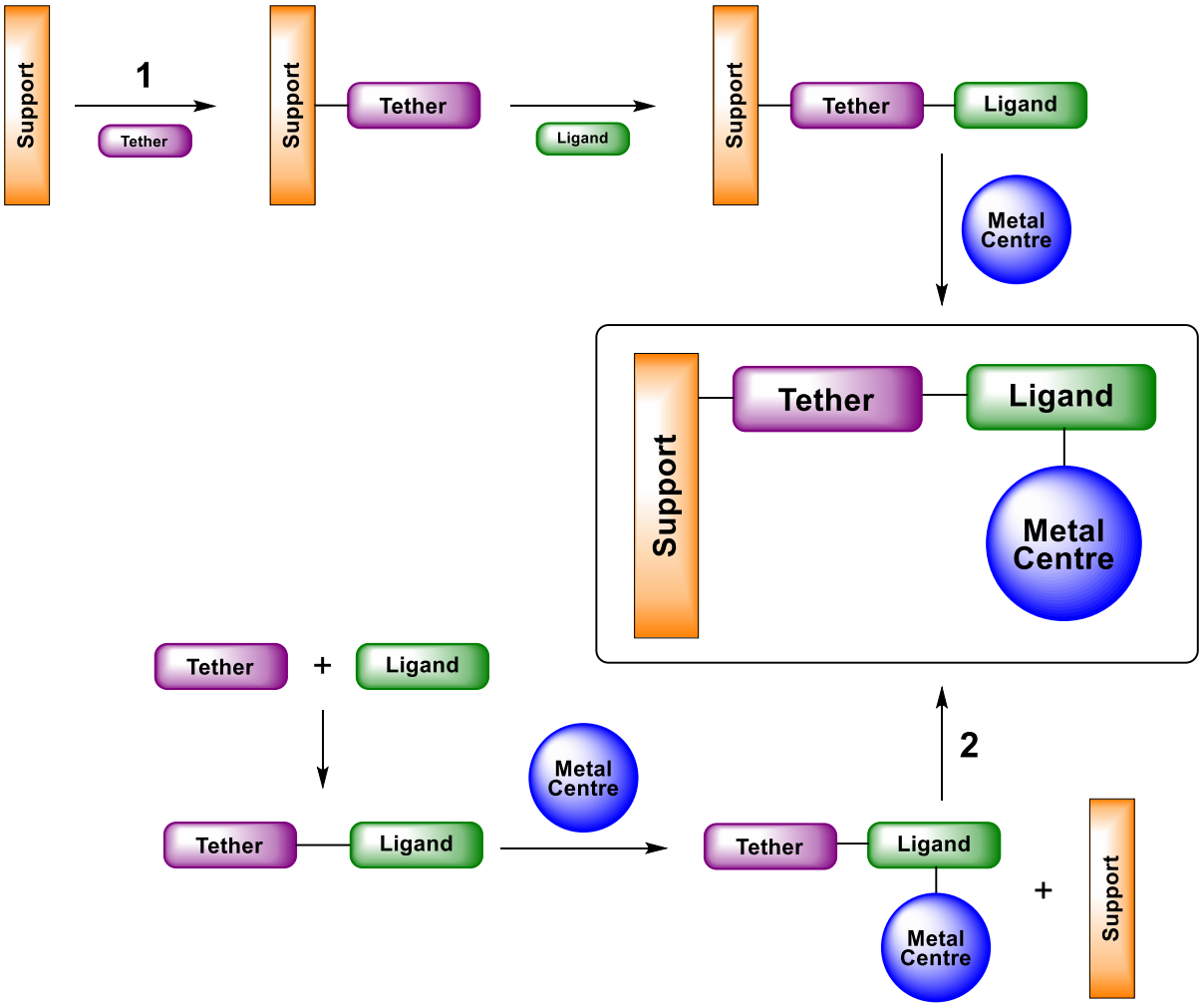

Scheme 2.1: Sequential (1) and convergent (2) approaches to the immobilization of catalysts onto inorganic supports.[5]

These compounds could also be used as ligand scaffolds in the synthesis of siloxane functionalized metal complexes, allowing the metal complexes to then be covalently bonded to inorganic supports, such as mesoporous silica, via an ethoxy siloxane tether. There are two modes for the immobilization of metal complexes onto inorganic supports, namely the sequential and the convergent approach. In the sequential approach (Pathway 1, Scheme 2.1) it becomes difficult to control the process at the point of metal addition. It was therefore decide to utilise the convergent approach (Pathway 2, Scheme 2.1) which allows for the synthesis and characterization of a discrete and stable metal complex before immobilization.[5]

2.2 Results and discussion

2.2.1.1. Synthesis and characterization of model and siloxane functionalized triazole ligands

Preparation of the 1,2,3-triazole ligands is based on a synthetic methodology utilising copper mediated click-type cycloaddition reactions. The synthesis of the model and siloxane functionalized ligands was adapted from literature procedures where the appropriate alkyne is 'clicked' with the desired alkyl or aryl azide using a Cu(I) species as catalysts. It should be noted that the synthesis of the siloxane functionalized ligands is tricky due to the fact that the siloxane functionality is sometimes susceptible to partial hydrolysis and subsequent self-condensation in refluxing aqueous reaction mixtures.[6] For this reason it was necessary to employ the copper catalyst, $CuBr(PPh_3)_3$, which could be used in an anhydrous click reaction.[6,7] The catalyst was synthesised according to a literature procedure.[8] The next point of departure was the synthesis of the organic azides, where both the octyl azide[9] and siloxane functionalized (3-azidopropyl triethoxysilane[10]) azide were synthesized according to literature procedures. Having both the copper catalyst and azide fragments in hand, **ML1** & **SL1** could be successfully synthesised by 'clicking' the appropriate azide with a commercially available alkyne, namely 2-ethynyl pyridine.[11] The reactions were carried out in a microwave reactor, with a THF/triethylamine (1:1 v/v) anhydrous solvent mixture (Scheme 2.2). The model and siloxane functionalized pyridine triazole ligands, **ML1** & **SL1**, were purified using column chromatography over silica and obtained in good yields as off-white powder and golden oil, respectively. The model pyridine triazole ligand, **ML1**, which contains an octyl substituent is not water sensitive and can be synthesized utilizing a one-pot reaction, employing copper sulphate as catalyst in a biphasic aqueous solvent mixture.[3]

However, using the $CuBr(PPh_3)_3$ catalyst in a microwave assisted reaction improved the yield of the compound and reduced the reaction time from 17 hours to only 0.5 hours.

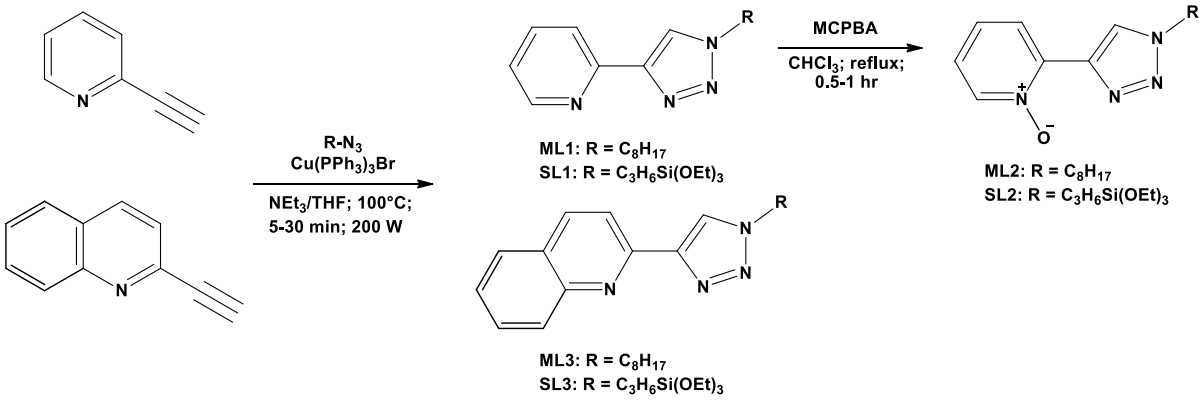

Scheme 2.2: Synthesis of model and siloxane functionalized triazole ligands ML1-ML3, SL1-SL3.

The pyridine N-oxide triazole ligands, **ML2** & **SL2**, were synthesized by subjecting the pyridine triazole ligands, **ML1** & **SL1**, to oxidation with mCPBA under reflux in dry chloroform (Scheme 2.2).[12] After aqueous work up, to quench the peroxide, **ML2** was purified using column chromatography over silica to afford the ligand as a white powder. The siloxane functionalized pyridine N-oxide triazole ligand, **SL2**, was obtained as a clear oil. It was found that the siloxane functionality could not be preserved (this was confirmed using FT-IR spectroscopy) after purification over silica column, resulting in an insoluble sticky white residue being obtained. In order to generate the quinoline triazole ligands, **ML3** & **SL3**, it was necessary to first synthesize 2-ethynyl quinoline from 2-chloroquinoline according to a literature procedure.[13] The transformation involves a Sonogoshira coupling of 2-chloroquinoline with trimethylsilylacetylene (TMS) utilising $PdCl_2(PPh_3)_2$ as catalyst. The Pd catalyst was synthesized according to a literature procedure.[14] This reaction is then followed by the cleavage of the TMS group using potassium bicarbonate to generate the desired 2-ethynyl quinoline. The quinoline triazole ligands were then synthesized and purified using the same procedure as for the pyridine-triazole derivatives (Scheme 2.2), where **ML3** & **SL3** were obtained as a white powder and yellow oil respectively.

2.2.1.2. Characterization of model and functionalized triazole ligands using FT IR spectroscopy

Whilst the formation of the triazole ring cannot be conclusively monitored using IR spectroscopy, it is still useful in determining the absence of the azide ($\upsilon_{N\equiv N}$ = 2085-2095 cm^{-1}) or alkyne ($\upsilon_{C\equiv C}$ = 2100-2200 cm^{-1} and $\upsilon_{C\equiv H}$ = 3150-3350 cm^{-1}) bands in the IR spectra of the compounds which confirms success of the reaction. For ligands **ML2** & **SL2** important vibrational bands are observed in the regions of 1251-1268 cm^{-1}, corresponding to the υ_{N-O} vibrations of the pyridine N-oxide functionality[15], which indicates the transformation of the pyridine triazole starting material. In the case of the siloxane functionalized ligands **SL1-SL3** very intense absorption bands are observed between 1099-939 cm^{-1}, which correspond to the stretching vibrations of the Si-O-Si bonds of the siloxane functionality. IR spectroscopy is therefore an invaluable tool for monitoring preservation of the siloxane functionality during reactions. Selected IR vibrations are summarized in Table 2. 1 below.

Table 2. 1: Selected IR vibrations of model and siloxane functionalized triazole ligands ML2, SL1-3.[a]

Ligand	Pyridine N-Oxide υ_{N-O} cm^{-1}	Siloxane [-Si(OEt)$_3$] $\upsilon_{Si-O-Si}$ cm^{-1}
ML2	1268	-
SL1	-	1070-953; 779
SL2	1251	1099-952; 760
SL3	-	1099-939; 757

[a] Oils recorded as neat samples using an ATR accessory

A typical IR spectrum for the siloxane functionalized pyridine N-oxide ligand (**SL2**) is shown in Figure 2.3. The vibrations resulting from the presence of the siloxane functionality are visible as very intense bands at 1068, 952 and 760 cm^{-1}. This distinct pattern observed is used as a guide to confirm that the siloxane functionality remains intact during subsequent reactions. The band observed at 1251 cm^{-1} is indicative of the υ_{N-O} cm^{-1} stretching vibration.

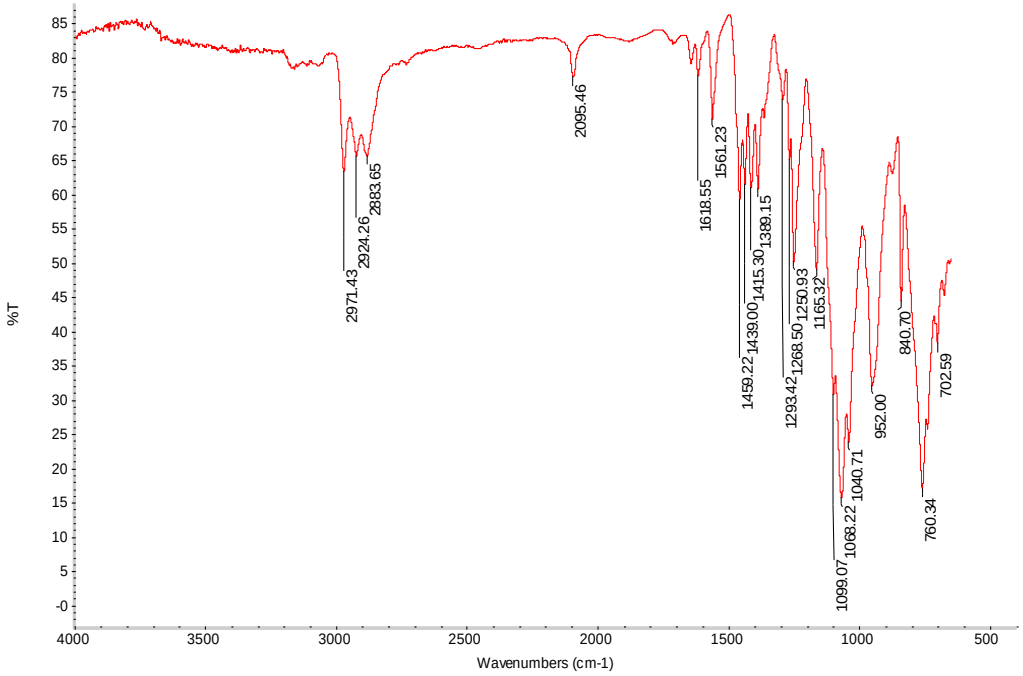

Figure 2.3: IR spectrum of siloxane functionalized pyridine N-oxide triazole ligand SL2

2.2.1.3. Characterization of model and functionalized triazole ligands using ^{1}H NMR spectroscopy

^{1}H NMR spectroscopy was used to confirm the synthesis of ligands bearing a triazole moeiety. The presence of a resonance corresponding to the proton of the newly formed triazole functionality in the aromatic region and the disappearance of the alkyne proton resonance was indicative of successful triazole formation for ligands **ML1**, **ML3**, **SL1** and **SL3**. Furthermore it was a useful tool in confirming the formation of the pyridine N-oxide functionality for ligands **ML2** & **SL2**. This was observed as a downfield shift of the triazole proton resonance in the aromatic region compared to the pyridine triazole starting material. For siloxane functionalized ligands **SL1-SL3** preservation of the siloxane functionality can be observed as a distinct quartet and triplet at about 3.81 ppm and 1.18 ppm, these resonances correspond to the ethyl and methyl protons respectively. Selected ^{1}H NMR resonances for ligands **ML1-ML3** and **SL1-SL3** are summarized in Table 2.2. The triazole proton resonances for all ligands appear in the range of 8.42-9.10 ppm.

Table 2.2: Selected ^{1}H NMR data for model and siloxane functionalized triazole ligands ML1-ML3 & SL1-SL3.[a]

Ligand	Triazole: C<u>H</u>	Ar<u>H</u>	Siloxane Functionality	
			Si(OC<u>H</u>$_2$CH$_3$)$_3$	Si(OCH$_2$C<u>H</u>$_3$)$_3$
ML1	8.41 (s)	8.57 (d, $^{3}J_{H\text{-}H}$ = 4.69), 8.11 (m), 7.85 (m), 7.29 (m)	-	-
ML2	9.07 (s)	8.43 (d, $^{3}J_{H\text{-}H}$ = 8.05), 8.32 (d, $^{3}J_{H\text{-}H}$ = 6.63), 7.45 (t, $^{3}J_{H\text{-}H}$ = 7.67), 7.37 (t, $^{3}J_{H\text{-}H}$ = 6.91)	-	-
ML3	8.63 (s)	8.40 (d, $^{3}J_{H\text{-}H}$ = 8.44), 8.32 (d, $^{3}J_{H\text{-}H}$ = 8.67), 8.01 (d, $^{3}J_{H\text{-}H}$ = 8.44), 7.96 (d, $^{3}J_{H\text{-}H}$ = 8.21), 7.75 (t, $^{3}J_{H\text{-}H}$ = 7.83), 7.57 (t, $^{3}J_{H\text{-}H}$ = 7.60)	-	-
SL1	8.42 (s)	8.57 (m), 8.12 (m), 7.85 (m), 7.29 (m)	3.81 (q, 6H)	1.18 (t, $^{3}J_{H\text{-}H}$ = 6.95, 9H)
SL2	9.10 (s)	8.43 (d, $^{3}J_{H\text{-}H}$ = 8.07), 8.35 (d, $^{3}J_{H\text{-}H}$ = 6.38), 7.46 (t, $^{3}J_{H\text{-}H}$ = 8.08), 7.37 (t, $^{3}J_{H\text{-}H}$ = 6.62)	3.81 (q, 6H)	1.17 (t, $^{3}J_{H\text{-}H}$ = 7.17, 9H)
SL3	8.64 (s)	8.41 (d, $^{3}J_{H\text{-}H}$ = 8.59), |8.32 (d, $^{3}J_{H\text{-}H}$ = 8.59), 8.01 (d, $^{3}J_{H\text{-}H}$ = 8.41), 7.96 (d, $^{3}J_{H\text{-}H}$ = 8.27), 7.75 (t, $^{3}J_{H\text{-}H}$ = 7.64), 7.57 (t, $^{3}J_{H\text{-}H}$ = 7.49)	3.82 (q, 6H)	1.18 (t, $^{3}J_{H\text{-}H}$ = 7.03, 9H)

[a] Recorded in Acetone-d_6

2.2.1.4. Characterization of model and functionalized complexes using ESI mass spectrometry, melting point determination and microanalyses

ESI-MS data, melting points and microanalyses of the model and functionalized ligands are summarized in Table 2.3. Model ligands, **ML1-3**, melted in the range of 60-77 °C. Microanalysis confirmed that the obtained ligands were isolated with reasonable purity. The only exception being siloxane functionalized pyridine N-oxide triazole ligand **SL2** where acceptable elemental analysis data could not be obtained due to the sensitive nature of the material. This result is most likely due to the loss of ethoxy groups on the siloxane functionality, because of the ligand reacting with itself.

Table 2.3: ESI-MS, microanalyses and melting points of model and siloxane functionalized ligands, ML1-3 and SL1-3.

Ligand	ESI-MS $[M+H]^+$; $[M+Na]^+$ (m/z)	Microanalysis: Calculated (Found)			Melting Point (°C)
	Calculated (Found)	C (%)	H (%)	N (%)	
ML1	259.19 (259.19); 281.17 (281.17);	69.73 (70.06)	8.58 (8.59)	21.69 (22.48)	72-75
ML2	275.19 (275.19); 297.17 (297.17)	65.67 (65.92)	8.08 (7.90)	20.42 (19.67)	60-63
ML3	309.21 (309.21); 331.19 (331.19)	73.99 (74.42)	7.84 (7.69)	18.17 (16.69)	74-77
SL1	351.19 (351.18); 373.17 (373.17)	54.83 (54.61)	7.48 (7.41)	15.99 (16.32)	-[b]
SL2	367.18 (367.18); 389.16 (389.16)	-[a]	-[a]	-[a]	-[b]
SL3	401.20 (401.20); 423.18 (423.18)	59.97 (59.75)	7.05 (6.85)	13.99 (13.48)	-[b]

[a] Acceptable elemental analysis data could not be obtained due to the sensitive nature of the material; [b] Ligands isolated as oils.

ESI-MS proved to be useful for confirming the successful synthesis of the model and functionalized ligands. The monoisotopic masses calculated for the proton and sodium adducts of the ligands correspond well with the obtained monoisotopic masses in the spectra (Table 2.3). Additional m/z peaks were however observed in the ESI-MS spectrum obtained for the siloxane functionalized pyridine N-oxide triazole ligand, **SL2** (Figure 2.4). These additional peaks (m/z 279.09, 301.08 and 405.14) are most likely due to the compound reacting with itself, which is likely given the presence of both the siloxane and pyridine N-oxide functionalities. It should be noted that ESI-MS analysis was conducted after storing the ligand under an inert atmosphere for an extended time.

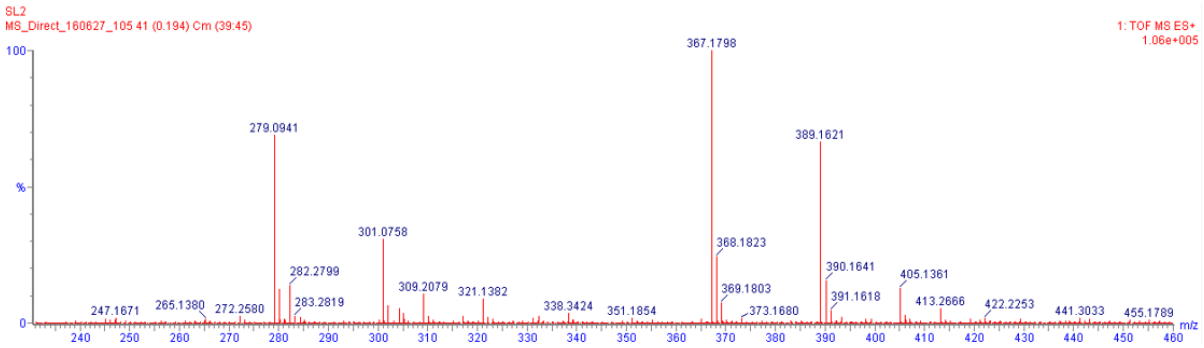

Figure 2.4: ESI-MS (positive mode) spectrum of siloxane functionalized ligand SL2.

It was also observed that the nature of the ligand had changed from a soluble, clear oil to a partially insoluble sticky white residue within a time period of one month. IR spectroscopy of **SL2** after several months showed a distortion of the signals corresponding to the siloxane vibration, between 1031-922 cm^{-1} and 761 cm^{-1}, as well as a shift in the pyridine N-oxide signal from 1251 cm^{-1} to 1242 cm^{-1} could also be observed. It can therefore be concluded that **SL2** is not stable even under inert conditions over time. However the ligand **SL2** appears to be stable over a short period of time (two weeks) and can be used for analysis or subsequent reactions within this window. The ligand could not be analysed by proton NMR after an extended storage time due to the insoluble nature of the resulting material.

2.2.2 Synthesis and characterization of model and functionalized triazole RuCl(*p*-cymene) complexes MC1-MC3 and SC1-SC3

The ligands were reacted with a ruthenium precursor, $[Ru(p\text{-cymene})(Cl)_2]_2$, in DCM (Scheme 2.3). The $[Ru(p\text{-cymene})(Cl)_2]_2$ dimer was synthesized according to a literature procedure.[16] The synthesis of the dimer involves a microwave assisted reaction between $RuCl_3 \cdot xH_2O$ and excess amounts of α-terpinine in ethanol, affording an orange solid in good yields. The counter-ion employed to stabilize the resulting cationic ruthenium species was tetraphenylborate.

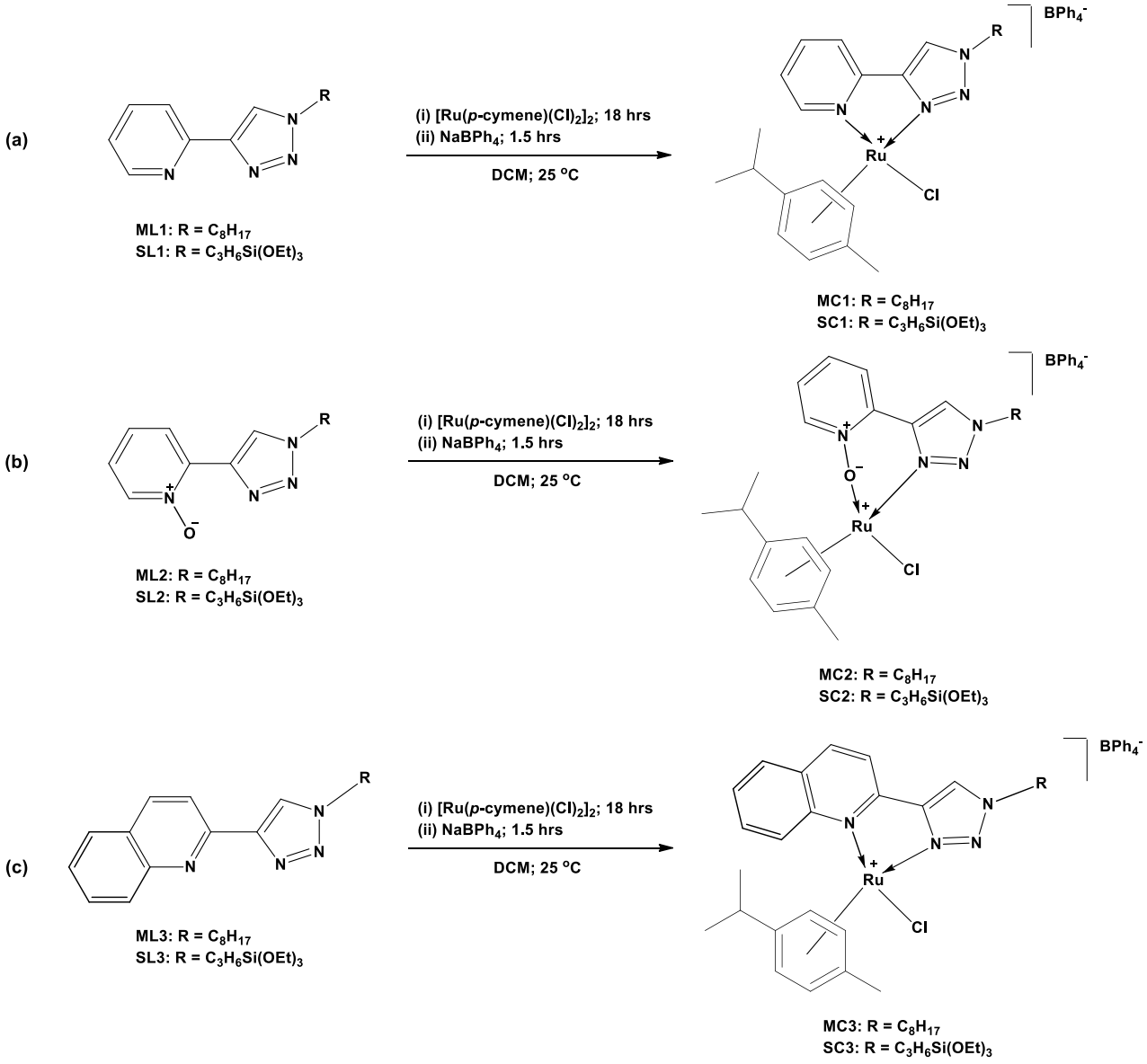

Scheme 2.3: Synthesis of model and siloxane functionalized cationic complexes MC1-MC3, SC1-SC3.

Once the formation of the cationic species could be observed (colour change from orange to yellow or brown) the sodium tetraphenylborate salt was added as a source of the counter-ion. Previous work done in our group on similar types of complexes showed that the tetraphenylborate counter-ion was capable of effectively stabilizing the model and more importantly the siloxane functionalized complexes, which is why it was employed in the reactions discussed here. The model, **MC1-MC3**, and siloxane functionalized, **SC1-SC3**, complexes were isolated in good yields (57-87 %) as yellow to brown solids (Scheme 2.3). The complexes were fully characterized using FTIR, ^{1}H and ^{13}C NMR spectroscopy, ESI mass spectrometry, melting point determination and microanalyses.

2.2.2.1. Characterization of model and functionalized complexes using FT-IR spectroscopy

The coordination of the pyridine and triazole ring cannot be conclusively monitored using IR spectroscopy, however for complexes **MC2** & **SC2** shifts in the vibrational bands from the ligands observed in the regions of 1263-1260 cm^{-1}, correspond to the $\upsilon_{N\text{-}O}$ vibrations of the pyridine N-oxide functionality, which indicates the coordination of the N-O functionality to the ruthenium centre. In the case of the siloxane functionalized complexes **SC1-SC3** very intense absorption bands are observed between 1071-953 cm^{-1} which correspond to the stretching vibrations of the Si-O-Si bonds of the siloxane functionality. The presence of these bands confirms the preservation of the siloxane functionality during the complexation, which is crucial for subsequent immobilization of the complexes (Chapter 3). The presence of the counter-ion, tetraphenylborate, can be observed as very intense absorption bands between 733-702 cm^{-1}. Selected FT-IR vibrations for all model and functionalized complexes, **MC1-MC3** and **SC1-SC3**, are summarized in Table 2.4 below.

Table 2.4: Selected IR vibrations of model and siloxane functionalized complexes MC1-MC3, SC1-SC3.[a]

Complex	Pyridine N-Oxide υ_{N-O} cm^{-1}		Siloxane [-Si(OEt)$_3$] $\upsilon_{Si-O-Si}$ cm^{-1}	B(Ph)$_4^-$ υ_{B-C} cm^{-1}
	Ligand	Complex		
MC1	-	-	-	733-705
MC2	1268	1260	-	731-702
MC3	-	-	-	731-702
SC1	-	-	1071-953	731-702
SC2	1251	1263	1070-953	731-702
SC3	-	-	1064-954	731-702

[a] Solids recorded as neat samples using a ZnSe crystal ATR accessory

2.2.2.2. Characterization of model and functionalized complexes using NMR spectroscopy

^{1}H NMR spectroscopy was used to confirm the coordination of selected ligands to the ruthenium centre. Selected ^{1}H NMR resonances for complexes **MC1-MC3** and **SC1-SC3** are summarized in Table 2.5.

Table 2.5: Selected ^{1}H NMR data for model and siloxane functionalized complexes ML1-3 & SL1-3.[a]

Complex	Triazole Proton		Arene Ring: *p*-cymene	
	Ligand	Complex	Aromatic	Aliphatic
MC1	8.41 (s)	8.60 (s)	6.08 (d), 6.03 (d), 5.86 (d), 5.77 (d)	2.76 (m), 2.20 (s), 1.13 (m)
MC2	9.07 (s)	8.44 (s)	5.85 (d), 5.81 (d), 5.54 (t)	2.98 (m), 2.25 (s), 1.31 (m)
MC3	8.63 (s)	8.87 (s)	6.12 (d), 6.07 (d), 5.99 (d), 5.94 (d)	2.52 (m), 2.21 (s), 1.00 (d), 0.94 (d)
SC1	8.42 (s)	8.66 (s)	6.09 (d), 6.03 (d), 5.88 (d), 5.79 (d)	2.77 (m), 2.21 (s), 1.09 (m)
SC2	9.10 (s)	8.33 (s)	5.83 (d), 5.79 (d), 5.52 (d)	2.98 (m), 2.24 (s), 1.31 (d)
SC3	8.64 (s)	8.90 (s)	6.11 (d), 6.07 (d), 6.00 (d), 5.94 (d)	2.53 (m), 2.21 (s), 1.01 (d), 0.95 (d)

[a] Recorded in Acetone-d_6

Successful complexation of the N,N' donor ligands **ML1**, **ML3**, **SL1** and **SL3** to the ruthenium centre could be observed in the ^{1}H NMR spectrum of the complexes as a general downfield shift of all the aromatic signals, including the triazole proton signal (Table 2.5), relative to the free ligand. This downfield shift is due to the cationic nature of the complexes. In the case of the pyridine N-oxide ligands **ML2** and **SL2** we see a slight downfield shift for the pyridine protons and an upfield shift for the triazole protons (Table 2.5) upon complexation. This can be attributed to the oxygen atom withdrawing electron density through the conjugated aromatic system in the free ligand, however upon complexation this electron density is then transferred to the metal centre which in turn shields the protons of the ligands in the complex. Changes in the coordination of the *p*-cymene ring could be observed with resonances in the monomer complexes corresponding to the arene ring protons in the range of 5.77-6.12 ppm for the N,N' donor ligands and between 5.52-5.85 ppm for the N,O donor ligands, this upfield shift points towards a larger electron density being present in the N,O complexes. The aliphatic protons of the *p*-cymene ring can be observed in a range of 0.94-2.98 ppm.

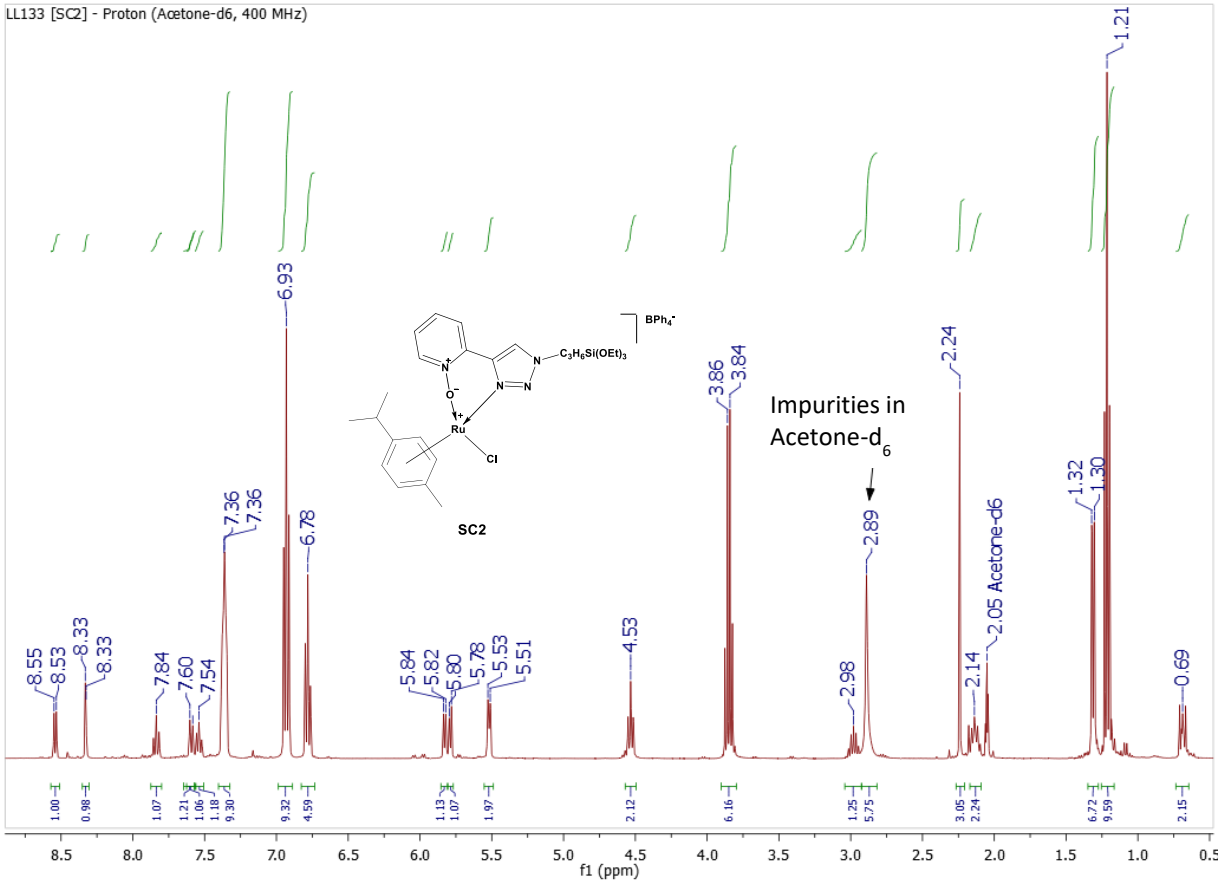

Figure 2.5: ^{1}H NMR spectrum of siloxane functionalized complex, SC2.

The ^{1}H NMR spectrum of complex **SC2** is shown as an example in Figure 2.5 above. The arene ring proton resonances of the *p*-cymene ligand are observed as three doublets resonating at 5.52, 5.79 and 5.83 ppm respectively. The methyl proton resonance of *p*-cymene are observed as a singlet at 2.24 ppm, while the methyl and methylene protons of the *iso*-propyl are observed in the form of a doublet and multiplet at 1.31 ppm and 2.98 ppm, respectively. Intense resonances are observed at 6.78, 6.93 and 7.36 ppm respectively corresponding to the protons of the tetraphenylborate counter-ion, integrating for a total of 20 protons. An upfield shift for the triazole proton resonance from 9.10 ppm for the free ligand to 8.33 ppm for the complex is observed confirming complexation of the N,O ligand. Furthermore, shifts in the pyridine protons can be observed compared to the free ligand, these signals appear in the aromatic region between 7.54-8.54 ppm and confirm successful coordination of the pyridine N-oxide ligand. The protons of the propyl chain of the siloxane tail can be observed as a triplet, pentet and multiplet at 4.53, 2.14 and 0.69 ppm respectively. Lastly, but most importantly the resonances corresponding to the ethyl and methyl protons of the siloxane functionality can be observed as a quartet and a triplet at 3.85 and 1.21 ppm respectively.

2.2.2.3. Characterization of model and functionalized complexes using ESI mass spectrometry, melting point determination and microanalyses

ESI-MS data, melting points and microanalyses of all the model and functionalized complexes are summarized in Table 2.6. The complexes have melting points in the range of 85-159 ˚C and they subsequently all decompose in the range of 153-227 ˚C. The complexes **MC2** and **SC2** bearing the N,O donor ligands appear to be the least thermally stable, while the highest melting point and decomposition temperatures are observed for complex **MC1**. Microanalysis confirmed that the obtained complexes were isolated in high purity.

Table 2.6: ESI-MS, microanalyses and melting points of model and siloxane functionalized complexes, MC1-3 and SC1-3.

Complex	ESI-MS $[M]^+$ (m/z)	Microanalyses: Calculated (Found)			Melting Point (°C) [Decomposition]
	Calculated (Found)	C (%)	H (%)	N (%)	
MC1	529.17 (529.17)	68.04 (68.34)[a]	6.55 (6.66)[a]	6.44 (6.68)[a]	155-159 [221-227]
MC2	545.16 (545.16)	68.09 (67.31)	6.53 (6.68)	6.48 (6.18)	81-85 [153-160]
MC3	579.18 (579.18)	70.86 (70.20)	6.51 (6.37)	6.24 (6.00)	99-106 [194-205]
SC1	621.16 (621.16)	61.71 (61.83)[b]	6.25 (6.00)[b]	5.70 (5.83)[b]	118-126 [209-215]
SC2	637.16 (637.16)	61.73 (61.56)[a]	6.24 (5.90)[a]	5.73 (5.60)[a]	85-90 [161-168]
SC3	671.18 (671.18)	64.40 (64.76)[a]	6.23 (6.13)[a]	5.54 (5.28)[a]	148-156 [218-224]

[a] M·0.25DCM; [b] M·0.5DCM

Ruthenium compounds give rise to very distinct isotopic splitting patterns in the mass spectra of the compounds, due to the metal having many naturally occurring isotopes. It is therefore possible to conclusively elucidate the structure of a certain fragment in the mass spectrum by comparing the experimentally obtained clusters with the theoretical simulation of the expected isotopic cluster. ESI-MS proved to be an important tool to confirm the successful synthesis of the model and functionalized ruthenium complexes. The theoretically calculated and obtained monoisotopic masses of the complexes are identical and are summarized in Table 2.6.

The mass spectrum (positive mode) of the model complex **MC1** is shown in Figure 2.6. The obtained spectrum corresponds very well with the simulated isotopic distribution of the cationic ruthenium complex, with the base peak being observed at a m/z of 529.17. No other significant low mass fragments could be observed. Also higher mass ions, which are often assigned to adducts or dimerization processes, could not be observed.

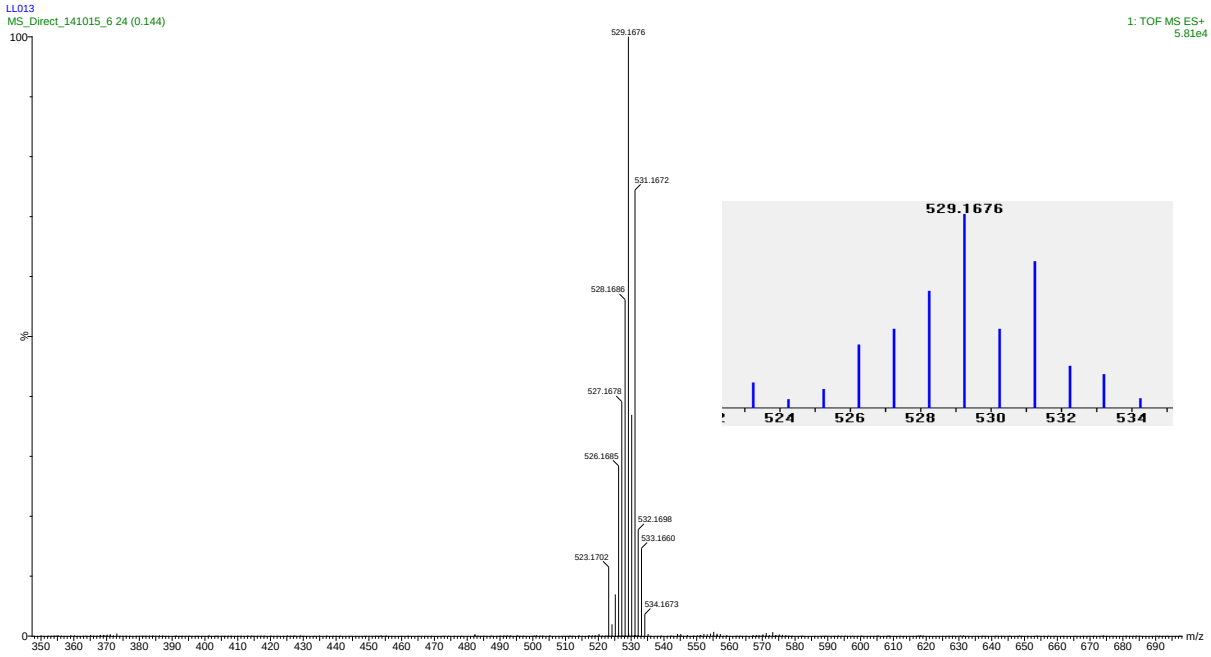

Figure 2.6: ESI-MS (positive mode) of model complex MC1

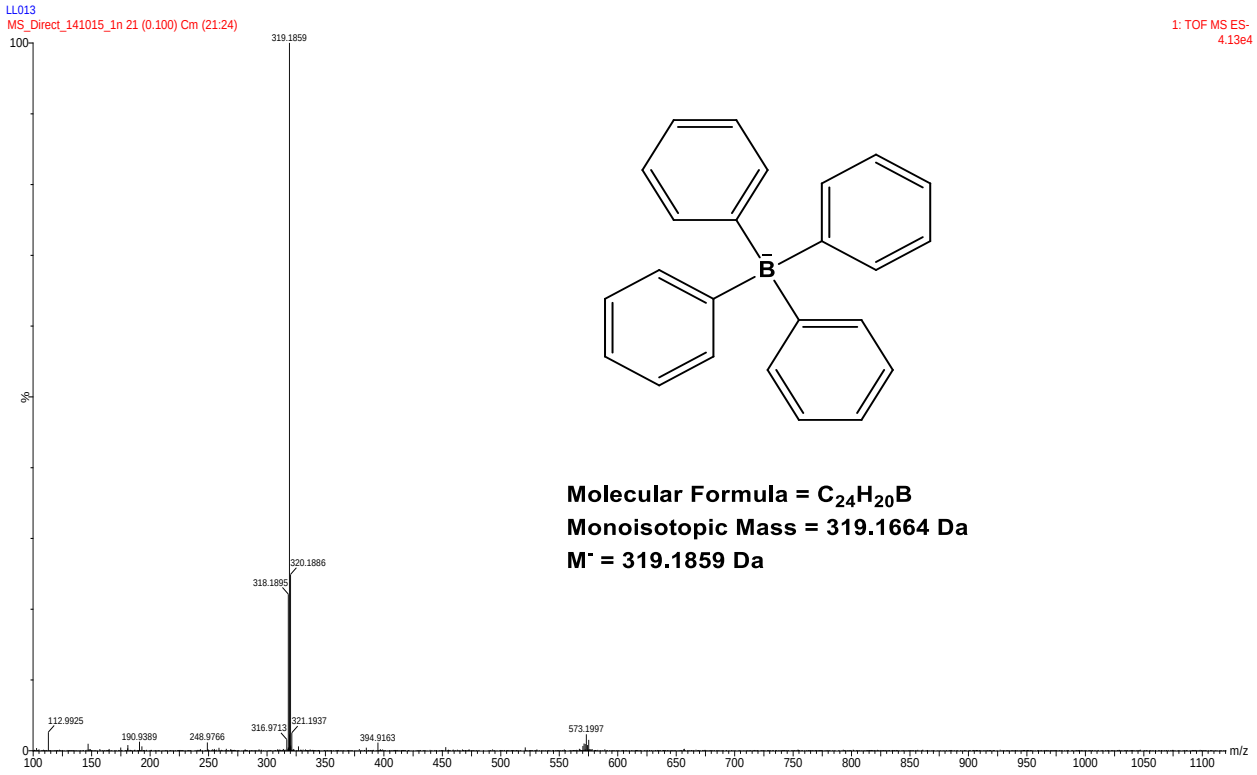

Figure 2.7: ESI-MS (negative mode) of model complex MC1

The mass spectrum of the model complex **MC1** was also recorded in the negative mode (Figure 2.7) to detect any negatively charged components. The base peak at a m/z of 319.19 corresponds to the tetraphenylborate counter-ion (Monoisotopic mass = 319.17 Da), as expected.

2.3 Concluding remarks

Model and functionalized ligands, **ML1-ML3** and **SL1-SL3**, were successfully synthesized and complexed to the ruthenium arene dimer, $RuCl_2$(*p*-cymene)]$_2$, in DCM to afford the model and functionalized complexes **MC1-MC3** and **SC1-SC3**. Tetraphenylborate was employed as the counterion and the cationic complexes were isolated as stable yellow to dark golden yellow solids in moderate to high yields (57-87 %). ^{1}H NMR spectroscopy was utilized to confirm the successful complexation of the N,N$'$ and N,O ligands to the ruthenium centre.

The preservation of the siloxane functionality was monitored throughout using IR and ^{1}H NMR spectroscopy. The siloxane functionality remained intact for all the ligands and complexes during the synthetic steps. It was observed for ligand **SL2** that the siloxane functionality decomposed over time, most likely due to the compound undergoing self-condensation.

In general, both the model and functionalized complexes showed decent thermal stability, melting point range between 99-159 ˚C. The N,O complexes, **MC2** and **SC2**, were found to be the least thermally stable with melting point range between 81-90 ˚C.

2.4 Experimental section

2.4.1 General remarks and instrumentation

All reactions were performed using standard Schlenk techniques under an inert atmosphere (Argon or Nitrogen) unless stated otherwise. Highly air-sensitive materials were stored in a nitrogen purged glovebox and all manipulations with these materials were carried out in the glovebox to prevent decomposition or oxidation.

In the case of microwave assisted reactions a CEM Microwave reactor was used. Fourier transform infrared (FT-IR) spectra were recorded using an ATR accessory on a Nicolet Avatar 330 FT-IR spectrometer equipped with a Smart Performer ATR attachment with a ZnSe crystal. NMR spectra were recorded on a Varian Unity Inova instrument at 300, 400 and 600 MHz for ^{1}H and ^{13}C. ESI-MS was performed using a Waters Synapt G2 Mass Spectrometer. A Thermo Elemental Analyzer (CHNS-O) was used for the accurate determination of the elemental composition of samples.

2.4.2 Materials

All reagents were acquired from Sigma-Aldrich and used without any further purification; these include 2-ethynyl pyridine, 2-chloroquinoline, copper iodide, octyl bromide, 3-chloropropyl triethoxysilane, *meta*-Chloroperoxybenzoic acid (mCPBA), α-terpinine and $RuCl_3 \cdot xH2O$. All solvents were purchased from Sigma-Aldrich or Kimix Chemicals. DCM, diethyl ether, hexane, toluene and THF were purified using a Pure SolvTM Micro solvent purifier fitted with activated alumina columns. Ethanol and methanol were purified by distillation over a mixture of magnesium filings and iodine. Acetonitrile was purified by distillation over phosphorous pentoxide.

2.4.3 Synthesis of model and functionalized ligands

2.4.3.1. Synthesis of pyridine (ML1, SL1) and quinoline (ML3, SL3) triazole ligands

For model ligand **ML1**: To a mixture of NEt_3/THF (1 mL, 1:1 v/v) in a microwave tube was added 2-ethynylpyridine (0.404 mL, 4.0 mmol), octyl azide (1.00 g, 6.44 mmol) and $Cu(PPh_3)_3Br$ (0.018 g, 0.02 mmol). The mixture was irradiated in a Discover microwave reactor at 100 °C for 30 min (200 Watts). The reaction mixture was brown with grey un-dissolved $Cu(PPh_3)_3Br$ before and dark brown with a brown precipitate after the reaction.

The solvent was removed under reduced pressure to obtain a brown solid. The crude mixture was washed with hexane (3×30 mL) and the hexane fractions decanted. To the remaining brown residue was added diethyl ether, at which point majority of the material dissolved and a brown solid insoluble residue remaining. The ether fraction was decanted, filtered over cotton wool and the solvent removed under reduced pressure to obtain a light brown powder. The powder was purified by flash column chromatography over silica gel eluted with DCM followed by a mixture of DCM/Acetone (9:1 v/v). The separation was monitored by TLC (DCM/Acetone (9:1 v/v)). The white powder obtained was further dried *in-vacuo* (0.631 g, 2.44 mmol, 61%).

Model ligand, **ML1**: White powder, 61% yield. ^{1}H NMR (400 MHz, $(CD_3)_2CO$): δ (ppm) = 8.57 (H_{py}, d, $^{3}J_{H-H}$ = 4.69, 1H), 8.41 (H_{trz}, s, 1H), 8.11 (H_{py}, m, 1H), 7.85 (H_{py}, m, 1H), 7.29 (H_{py}, m, 1H), 4.49 (N-C**H**$_2$, t, $^{3}J_{H-H}$ = 7.04, 2H), 1.98 (C**H**$_2$, m, 2H), 1.32 (C**H**$_2$, m, 10H), 0.85 (C**H**$_3$, t, $^{3}J_{H-H}$ = 6.77, 3H). ^{13}C {^{1}H} NMR (400 MHz, $(CD_3)_2CO$): δ (ppm) = 152.01, 150.56, 148.99, 137.70, 123.57, 123.44, 120.37, 50.93, 32.63, 31.15, 29.83, 27.29, 23.41, 14.46. Elemental Analysis (%): Calc. For $C_{15}H_{22}N_4$ (258.36 g/mol): C, 69.73; H, 8.58; N, 21.69; Found: C, 70.06; H, 8.59; N, 22.48. MS (ESI, *m*/*z*): 259.19 $[M+H]^+$, 281.17 $[M+Na]^+$. Melting Point: 72-75 ˚C.

Model ligand, **ML3**: White powder, 60% yield. ^{1}H NMR (400 MHz, $(CD_3)_2CO$): δ (ppm) = 8.63 (H_{trz}, s, 1H), 8.40 (H_{qu}, d, $^{3}J_{H-H}$ = 8.44, 1H), 8.32 (H_{qu}, d, $^{3}J_{H-H}$ = 8.67, 1H), 8.01 (H_{qu}, d, $^{3}J_{H-H}$ = 8.44, 1H), 7.96 (H_{qu}, d, $^{3}J_{H-H}$ = 8.21, 1H), 7.75 (H_{qu}, t, $^{3}J_{H-H}$ = 7.83, 1H), 7.57 (H_{qu}, t, $^{3}J_{H-H}$ = 7.60, 1H), 4.54 (N-C**H**$_2$, t, $^{3}J_{H-H}$ = 7.08, 2H), 2.01 (C**H**$_2$, m, 2H), 1.38 & 1.27 (C**H**$_2$, m, 10H), 0.86 (C**H**$_3$, t, $^{3}J_{H-H}$ = 6.76, 3H). ^{13}C {^{1}H} NMR (300 MHz, $(CD_3)_2CO$): δ (ppm) = 151.93, 149.05, 148.99, 137.65, 130.59, 129.80, 128.80, 128.62, 127.11, 124.10, 119.12, 50.94, 32.50, 31.04, 29.72, 27.19, 23.28, 14.33. Elemental Analysis (%): Calc. For $C_{19}H_{24}N_4$ (308.42 g/mol): C, 73.99; H, 7.84; N, 18.17; Found: C, 74.42; H, 7.69; N, 16.69. MS (ESI, *m*/*z*): 309.21 $[M+H]^+$, 331.19 $[M+Na]^+$. Melting Point: 74-77 ˚C.

Functionalized ligand, **SL1**: Yellow oil, 96% yield. IR: FT-IR, υ/cm^{-1}: 1070-953 and 779 (siloxane, Si-O-Si). ^{1}H NMR (400 MHz, $(CD_3)_2CO$): δ (ppm) = 8.57 (H_{py}, m, 1H), 8.42 (H_{trz}, s, 1H), 8.12 (H_{py}, m, 1H), 7.85 (H_{py}, m, 1H), 7.29 (H_{py}, m, 1H), 4.50 (NC**H**$_2$CH$_2$CH$_2$Si, t, $^{3}J_{H-H}$ = 7.02, 2H), 3.81 (CH$_2$CH$_2$Si(OC**H**$_2$CH$_3$)$_3$, q, 6H), 2.09 (NCH$_2$C**H**$_2$CH$_2$Si, m, 2H), 1.18 (CH$_2$CH$_2$Si(OCH$_2$C**H**$_3$)$_3$, t, $^{3}J_{H-H}$ = 6.95, 9H), 0.65 (NCH$_2$CH$_2$C**H**$_2$Si, m, 2H). ^{13}C {^{1}H} NMR (400 MHz, $(CD_3)_2CO$): δ (ppm) = 151.97, 150.54, 148.91, 137.68, 123.61, 123.55, 120.36, 59.03, 53.18, 25.22, 18.74, 8.19. Elemental Analysis (%): Calc. For $C_{16}H_{26}N_4O_3Si$ (350.49

g/mol): C, 54.83; H, 7.48; N, 15.99; Found: C, 54.605; H, 7.405; N, 16.32. MS (ESI, *m*/*z*): 351.18 $[M+H]^+$, 373.17 $[M+Na]^+$.

Functionalized ligand, **SL3**: Yellow oil, 29% yield. IR: FT-IR, υ/cm^{-1}: 1099-939 and 757 (siloxane, Si-O-Si). ^1H NMR (400 MHz, $(CD_3)_2CO$): δ (ppm) = 8.64 (H_{trz}, s, 1H), 8.41 (H_{qu}, d, $^3J_{H-H}$ = 8.59, 1H), 8.32 (H_{qu}, d, $^3J_{H-H}$ = 8.59, 1H), 8.01 (H_{qu}, d, $^3J_{H-H}$ = 8.41, 1H), 7.96 (H_{qu}, d, $^3J_{H-H}$ = 8.27, 1H), 7.75 (H_{qu}, t, $^3J_{H-H}$ = 7.64, 1H), 7.57 (H_{qu}, t, $^3J_{H-H}$ = 7.49, 1H), 4.55 ($NC\mathbf{H}_2CH_2CH_2Si$, t, $^3J_{H-H}$ = 7.12, 2H), 3.82 ($CH_2CH_2Si(OC\mathbf{H}_2CH_3)_3$, q, 6H), 2.11 ($NCH_2C\mathbf{H}_2CH_2Si$, m, 2H), 1.18 ($CH_2CH_2Si(OCH_2C\mathbf{H}_3)_3$, t, $^3J_{H-H}$ = 7.03, 9H), 0.67 ($NCH_2CH_2C\mathbf{H}_2Si$, m, 2H). ^{13}C $\{^1H\}$ NMR (400 MHz, $(CD_3)_2CO$): δ (ppm) = 151.87, 140.00, 148.88, 137.61, 130.54, 129.75, 128.77, 128.58, 127.06, 124.22, 58.90, 53.15, 25.08, 18.64, 8.06. Elemental Analysis (%): Calc. For $C_{20}H_{28}N_4O_3Si$ (400.55 g/mol): C, 59.97; H, 7.05; N, 13.99; Found: C, 59.75; H, 6.85; N, 13.48. MS (ESI, *m*/*z*): 401.20 $[M+H]^+$, 423.18 $[M+Na]^+$.

2.4.3.2. Synthesis of pyridine N-oxide triazole ligands

For model ligand **ML2**: MCPBA (0.642 g, 3.72 mmol) was dissolved in chloroform (5 mL) in a Schlenk tube at room temperature in air. To this was added a solution of **ML1** (0.480 g, 1.86 mmol) in chloroform (5 mL). The clear reaction mixture was placed in an oil bath and left to stir for 0.5 hrs at 61 °C under N_2. After 0.5 hrs the Schlenk tube was removed from the heat and cooled to room temperature. A clear solution was obtained after the reaction was completed. The contents of the Schlenk tube were transferred to a separating funnel. An aqueous solution of $Na_2S_2O_3$ (0.5 M) was added to the reaction mixture (50 mL). The organic layer was extracted with DCM (2×50 mL). The combined organic layers were washed with aqueous NaOH (1 M) solution (1×100 mL). The NaOH fraction was then extracted with DCM (3×50 mL). The mixture was dried over $MgSO_4$ and filtered. The solvent was removed from the filtrate under reduced pressure to afford a white solid. The solid was dissolved in acetone and recrystallized by layering the solution with water. The solid was purified using flash column chromatography over silica gel eluted with DCM followed by Acetone. The white powder was dried *in-vacuo* for 6 hrs at room temperature (0.170 g; 33.3% yield).

Model ligand, **ML2**: White powder, 33% yield. IR: FT-IR, υ/cm^{-1}: 1268 (pyridine N-O). ^1H NMR (600 MHz, $(CD_3)_2CO$): δ (ppm) = 9.07 (H_{trz}, s, 1H), 8.43 (H_{py}, d, $^3J_{H-H}$ = 8.05, 1H), 8.32 (H_{py}, d, $^3J_{H-H}$ = 6.63, 1H), 7.45 (H_{py}, t, $^3J_{H-H}$ = 7.67, 1H), 7.37 (H_{py}, t, $^3J_{H-H}$ = 6.91, 1H), 4.54 (N-$C\mathbf{H}_2$, t, $^3J_{H-H}$ = 7.14, 2H), 1.98 ($C\mathbf{H}_2$, m, 2H), 1.32 ($C\mathbf{H}_2$, m, 10H), 0.85 ($C\mathbf{H}_3$, t, $^3J_{H-H}$ = 6.88, 3H). ^{13}C $\{^1H\}$ NMR (400 MHz, $(CD_3)_2CO$): δ (ppm) = 142.11, 140.82, 139.46, 127.13, 125.44,

124.98, 124.31, 50.80, 32.52, 31.08, 29.90, 27.18, 23.30, 14.37. Elemental Analysis (%): Calc. For $C_{15}H_{22}N_4O$ (274.36 g/mol): C, 65.67; H, 8.08; N, 20.42; Found: C, 65.92; H, 7.90; N, 19.67. MS (ESI, *m*/*z*): 275.19 $[M+H]^+$, 297.17 $[M+Na]^+$. Melting Point: 60-63 ˚C.

Functionalized ligand, **SL2**: Clear oil, 67% yield. IR: FT-IR, υ/cm^{-1}: 1251 (pyridine, N-O), 1099.07-952.00 and 760.34 (siloxane, Si-O-Si). ^{1}H NMR (400 MHz, $(CD_3)_2CO$): δ (ppm) = 9.10 (H_{trz}, s, 1H), 8.43 (H_{py}, d, $^3J_{H-H}$ = 8.07, 1H), 8.35 (H_{py}, d, $^3J_{H-H}$ = 6.38, 1H), 7.46 (H_{py}, t, $^3J_{H-H}$ = 8.08, 1H), 7.37 (H_{py}, t, $^3J_{H-H}$ = 6.62, 1H), 4.53 ($NC\mathbf{H}_2CH_2CH_2Si$, t, $^3J_{H-H}$ = 6.89, 2H), 3.81 ($CH_2CH_2Si(OC\mathbf{H}_2CH_3)_3$, q, 6H), 2.09 ($NCH_2C\mathbf{H}_2CH_2Si$, t, $^3J_{H-H}$ = 6.90, 2H), 1.17 ($CH_2CH_2Si(OCH_2C\mathbf{H}_3)_3$, t, $^3J_{H-H}$ = 7.17, 9H), 0.63 ($NCH_2CH_2C\mathbf{H}_2Si$, m, 2H). ^{13}C {^{1}H} NMR (600 MHz, $(CD_3)_2CO$): δ (ppm) = 142.19, 140.92, 139.42, 127.41, 125.73, 125.00, 124.38, 59.01, 53.09, 25.20, 18.76, 8.13. Acceptable micro analysis could not be obtained due the sensitive nature of the material. MS (ESI, *m*/*z*): 367.18 $[M+H]^+$, 389.16 $[M+Na]^+$.

2.4.4 Synthesis of model and functionalized complexes

For model complex **MC1**: The precursor $[Ru(p\text{-cymene})(Cl)_2]_2$ (0.202 g, 0.329 mmol) was dissolved with stirring in DCM (15 mL). To this was added **ML1** (0.170 g, 0.658 mmol), dissolved in DCM (10 mL), and the mixture was stirred for 18 hrs at 25 °C. The solution was a clear orange and turned a clear yellow during this period. At 18 hrs the counter ion $NaBPh_4$ (0.226 g, 0.658 mmol) was added as a solid. The mixture was left to stir for a further 1.5 hrs, at which point it was still a yellow solution. The reaction mixture was then filtered over a plug of celite and cotton wool. The clear yellow filtrate was then collected and the solvent removed under reduced pressure. The resulting yellow flaky powder was dissolved in MeCN (2 mL) and the solution was then layered with ether (20 mL) and hexane (20 mL) and triturated (the solution was physically agitated). A yellow precipitate formed and the mixture was placed in the freezer overnight. The yellow solid was then filtered off and washed with ether. The product was dried *in-vacuo* (0.470 g, 0.554 mmol, 84%).

Model complex **MC1**: Yellow solid, yield 84 %. IR: FT-IR, υ/cm^{-1}: 733-705 (BPh_4, B-C). ^{1}H NMR (300 MHz, $(CD_3)_2CO$): δ (ppm) = 9.42 (H_{py}, m, 1H), 8.60 (H_{trz}, s, 1H), 8.11 (H_{py}, m, 1H), 7.97 (H_{py}, m, 1H), 7.60 (H_{py}, m, 1H), 7.36 (BPh_4, m, 8H), 6.93 (BPh_4, t, $^3J_{H-H}$ = 7.01, 8H), 6.78 (BPh_4, t, $^3J_{H-H}$ = 7.01, 4H), 6.08 (H_{cym} aromatic, d, $^3J_{H-H}$ = 6.13, 1H), 6.03 (H_{cym} aromatic, d, $^3J_{H-H}$ = 6.13, 1H), 5.86 (H_{cym} aromatic, d, $^3J_{H-H}$ = 6.13, 1H), 5.77 (H_{cym} aromatic, d, $^3J_{H-H}$ = 6.13, 1H), 4.62 (octyl N-CH_2, t, $^3J_{H-H}$ = 6.95, 2H), 2.76 (H_{cym} *i*-Pr $C\mathbf{H}(CH_3)_2$, m, 1H), 2.20 (H_{cym}

CH_3, s, 3H), 2.01 (octyl CH_2, m, 2H), 1.33 (octyl CH_2, m, 10H), 1.13 (H_{cym} *i*-Pr CH($C\mathbf{H}_3$)$_2$, m, 6H), 0.88 (octyl CH_3, m, 3H). ^{13}C {^1H} NMR (300 MHz, $(CD_3)_2CO$): δ (ppm) = 166.01 (BPh_4), 165.35 (BPh_4), 164.69 (BPh_4), 164.04 (BPh_4), 156.31, 149.44, 147.22, 140.98, 137.09 (BPh_4), 126.86, 126.16 (BPh_4), 125.79, 123.23, 122.39 (BPh_4), 105.70 (C_{cym} aromatic), 103.22 (C_{cym} aromatic), 86.96 (C_{cym} aromatic), 85.59 (C_{cym} aromatic), 84.86 (C_{cym} aromatic 84.23 (C_{cym} aromatic), 53.44, 32.54, 31.87, 30.64, 26.99, 23.36, 22.67, 21.92, 18.81, 14.44. Elemental Analysis (%): Calc. For $C_{49}H_{56}BClN_4Ru{\cdot}0.25CH_2Cl_2$ (529.16 g/mol): C, 68.04; H, 6.55; N, 6.44; Found: C, 68.335; H, 6.66; N, 6.675. MS (ESI, *m*/*z*): 529.17 $[M]^+$, 319.19 $[BPh_4]^-$. Melting Point: 142-146 ˚C

Model complex **MC2**: Golden brown solid, yield 57 %. IR: FT-IR, *υ*/cm^{-1}: 1260 (pyridine, N-O), 731-702 (BPh_4, B-C). ^1H NMR (600 MHz, $(CD_3)_2CO$): δ (ppm) = 8.58 (H_{py}, d, $^3J_{H-H}$ = 6.37, 1H), 8.44 (H_{trz}, s, 1H), 7.87 (H_{py}, t, $^3J_{H-H}$ = 7.60, 1H), 7.64 (H_{py}, d, $^3J_{H-H}$ = 8.38, 1H), 7.35 (H_{py}, d, $^3J_{H-H}$ = 6.85, 1H), 7.35 (BPh_4, m, 8H), 6.92 (BPh_4, t, $^3J_{H-H}$ = 7.28, 8H), 6.78 (BPh_4, t, $^3J_{H-H}$ = 7.18, 4H), 5.85 (H_{cym} aromatic, d, $^3J_{H-H}$ = 6.09, 1H), 5.81 (H_{cym} aromatic, d, $^3J_{H-H}$ = 6.09, 1H), 5.54 (H_{cym} aromatic, t, $^3J_{H-H}$ = 5.25, 2H), 4.57 (octyl N-CH_2, t, $^3J_{H-H}$ = 7.16, 2H), 2.98 (H_{cym} *i*-Pr $C\mathbf{H}(CH_3)_2$, m, 1H), 2.25 (H_{cym} CH_3, s, 3H), 1.39-1.31 (octyl CH_2 & H_{cym} *i*-Pr CH($C\mathbf{H}_3$)$_2$, m, 18H), 0.89 (octyl CH_3, t, $^3J_{H-H}$ = 6.85, 3H). ^{13}C {^1H} NMR (300 MHz, $(CD_3)_2CO$): δ (ppm) = 165.67 (BPh_4), 165.17 (BPh_4), 164.68 (BPh_4), 164.19 (BPh_4), 142.50, 140.75, 136.97, 136.60, 128.16, 127.14, 126.78, 126.11, 122.34, 102.05 (C_{cym} aromatic), 100.18 (C_{cym} aromatic), 85.98 (C_{cym} aromatic), 84.10 (C_{cym} aromatic), 82.43 (C_{cym} aromatic), 81.17 (C_{cym} aromatic), 53.19, 32.44, 31.61, 29.83, 26.95, 23.28, 22.56, 22.33, 18.24, 14.35. Elemental Analysis (%): Calc. For $C_{49}H_{56}BClN_4ORu$ (545.16 g/mol): C, 68.09; H, 6.53; N, 6.48; Found: C, 67.31; H, 6.68; N, 6.18. MS (ESI, *m*/*z*): 545.16 $[M]^+$. Melting Point: 81-85 ˚C (Decomposition: 153-160 ˚C).

Model complex **MC3**: Dark yellow solid, yield 61 %. IR: FT-IR, *υ*/cm^{-1}: 731-702 (BPh_4, B-C). ^1H NMR (400 MHz, $(CD_3)_2CO$): δ (ppm) = 8.88 (H_{qu}, d, $^3J_{H-H}$ = 8.77, 1H), 8.87 (H_{trz}, s, 1H), 8.67 (H_{qu}, d, $^3J_{H-H}$ = 8.56, 1H), 8.17 (H_{qu}, d, $^3J_{H-H}$ = 8.09, 1H), 8.08 (H_{qu}, m, 2H), 7.86 (H_{qu}, t, $^3J_{H-H}$ = 7.62, 1H), 7.36 (BPh_4, m, 8H), 6.92 (BPh_4, t, $^3J_{H-H}$ = 7.46, 8H), 6.77 (BPh_4, t, $^3J_{H-H}$ = 6.94, 4H), 6.12 (H_{cym} aromatic, d, $^3J_{H-H}$ = 6.25, 1H), 6.07 (H_{cym} aromatic, d, $^3J_{H-H}$ = 6.25, 1H), 5.99 (H_{cym} aromatic, d, $^3J_{H-H}$ = 6.25, 1H), 5.94 (H_{cym} aromatic, d, $^3J_{H-H}$ = 6.25, 1H), 4.69 (octyl N-CH_2, t, $^3J_{H-H}$ = 7.20, 2H), 2.52 (H_{cym} *i*-Pr $C\mathbf{H}(CH_3)_2$, m, 1H), 2.21 (H_{cym} CH_3, s, 3H), 2.09 (octyl CH_2, m, 2H), 1.41 & 1.30 (octyl CH_2, m, 10H), 1.00 (H_{cym} *i*-Pr CH($C\mathbf{H}_3$)$_2$, d, $^3J_{H-H}$ = 6.91, 3H), 0.94 (H_{cym} *i*-Pr CH($C\mathbf{H}_3$)$_2$, d, $^3J_{H-H}$ = 6.91, 3H), 0.88 (octyl CH_3, t, $^3J_{H-H}$ = 6.91, 3H). ^{13}C

{^{1}H} NMR (400 MHz, $(CD_3)_2CO$): δ (ppm) = 165.64 (BPh_4), 165.15 (BPh_4), 164.66 (BPh_4), 164.17 (BPh_4), 150.67, 149.14, 148.04, 141.93, 136.94, 133.40, 130.53, 130.10, 129.72, 129.56, 127.43, 126.04, 122.28, 119.34, 105.23 (C_{cym} aromatic), 104.48 (C_{cym} aromatic), 88.24 (C_{cym} aromatic), 85.61 (C_{cym} aromatic), 85.20 (C_{cym} aromatic), 83.42 (C_{cym} aromatic), 53.52, 32.43, 31.71, 30.51, 29.59, 26.95, 23.24, 22.59, 21.60, 18.78, 14.31. Elemental Analysis (%): Calc. For $C_{53}H_{58}BClN_4Ru$ (579.16 g/mol): C, 70.86; H, 6.51; N, 6.24; Found: C, 70.20; H, 6.37; N, 6.00. MS (ESI, *m*/*z*): 579.18 $[M]^+$. Melting Point: 99-106 ˚C (Decomposition: 194-205 ˚C).

Functionalized complex **SC1**: Yellow solid, yield 87 %. IR: FT-IR, *υ*/cm^{-1}: 1071-953 (siloxane, Si-O-Si), 731-702 (BPh_4, B-C). ^{1}H NMR (300 MHz, $(CD_3)_2CO$): δ (ppm) = 9.43 (H_{py}, m, 1H), 8.66 (H_{trz}, s, 1H), 8.12 (H_{py}, m, 1H), 8.01 (H_{py}, m, 1H), 7.61 (H_{py}, m, 1H), 7.36 (BPh_4, m, 8H), 6.92 (BPh_4, t, $^3J_{H\text{-}H}$ = 7.26, 8H), 6.77 (BPh_4, t, $^3J_{H\text{-}H}$ = 7.07, 4H), 6.09 (H_{cym} aromatic, d, $^3J_{H\text{-}H}$ = 6.08, 1H), 6.03 (H_{cym} aromatic, d, $^3J_{H\text{-}H}$ = 6.08, 1H), 5.88 (H_{cym} aromatic, d, $^3J_{H\text{-}H}$ = 6.08, 1H), 5.79 (H_{cym} aromatic, d, $^3J_{H\text{-}H}$ = 6.08, 1H), 4.64 ($NC\mathbf{H}_2CH_2CH_2Si$, t, $^3J_{H\text{-}H}$ = 6.88, 2H), 3.83 ($CH_2CH_2Si(OC\mathbf{H}_2CH_3)_3$, q, 6H), 2.77 ($H_{cym}$ *i*-Pr $C\mathbf{H}(CH_3)_2$, m, 1H), 2.21 (H_{cym} CH_3, s, 3H), 2.14 ($NCH_2C\mathbf{H}_2CH_2Si$, m, 2H), 1.22-1.09 ($CH_2CH_2Si(OCH_2C\mathbf{H}_3)_3$ & H_{cym} *i*-Pr $CH(C\mathbf{H}_3)_2$, m, 15H), 0.64 ($NCH_2CH_2C\mathbf{H}_2Si$, m, 2H). ^{13}C {^{1}H} NMR (400 MHz, $(CD_3)_2CO$): δ (ppm) = 165.76 (BPh_4), 165.28 (BPh_4), 164.79 (BPh_4), 164.30 (BPh_4), 156.33, 149.47, 147.22, 140.99, 137.08 (BPh_4), 126.90, 126.17 (BPh_4), 125.95, 123.27, 122.40 (BPh_4), 105.77 (C_{cym} aromatic), 103.16 (C_{cym} aromatic), 86.97 (C_{cym} aromatic), 85.51 (C_{cym} aromatic), 84.95 (C_{cym} aromatic), 84.36 (C_{cym} aromatic), 59.12, 55.61, 31.88, 24.95, 22.73, 21.88, 18.81, 8.00. Elemental Analysis (%): Calc. For $C_{50}H_{60}BClN_4O_3RuSi{\cdot}0.5CH_2Cl_2$ (621.23 g/mol): C, 61.71; H, 6.25; N, 5.70; Found: C, 61.83; H, 5.995; N, 5.825. MS (ESI, *m*/*z*): 621.16 $[M]^+$. Melting Point: 78-85 ˚C.

Functionalized complex **SC2**: Dark yellow solid, yield 75 %. IR: FT-IR, *υ*/cm^{-1}: 1263 (pyridine, N-O), 1070-953 (siloxane, Si-O-Si), 731.39-702.37 (BPh_4, B-C). ^{1}H NMR (600 MHz, $(CD_3)_2CO$): δ (ppm) = 8.54 (H_{py}, d, $^3J_{H\text{-}H}$ = 6.49, 1H), 8.33 (H_{trz}, s, 1H), 7.84 (H_{py}, t, $^3J_{H\text{-}H}$ = 7.80, 1H), 7.59 (H_{py}, d, $^3J_{H\text{-}H}$ = 7.80, 1H), 7.54 (H_{py}, t, $^3J_{H\text{-}H}$ = 6.82, 1H), 7.36 (BPh_4, s, 8H), 6.93 (BPh_4, t, $^3J_{H\text{-}H}$ = 7.33, 8H), 6.78 (BPh_4, t, $^3J_{H\text{-}H}$ = 7.25, 4H), 5.83 (H_{cym} aromatic, d, $^3J_{H\text{-}H}$ = 6.14, 1H), 5.79 (H_{cym} aromatic, d, $^3J_{H\text{-}H}$ = 6.09, 1H), 5.52 (H_{cym} aromatic, d, $^3J_{H\text{-}H}$ = 6.04, 2H), 4.53 ($NC\mathbf{H}_2CH_2CH_2Si$, t, $^3J_{H\text{-}H}$ = 7.25, 2H), 3.85 ($CH_2CH_2Si(OC\mathbf{H}_2CH_3)_3$, q, 6H), 2.98 ($H_{cym}$ *i*-Pr $C\mathbf{H}(CH_3)_2$, m, 1H), 2.24 (H_{cym} CH_3, s, 3H), 2.14 ($NCH_2C\mathbf{H}_2CH_2Si$, p, 2H), 1.31 (H_{cym} *i*-Pr $CH(C\mathbf{H}_3)_2$, d, $^3J_{H\text{-}H}$ = 7.10, 6H), 1.21 ($CH_2CH_2Si(OCH_2C\mathbf{H}_3)_3$, t, $^3J_{H\text{-}H}$ = 6.92, 9H), 0.69

($NCH_2CH_2C\mathbf{H}_2Si$, m, 2H). ^{13}C {^1H} NMR (300 MHz, $(CD_3)_2CO$): δ (ppm) = 206.12, 165.53 (BPh_4), 165.21 (BPh_4), 164.88 (BPh_4), 164.55 (BPh_4), 142.53, 140.81, 137.05, 136.62, 128.29, 127.17, 126.85, 126.18, 122.41, 100.25 (C_{cym} aromatic), 85.95 (C_{cym} aromatic), 84.15 (C_{cym} aromatic), 82.55 (C_{cym} aromatic), 81.27 (C_{cym} aromatic), 59.13, 55.39, 31.69, 24.67, 22.64, 22.44, 18.80, 18.33, 8.17. Elemental Analysis (%): Calc. For $C_{50}H_{60}BClN_4O_4RuSi{\cdot}0.25CH_2Cl_2$ (637.23): C, 61.73; H, 6.24; N, 5.73; Found: C, 61.56; H, 5.90; N, 5.60. MS (ESI, *m*/*z*): 637.16 $[M]^+$. Melting Point: 85-90 ˚C (Decomposition: 161-168 ˚C).

Functionalized complex **SC3**: Yellow solid, yield 85 %. IR: FT-IR, υ/cm^{-1}: 1605 (pyridine, C=N), 1579 (pyridine, C=C), 1064-954 (siloxane, Si-O-Si), 731-702 (BPh_4, B-C). ^1H NMR (300 MHz, $(CD_3)_2CO$): δ (ppm) = 8.90 (H_{trz}, s, 1H), 8.89 (H_{qu}, d, $^3J_{H\text{-}H}$ = 8.46, 1H), 8.69 (H_{qu}, d, $^3J_{H\text{-}H}$ = 8.46, 1H), 8.17 (H_{qu}, d, $^3J_{H\text{-}H}$ = 8.24, 1H), 8.09 (H_{qu}, m, 2H), 7.87 (H_{qu}, t, $^3J_{H\text{-}H}$ = 7.45, 1H), 7.36 (BPh_4, m, 8H), 6.92 (BPh_4, t, $^3J_{H\text{-}H}$ = 7.22, 8H), 6.77 (BPh_4, t, $^3J_{H\text{-}H}$ = 7.22, 4H), 6.11 (H_{cym} aromatic, d, $^3J_{H\text{-}H}$ = 5.98, 1H), 6.07 (H_{cym} aromatic, d, $^3J_{H\text{-}H}$ = 5.98, 1H), 6.00 (H_{cym} aromatic, d, $^3J_{H\text{-}H}$ = 5.98, 1H), 5.94 (H_{cym} aromatic, d, $^3J_{H\text{-}H}$ = 5.98, 1H), 4.70 ($NC\mathbf{H}_2CH_2CH_2Si$, t, $^3J_{H\text{-}H}$ = 7.16, 2H), 3.85 ($CH_2CH_2Si(OC\mathbf{H}_2CH_3)_3$, q, 6H), 2.53 ($H_{cym}$ *i*-Pr $C\mathbf{H}(CH_3)_2$, m, 1H), 2.21 (H_{cym} CH_3, s, 3H), 2.18 ($NCH_2C\mathbf{H}_2CH_2Si$, m, 2H), 1.21 ($CH_2CH_2Si(OCH_2C\mathbf{H}_3)_3$, t, $^3J_{H\text{-}H}$ = 7.00, 9H), 1.01 (H_{cym} *i*-Pr $CH(C\mathbf{H}_3)_2$, d, $^3J_{H\text{-}H}$ = 7.22, 3H), 0.95 (H_{cym} *i*-Pr $CH(C\mathbf{H}_3)_2$, d, $^3J_{H\text{-}H}$ = 7.00, 3H), 0.70 ($NCH_2CH_2C\mathbf{H}_2Si$, m, 2H). ^{13}C {^1H} NMR (400 MHz, $(CD_3)_2CO$): δ (ppm) = 165.60 (BPh_4), 165.10 (BPh_4), 164.61 (BPh_4), 164.12 (BPh_4), 150.63, 149.09, 147.98, 141.86, 136.91, 133.34, 130.49, 130.04, 129.67, 129.51, 127.47, 125.98, 122.21, 119.29, 105.25 (C_{cym} aromatic), 104.35 (C_{cym} aromatic), 88.14 (C_{cym} aromatic), 85.60 (C_{cym} aromatic), 85.09 (C_{cym} aromatic), 83.48 (C_{cym} aromatic), 58.97, 55.59, 31.67, 24.71, 22.59, 21.50, 18.72, 18.63, 7.89. Elemental Analysis (%): Calc. For $C_{54}H_{62}BClN_4O_3RuSi{\cdot}0.25CH_2Cl_2$ (671.18 g/mol): C, 64.40; H, 6.23; N, 5.54; Found: C, 64.76; H, 6.13; N, 5.28. MS (ESI, *m*/*z*): 671.18 $[M]^+$. Melting Point: 148-156 ˚C (Decomposition: 218-224 ˚C).

2.5 References

1 A. Habtemariam, M. Melchart, R. Fernández, S. Parsons, I. D. H. Oswald, A. Parkin, F. P. A. Fabbiani, J. E. Davidson, A. Dawson, R. E. Aird, D. I. Jodrell and P. J. Sadler, *J. Med. Chem.*, 2006, **49**, 6858–6868.

2 A. Bolje, S. Hohloch, D. Urankar, A. Pevec, M. Gazvoda, B. Sarkar and J. Košmrlj, *Organometallics*, 2014, **33**, 2588–2598.

3 L. Bernet, R. Lalrempuia, W. Ghattas, H. Mueller-Bunz, L. Vigara, A. Llobet and M. Albrecht, *Chem. Commun. (Camb).*, 2011, **47**, 8058–8060.

4 D. Huang, P. Zhao and D. Astruc, *Coord. Chem. Rev.*, 2014, **272**, 145–165.

5 H. Kotze, Immobilized Ru(II) Catalysts for Transfer Hydrogenation and Oxidative Alkene Cleavage Reactions, Stellenbosch University, 2015.

6 K. Bürglová, N. Moitra, J. Hodačová, X. Cattoën and M. Wong Chi Man, *J. Org. Chem.*, 2011, **76**, 7326–7333.

7 N. Moitra, J. J. E. Moreau, X. Cattoën and M. Wong Chi Man, *Chem. Commun. (Camb).*, 2010, **46**, 8416–8418.

8 Z. Yu, L. S. Tan and E. Fossuma, *Arkivoc*, 2009, **2009**, 255–265.

9 M. H. Ngai, P.-Y. Yang, K. Liu, Y. Shen, M. R. Wenk, S. Q. Yao and M. J. Lear, *Chem. Commun.*, 2010, **46**, 8335–8337.

10 K. K. K. Ho, R. Chen, M. D. P. Willcox, S. A. Rice, N. Cole, G. Iskander and N. Kumar, *Biomaterials*, 2014, **35**, 2336–2345.

11 R. G. Kultyshev, Y. Kawanishi, M. Nishioka and A. Miyazawa, *Synth. Commun.*, 2014, **44**, 556–563.

12 A. Bolje and J. Kosmrlj, *Org. Lett.*, 2013, **15**, 5084–5087.

13 M. Son, J. Young, E. Jeong, D. Baek, K. Choi, J. Kyun, A. Nim, S. Min and Y. Seo, *Bioorg. Med. Chem. Lett.*, 2013, **23**, 1472–1476.

14 P. Pta, A. M. M. Meij, S. Otto and A. Roodt, *Inorg. Chim. Acta*, 2006, **358**, 1005–1011.

15 S. Kida, J. V Quagliano, J. A. Walmsley and S. Y. Tyree, *Spectrochim. Acta*, 1963, **19**, 189-199.

16 J. Tönnemann, J. Risse, Z. Grote, R. Scopelliti and K. Severin, *Eur. J. Inorg. Chem.*, 2013, 4558–4562.

Chapter 3: Immobilization of functionalized Ru arene triazole complexes on MCM-41 and SBA-15

3.1 Introduction

Mesoporous silicate materials have been found to be very useful in various applications since their discovery in the 1990's. These materials have been employed for applications in membrane separation, adsorption of gases and liquids, electronics/optics, heterogeneous catalysis and drug delivery systems.[1–3] Wide-spread application of these materials is made possible due to the mesoporous nature of the silicate materials, which contain cylindrical pores in an ordered hexagonal array, with pore sizes between 20-500 Å in conjunction with large surface areas. These mesoporous silica have the added advantage of ease of synthesis and good stability under harsh conditions.[1] The general synthesis of templated mesoporous silicate materials involves the addition of a silica source to a solution of the template molecules at the necessary pH and temperature. The synthesis of these materials has been widely studied along with solid state characterization techniques which can be used to verify the synthesis of different mesoporous silica.[4]

The application of mesoporous silicate materials, such as MCM-41 and SBA-15, as catalyst supports is most relevant to this project. These materials have been successful in reactions such as oxidations, hydroxylations, polymerizations and acid catalyzed reactions.[1] The potential for functionalization of these supports is the reason they can be transformed into heterogeneous catalysts. Various methods for the synthesis of the heterogeneous catalysts based on mesoporous materials exist and many of these catalytic reactions are successful due to the intrinsic features and properties of the support employed.[5]

Tuel *et al.* post-synthetic modification to obtain a Ti-doped mesoporous material. This material is capable of catalytic oxidations in the presence of aqueous hydrogen peroxide or anhydrous TBHP.[6]

Another example of such a mesoporous material was shown by Xu *et al.* who used a surface sol–gel process to dope amorphous silica with Ti. This material was then used as a support for gold which was then used as a catalyst for the oxidation of cyclohexane (8.4% conversion). The catalyst selectively transformed the cyclohexane to cyclohexanone and cyclohexanol at 150 °C, 1.5 MPa and with oxygen as the terminal oxidant. The catalyst could be recycled up to four times with no significant change in the activity and selectivity in the oxidation reaction.[7]

The immobilization and coordination of a $RuCl_2(PPh_3)_3$ complex onto amine functionalized SBA-15 was demonstrated by Wan *et al.* The authors used various solid state analytical techniques to confirm the presence of the amine functionality and Ru complex on the support. The heterogenized homogeneous catalyst was applied in a homoallylic alcohol isomerization reaction, exhibiting similar activity to its homogeneous counterpart. However the heterogenized catalyst could be recycled for several runs without a drop in the activity.[8] Bleloch *et al.* showed that perruthenate could be immobilized onto MCM-41 and applied as a heterogeneous catalyst for the oxidation of alcohols to carbonyl derivatives using molecular oxygen as the terminal oxidant. The catalyst was synthesized using a tethering method followed by ion exchange with potassium perruthenate. The heterogeneous catalyst was found to be recyclable and highly active.[9]

The synthesis and characterization of the native silica, MCM-41 and SBA-15, as well as the synthesis and characterization of the ‘heterogenized’ catalysts based on the Ru arene triazole complexes discussed in Chapter 2 are reported in the sections to follow.

The native MCM-41 and SBA-15 supports as well as the immobilized and adsorbed catalysts are characterized using a range of solid state analytical techniques to verify the synthesis of the native silica as well as to ensure the structural integrity of the supports after immobilization/adsorption of the ruthenium complexes. The characterization techniques include infrared spectroscopy, nitrogen adsorption/desorption (BET) surface analysis, low-angle powder X-ray diffraction, transmission electron microscopy (TEM), scanning electron microscopy (SEM), thermal gravimetric analysis (TGA) and ICP-OES.

3.2 Results and discussion

3.2.1 Synthesis and characterization of mesoporous silica, MCM-41 and SBA-15

The native silica materials MCM-41[10] and SBA-15[11] were synthesized according to adapted literature procedures. MCM-41 was synthesized using cetyltrimethylammonium bromide (CTAB) as surfactant and tetraethyl orthosilicate (TEOS) as the silica source under basic conditions (pH = 12). In the case of SBA-15, TEOS was again employed as the source of silica and the surfactant was changed to poly(ethyleneglycol)-blockpoly(propyleneglycol)-block-poly(ethyleneglycol) (PEG-PPG copolymer) allowing SBA-15 to be synthesized under acidic conditions. After filtering, washing with water and drying under vacuum the native silica materials were both isolated as white powders. Both silica were calcined at 550 ˚C to remove templating agents.

The native MCM-41 and SBA-15 powders were characterized by infrared spectroscopy, nitrogen adsorption/desorption (BET) surface analysis, low-angle powder X-ray diffraction, transmission electron microscopy (TEM), scanning electron microscopy (SEM) and thermal gravimetric analysis (TGA).

3.2.1.1. Characterization of MCM-41 and SBA-15 native silica by means of FT-IR spectroscopy (ATR)

The successful synthesis of the native silicate materials, MCM-41 and SBA-15, was confirmed by means of FT-IR spectroscopy. In both cases the spectra obtained, exhibited characteristic absorption bands for these types of materials and the spectra correlate well with those reported in the literature. In Figure 3.1 the bands around 3383/3411 and 1628.50/1634.83 cm^{-1} can be assigned to water -OH stretching and water -OH bending respectively.[12] Furthermore the bands near 1058/1055 cm^{-1}, 970/965 cm^{-1} and 802/800 cm^{-1} can be assigned to Si-O, Si-OH and the O-Si-O stretching vibration respectively.[12] The only significant difference between the IR spectra of the two native materials is the Si-O-Si asymmetric stretching at 1245 cm^{-1} observed for MCM-41, whereas for SBA-15 only a shoulder can be observed in the same region.[13]

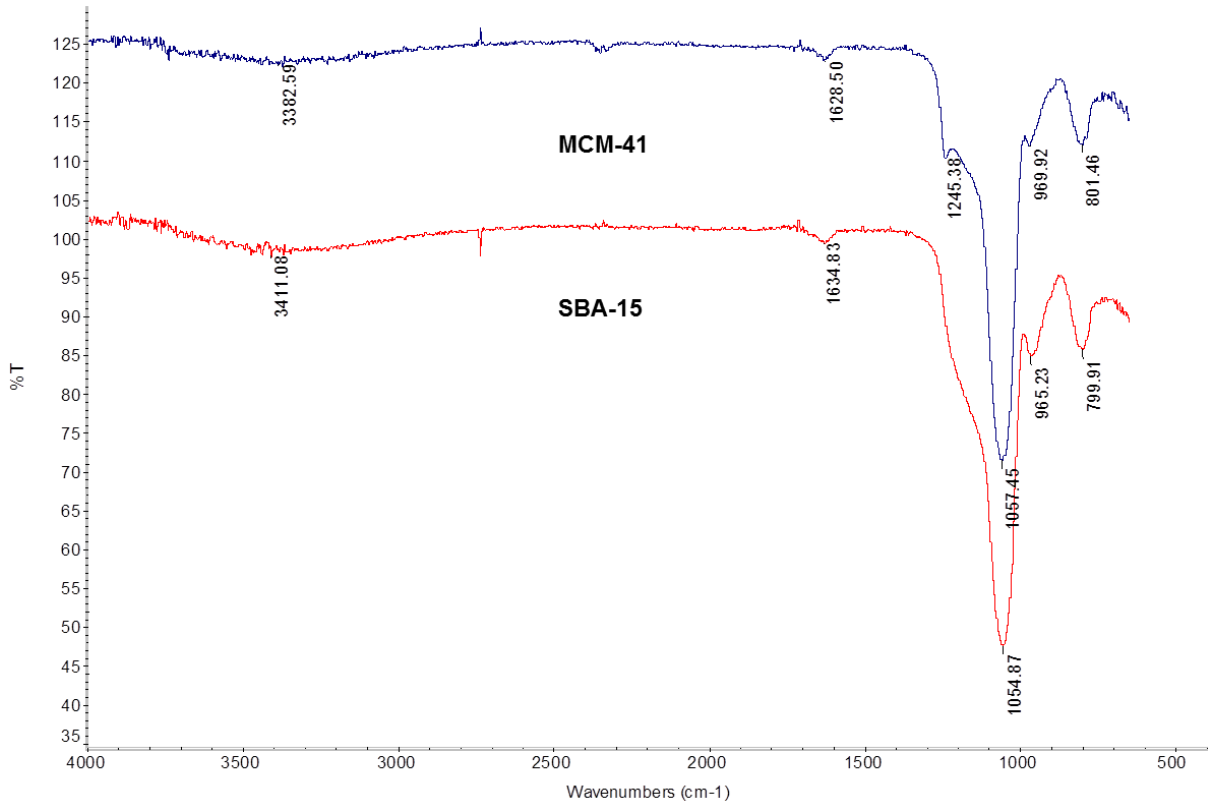

Figure 3.1: FT-IR spectra of native MCM-41 (blue) and SBA-15 (red).

3.2.1.2. Characterization of MCM-41 and SBA-15 by means of BET (Brunauer Emmett Teller) surface analysis

The surface area (m^2/g), average pore diameter (Å) and total pore volume (cm^3/g) of the native silica supports were determined by means of BET (Brunauer Emmett Teller) surface analysis. To ensure that the samples were completely dry and solvent free, they were degassed in the range of 150-230 °C for 18 hours before the analysis. BET analysis can give rise to five different types of nitrogen adsorption isotherms which are classified by the adsorption profile they exhibit. The various types of isotherm profiles (type I-V) observed are characteristic of different materials and the micro/meso-porous structures they contain.[14]

Type IV isotherm plots were obtained for both MCM-41 and SBA-15, depicted in Figure 3.2, where the volume of nitrogen adsorbed was plotted against the relative pressure (0 to 1, P/Po). A pronounced H1 hysteresis loop can be observed for SBA-15 but not for MCM-41. The presence of the H1 hysteresis loop is characteristic for materials with large pores of constant cross-section (cylindrical or hexagonal).[15]

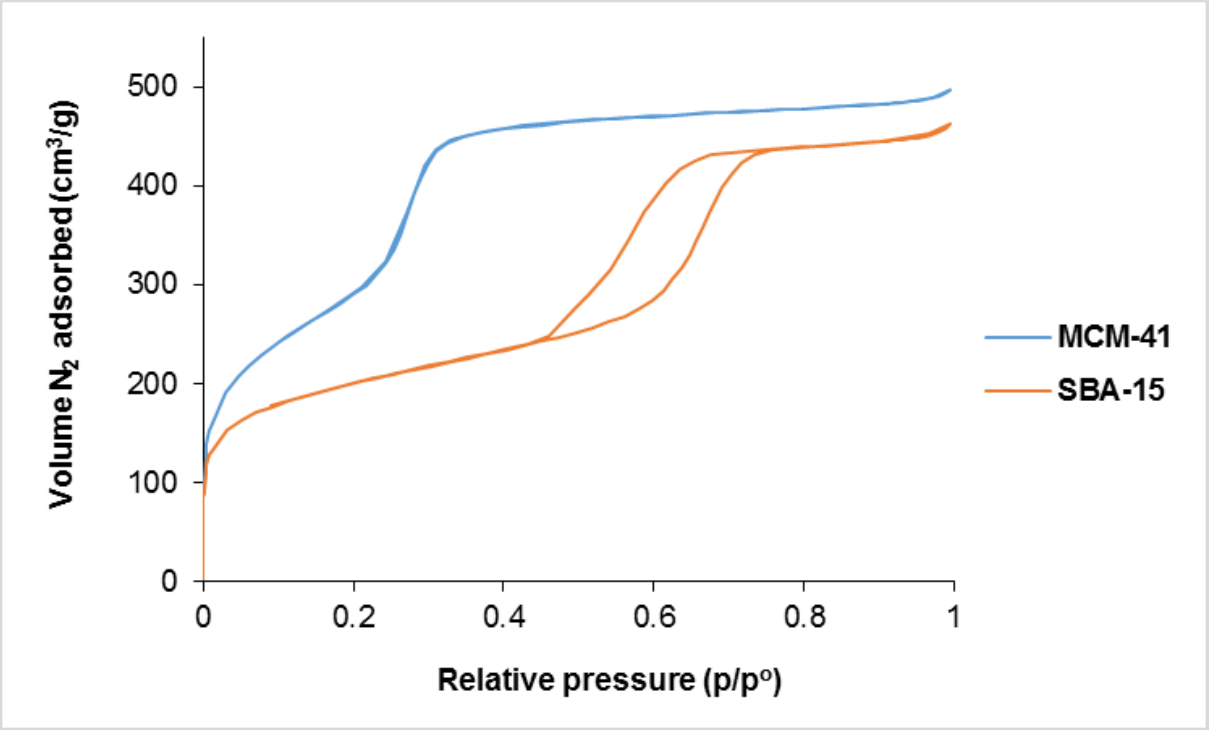

Figure 3.2: BET isotherm plots for native MCM-41 and SBA-15.

The absence of the hysteresis loop in the isotherm obtained for MCM-41 can be explained by the size of the mesopores of the native support. Literature has shown that the nitrogen adsorption hysteresis loop mainly appears at temperatures below 70 K or in materials where the average pore diameter is greater than 40 Å.[16,17] The BET analysis for our native silica was conducted at 77 K. The absence of the hysteresis loop for MCM-41 would therefore have to be due to the material having a pore diameter of less than 40 Å. This is exactly what was observed for our results, where MCM-41 has an average pore diameter of 29 Å compared to SBA-15 with a larger average pore diameter of 41 Å.

In Figure 3.2 it can be observed that a slightly higher volume of nitrogen gas was adsorbed onto the surface of MCM-41 (497 cm^3/g) compared to that of SBA-15 (463 cm^3/g). This meant that MCM-41 has a larger surface area than SBA-15 and due to the fact that wall thickness is inversely proportional to surface area it can be concluded that SBA-15 has thicker silica walls.[18] It was also observed that the pores of MCM-41 are filled over a slightly smaller range than SBA-15. The pore-filling steps occur at P/Po 0.24-0.33 and 0.56-0.69 relative pressures for MCM-41 and SBA-15 respectively. This therefore indicates that MCM-41 has a narrower pore size distribution compared to SBA-15.

Table 3.1: Summary of BET surface area, average pore diameter and total pore volume of native MCM-41 and SBA-15

Material	BET Surface Area (m^2/g)	Average Pore Diameter (Å)	Total Pore Volume (cm^3/g)
MCM-41	1 079.11	28.56	0.77
SBA-15	708.52	40.52	0.72

The surface area, average pore diameter and total pore volume for MCM-41 and SBA-15 calculated from BET analysis are summarized above in Table 3.1. The results correspond well with that in the literature.[19,7] It was observed that MCM-41 has a higher surface area than SBA-15 (difference ~370 m^2/g), whereas with regards to average pore diameter SBA-15 has larger pores than MCM-41 (difference ~12 Å). A negligible difference in the total pore volumes was observed for MCM-41 and SBA-15 (difference ~0.05 cm^3/g).

3.2.1.3. Characterization of native MCM-41 and SBA-15 by means of powder XRD

Typical powder X-ray diffraction (PXRD) patterns were obtained for the mesoporous silica materials MCM-41 and SBA-15.[15,20] In Figure 3.3 four well resolved peaks can be identified, for both native silica, which is indicative of a well-ordered mesostructure. These peaks are associated with a 2-D hexagonal symmetry and can be indexed as (100), (110), (200) and (210) diffractions.

From Figure 3.3 an intense reflection peak can be observed for MCM-41 at 2θ = 2.10 ˚ corresponding to the (100) reflection planes. Three additional peaks corresponding to the (110), (200) and (210) reflection planes can also be observed at 2θ = 3.72 ˚, 4.35 ˚ and 5.83 ˚ respectively. The presence of this fourth reflection peak (210) indicates that the material is of good quality.[21] Figure 3.3 also shows the intense (100) reflection planes at 2θ = 2.10 ˚ for SBA-15, with less intense peaks at 2θ = 3.72 ˚, 4.35 ˚ and 5.83 ˚ corresponding to the (110), (200) and (210) reflection planes respectively.

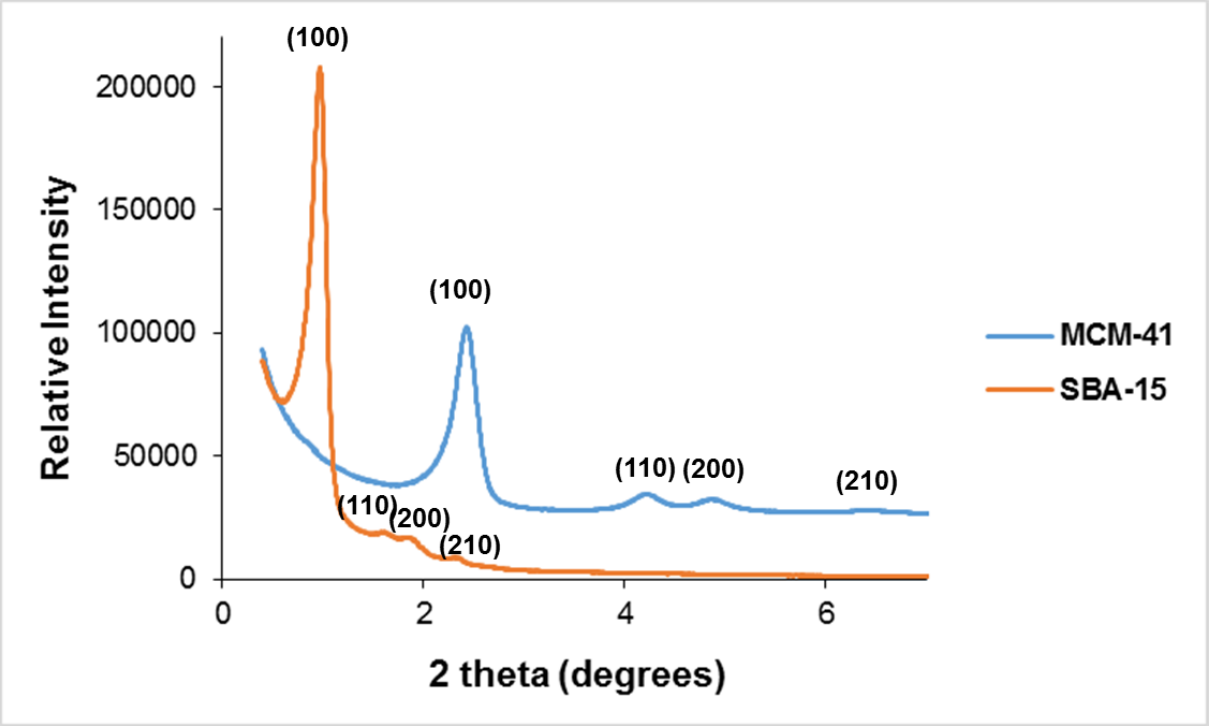

Figure 3.3: Powder XRD plot of MCM-41 (blue) and SBA-15 (orange).

The results are in good agreement with reported 2-D hexagonal ordered structures for these types of mesoporous materials which are summarized in Table 3.2 below.[22]

Table 3.2: Powder XRD diffractions of MCM-41 and SBA-15[a]

Material	(100)	(110)	(200)	(210)
MCM-41	2.48	4.34	5.02	6.42
SBA-15	0.99	1.65	1.94	2.39

[a] Angles given as 2 theta degrees.

3.2.1.4. Characterization of MCM-41 and SBA-15 by means of transmission electron microscopy (TEM) and scanning electron microscopy (SEM)

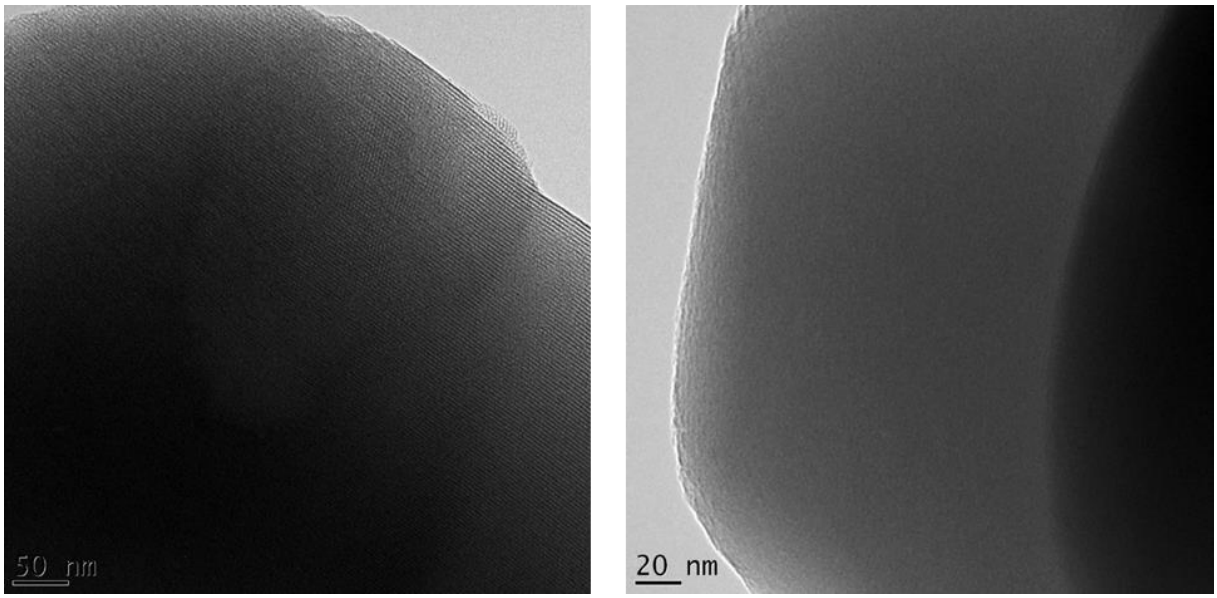

Figure 3.4: Transmission electron micrographs (TEM) of native MCM-41.

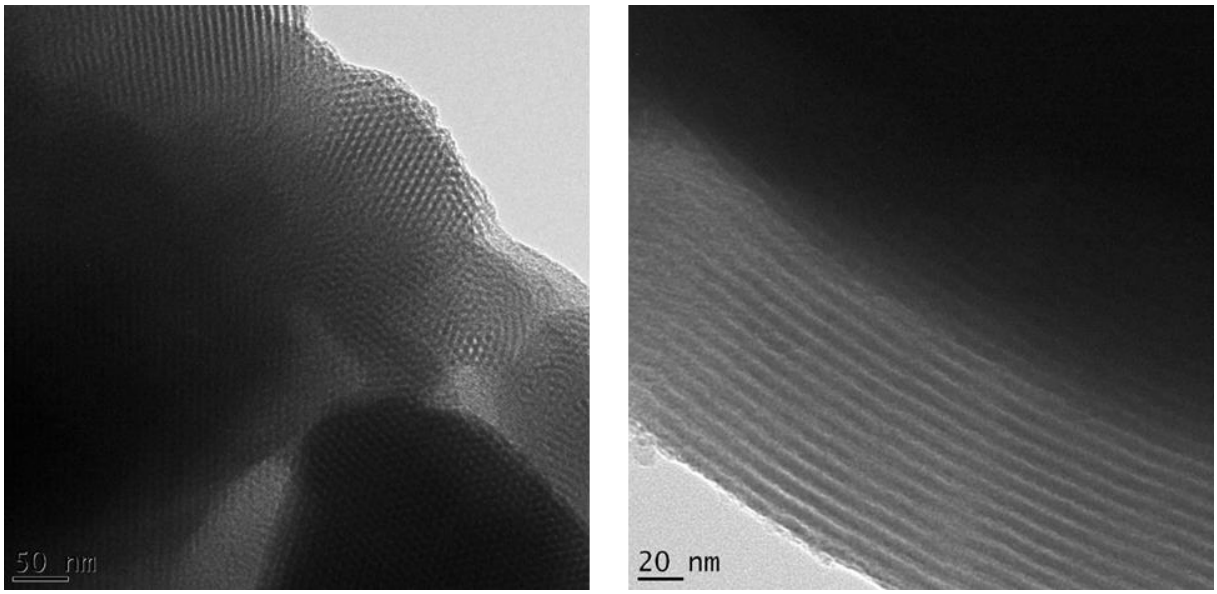

Figure 3.5: Transmission electron micrographs (TEM) of native SBA-15.

The TEM micrographs of the native MCM-41 and SBA-15 silica are shown above in Figure 3.4 and Figure 3.5 respectively. It can be observed that the supports exhibit regular arrays of mesoporous channels packed in a hexagonal arrangement.[4,5]

The morphology of the native silica was determined using scanning electron microscopy (SEM). The micrographs show clear hexagonal structures and the morphologies obtained are characteristic of MCM-41 and SBA-15 (Figure 3.6 and Figure 3.7).[15,20,4]

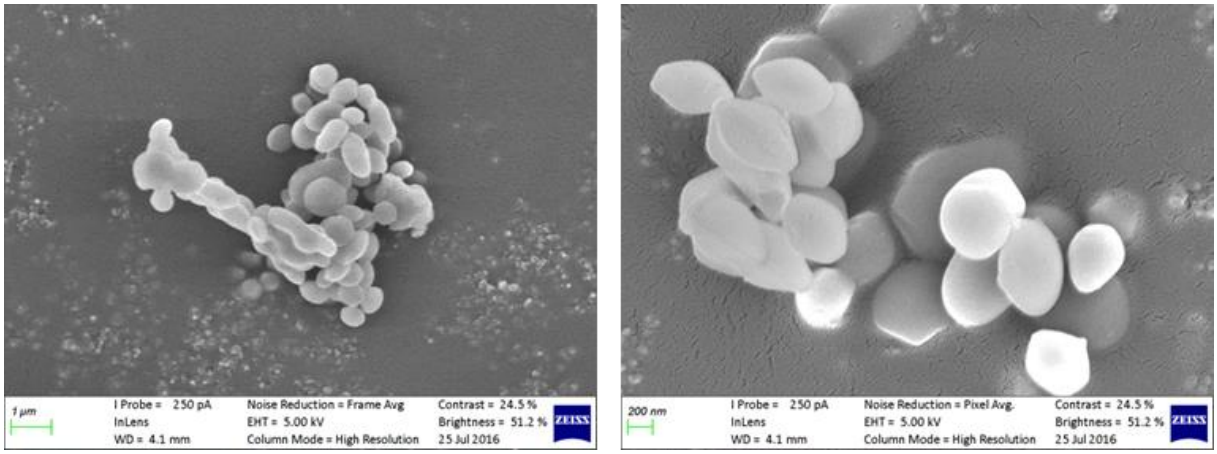

Figure 3.6: Scanning electron microscopy (SEM) micrographs of native MCM-41.

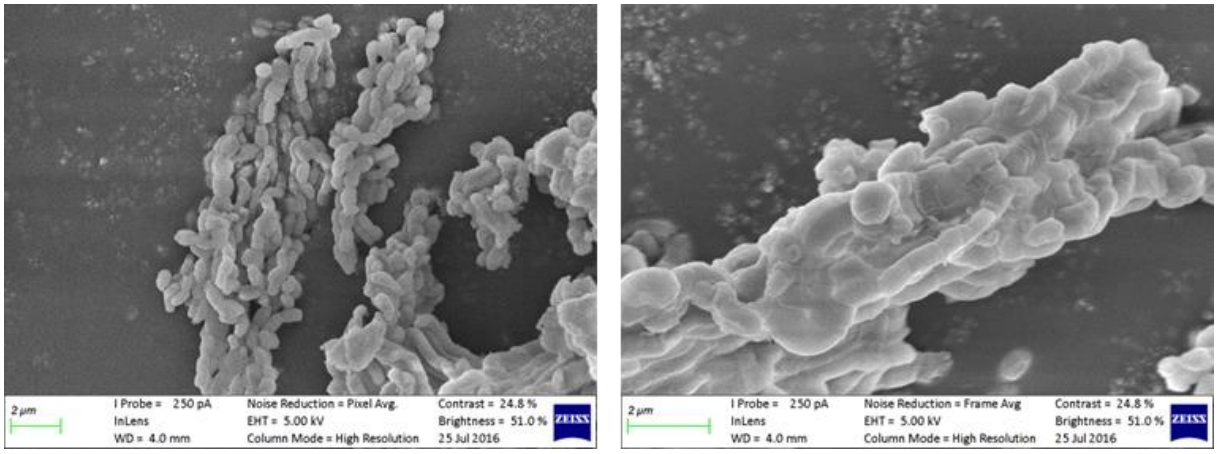

Figure 3.7: Scanning electron microscopy (SEM) micrographs of native SBA-15.

It can be observed that MCM-41 shows discrete, smaller particles compared to SBA-15 which are arranged in chain-like structures with larger particles. The different appearance of such mesoporous silica as well as the difference in particle size is due to the use of different templating agents and pH during synthesis of the materials.[4]

3.2.1.5. Characterization of MCM-41 and SBA-15 by means of thermal gravimetric analysis (TGA)

Thermal gravimetric analysis (TGA) provides useful information regarding the thermal stability of silicate materials. For both MCM-41 and SBA-15 the loss of water adsorbed onto the surface of the materials can be observed just below 100 °C (Figure 3.8 and Figure 3.9). The weight loss of water is considerably more significant for SBA-15 (9 % loss) compared to MCM-41 (2 % loss). Only a slight drop in the weight of the silica (1-4 %) can be observed between 100 and 600 °C due to small amounts of unreacted TEOS or templating agent that was not effectively removed during calcination. From the TGA analysis it can therefore be concluded that the native silica are suitable for use as catalyst supports due to their good thermal stabilities at high temperatures.[22]

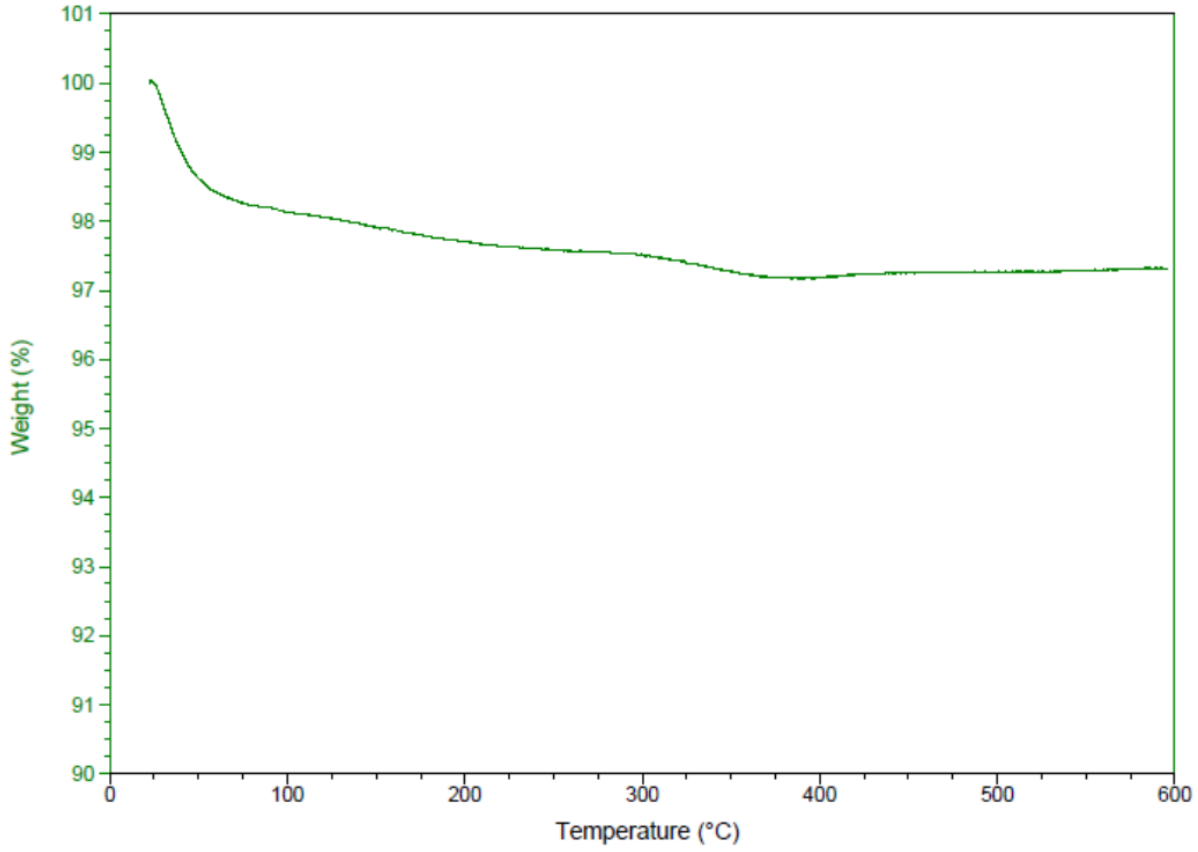

Figure 3.8: TGA analysis of native MCM-41.

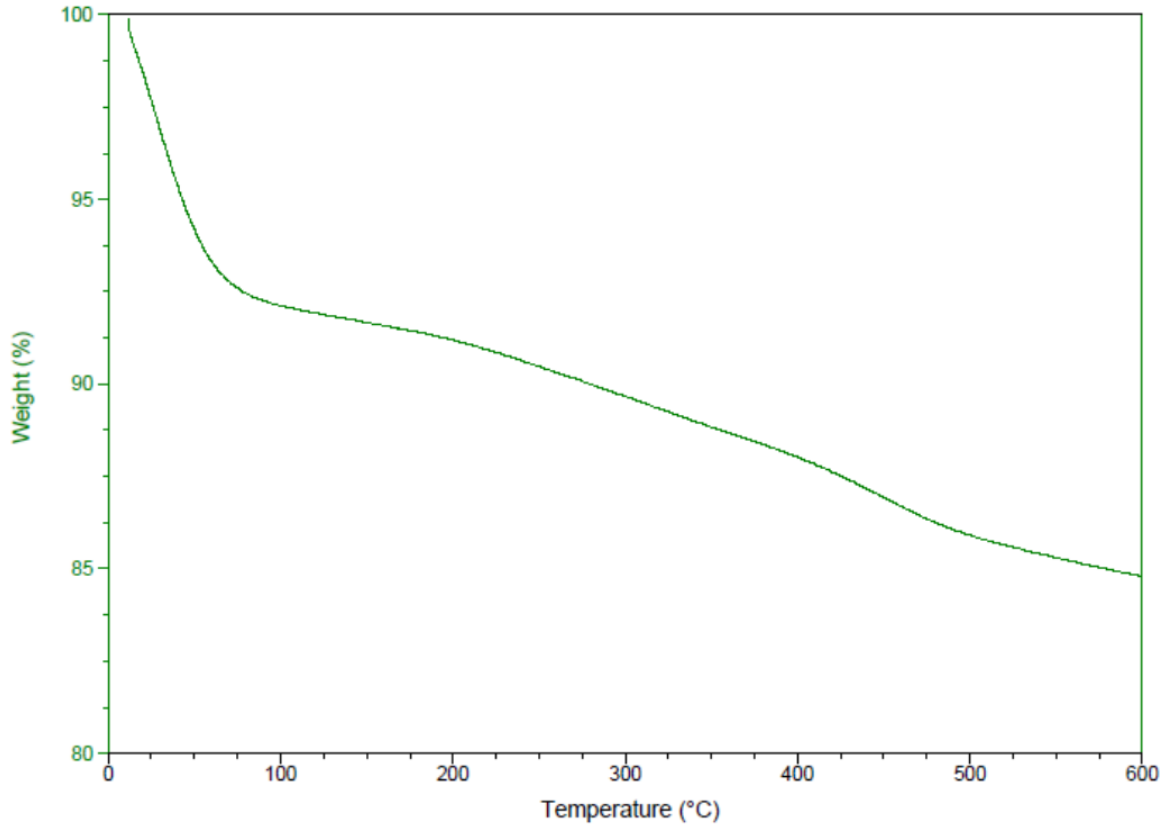

Figure 3.9: TGA analysis of native SBA-15.

3.2.2 Synthesis and characterization of heterogeneous ruthenium catalysts

The synthesis of the immobilized catalysts **IC1-IC6** is depicted in Scheme 3.1. The siloxane functionality of the complexes **SC1-SC3** was reacted with the surface silanols of MCM-41 and SBA-15, thereby effecting their covalent immobilization onto the silica supports. The functionalized complex was dissolved in THF (2 ml) and then added to a slurry of the silica (MCM-41 or SBA-15) in toluene (8 ml). A 1:10 (w/w) ratio of complex to silica support was employed for the reactions. The reaction mixture was refluxed for 24 hours at 110 °C, at which point the slurry was filtered and the powders dried *in vacuo*. For all the immobilizations a significant colour change from the native white silica could be observed. The immobilized complexes were obtained as light yellow to brown powders.

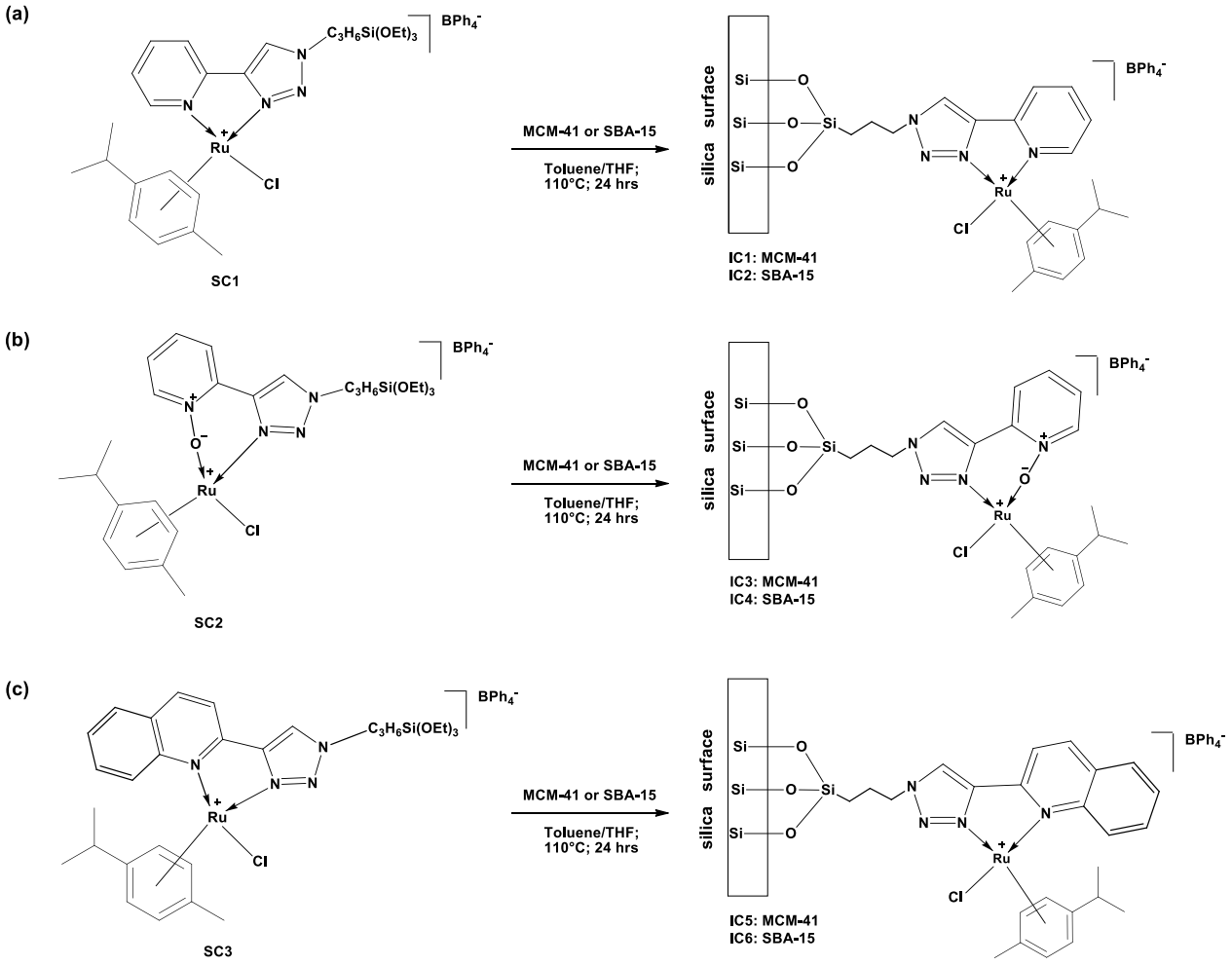

Scheme 3.1: Immobilization of complexes SC1-SC3 on MCM-41 and SBA-15 to generate catalysts IC1-IC6.

The preparation of the immobilized catalysts **IC1-IC6** is depicted below in Scheme 3.2. The siloxane functionality of the complexes **SC1-SC3** was reacted with the surface silanols of MCM-41 and SBA-15, thereby effecting their covalent immobilization onto the silica supports. The functionalized complex was dissolved in THF (2 ml) and then added to a slurry of the silica (MCM-41 or SBA-15) in toluene (8 ml). A 1:10 (w/w) ratio of complex to silica support was employed for the reactions. The reaction mixture was refluxed for 24 hours at 110 °C, at which point the slurry was filtered and the powder dried *in vacuo*. For all the immobilizations a significant colour change from the native white silica could be observed. The immobilized complexes were obtained as light yellow to brown powders.

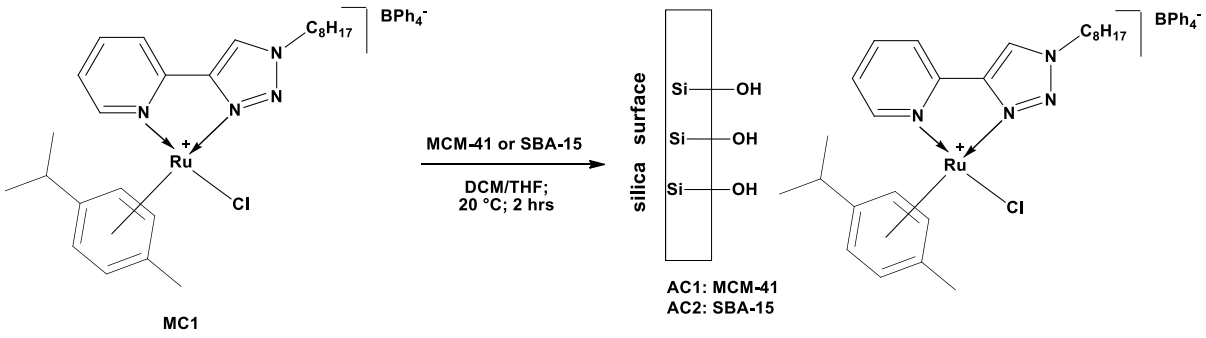

Scheme 3.2: Adsorption of complex MC1 on MCM-41 and SBA-15 to generate catalysts AC1 and AC2.

The immobilized and adsorbed MCM-41 and SBA-15 catalysts were characterized by infrared spectroscopy, nitrogen adsorption/desorption (BET) surface analysis, low-angle powder X-ray diffraction, transmission electron microscopy (TEM), scanning electron microscopy (SEM), thermal gravimetric analysis (TGA) and ICP-OES.

3.2.2.1. Characterization of immobilized catalysts IC1-IC6 and adsorbed catalysts AC1 and AC2 by means of FT-IR spectroscopy (ATR)

The FT-IR spectra of the immobilized and adsorbed MCM-41 and SBA-15 catalysts are shown in Figure 3.10 and Figure 3.11 respectively. No definite change in the spectra can be observed for both the MCM-41 and SBA-15 derivatives when comparing the immobilized and adsorbed catalysts to the native support materials. The signals corresponding to the immobilized or adsorbed organometallic complex cannot be observed in the IR spectra due to the low ratio of immobilization of the complex (1:10 w/w, complex:silica). We therefore observe the spectra being dominated by the intense bands of the silica support.

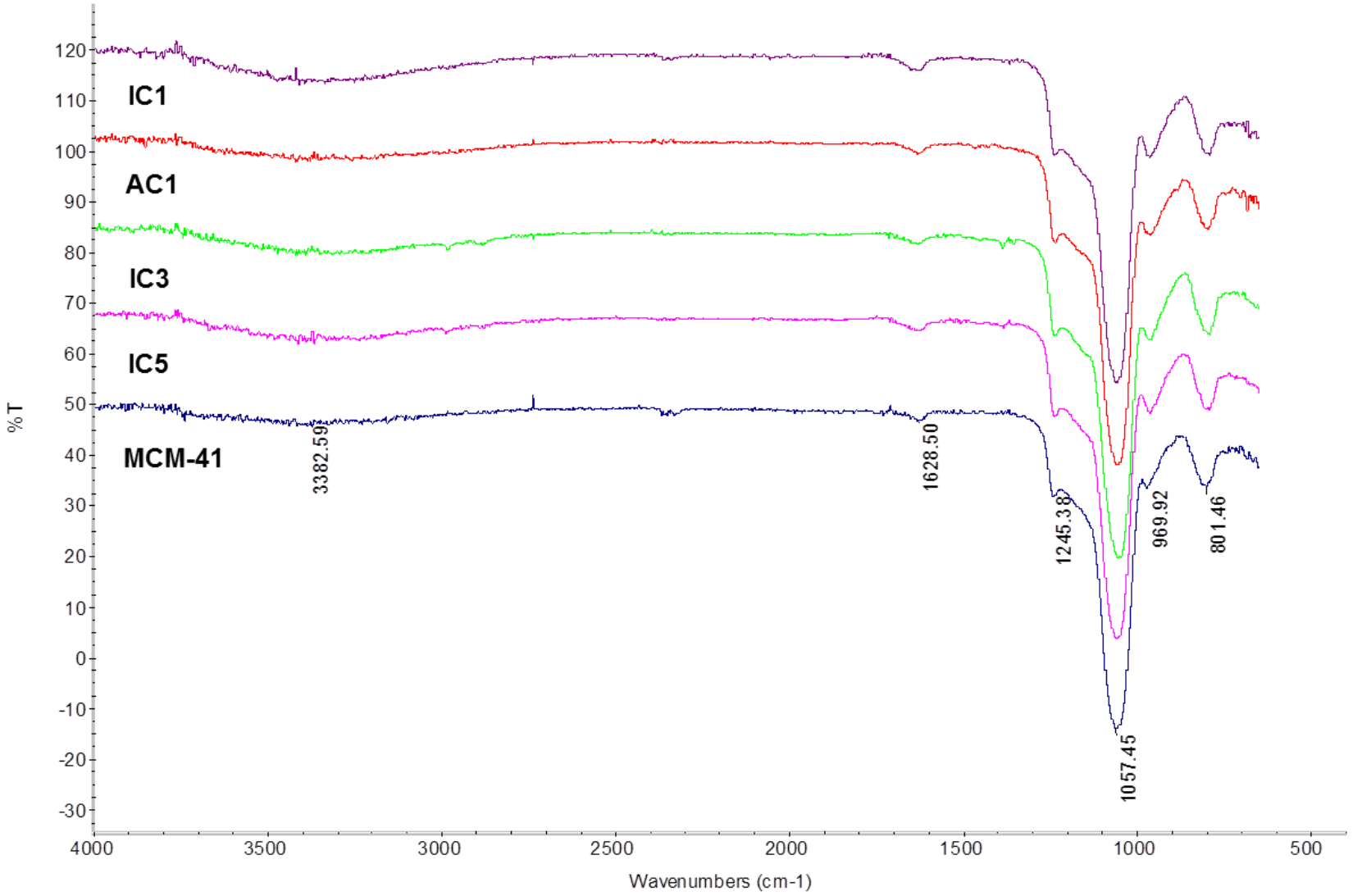

Figure 3.10: FT-IR spectra of immobilized and adsorbed MCM-41 catalysts.

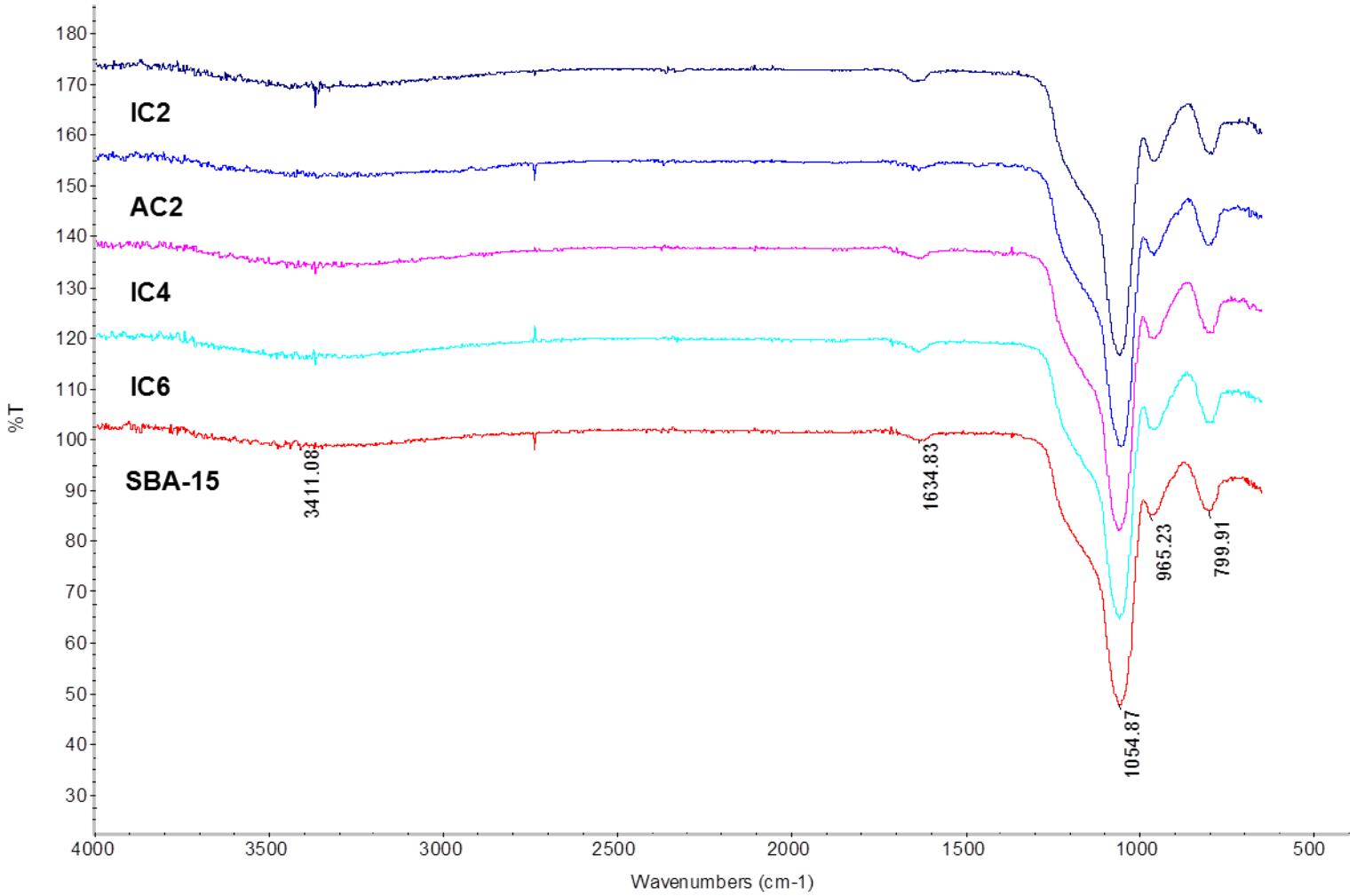

Figure 3.11: FT-IR spectra of immobilized and adsorbed SBA-15 catalysts.

3.2.2.2. Characterization of immobilized catalysts IC1-IC6 and adsorbed catalysts AC1 and AC2 by means of BET (Brunauer Emmett Teller) surface analysis

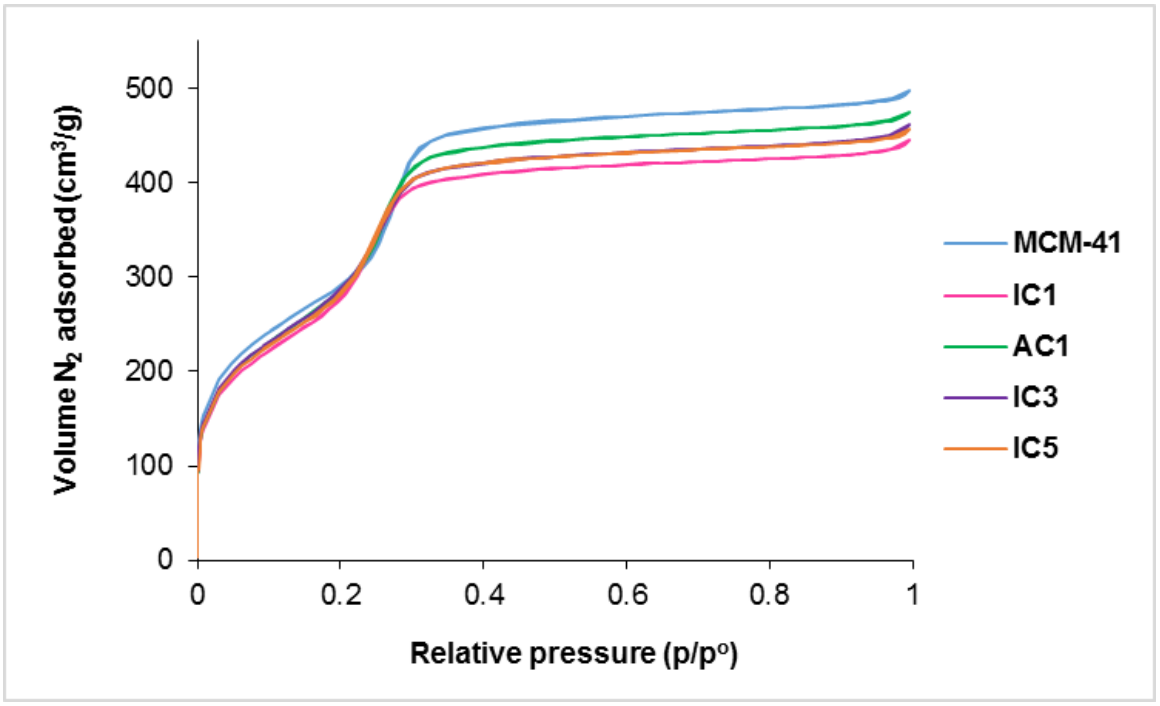

Figure 3.12: Isotherm plots for MCM-41 immobilized and adsorbed catalysts IC1,3,5 and AC1.

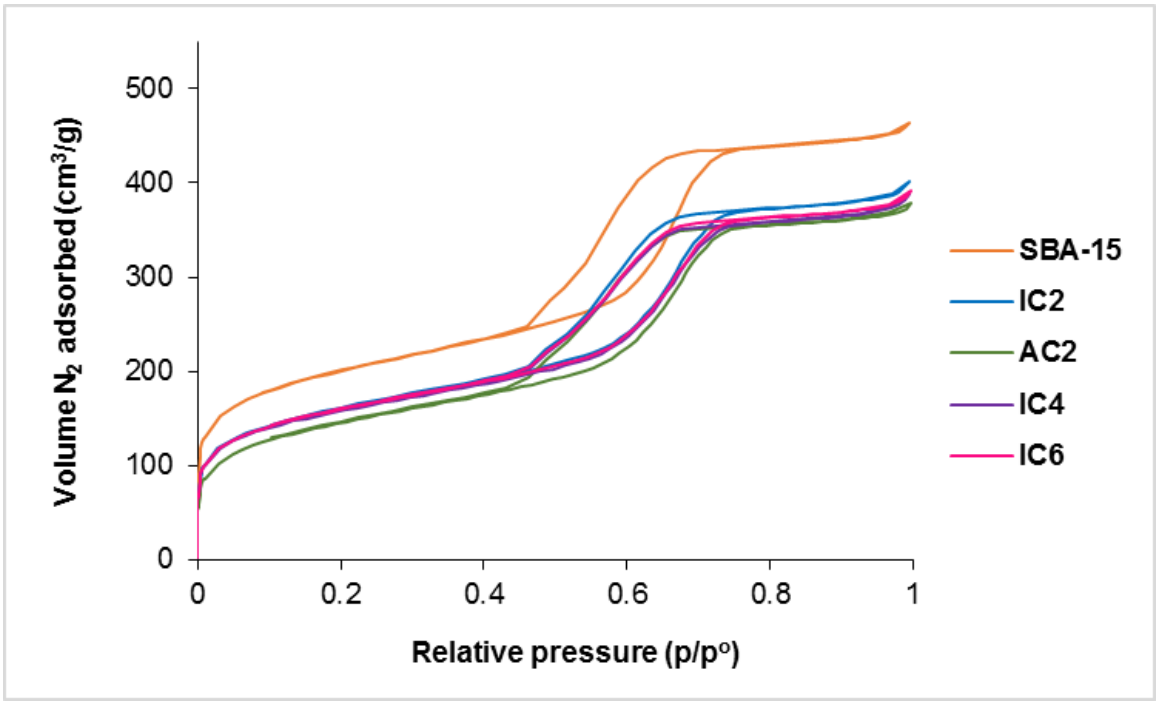

Figure 3.13: Isotherm plots for SBA-15 immobilized and adsorbed catalysts IC2,4,6 and AC2.

The characteristic type IV BET isotherms obtained for the complexes immobilized on MCM-41 and SBA-15 are shown in Figure 3.12 and Figure 3.13 respectively. For **IC1-IC6** and **AC1-AC2** a decrease in the total volume of nitrogen adsorbed can be observed relative to the native silica. This can be ascribed to the immobilization of the siloxane functionalized complexes which then occupy surface space within the support. Decreases in the BET surface area and total pore volume of all the immobilized and adsorbed catalysts relative to the native silica (Table 3.3) is a further illustration of the presence of the complexes within the pores and on the surface of the supports. The adsorbed systems show a greater reduction in surface area and the pore sizes and pore volumes hardly change after simple adsorption, compared to the immobilized systems. This would seem to suggest that adsorption is essentially on the surface of the support and not inside the pores of the silica.

Table 3.3: Summary of BET surface area, average pore diameter and total pore volume of immobilized catalysts IC1-IC6 and adsorbed catalysts AC1 and AC2

Material	BET Surface Area (m^2/g)	Average Pore Diameter (Å)	Total Pore Volume (cm^3/g)
MCM-41	1 079.11	28.56	0.77
IC1 (MCM-41)	1 057.87	26.09	0.69
AC1 (MCM-41)	1 038.63	28.38	0.74
IC3 (MCM-41)	1 043.12	27.41	0.72
IC5 (MCM-41)	1 041.01	27.16	0.71
SBA-15	708.52	40.52	0.72
IC2 (SBA-15)	568.04	43.86	0.62
AC2 (SBA-15)	492.29	46.38	0.58
IC4 (SBA-15)	567.96	42.30	0.60
IC6 (SBA-15)	536.64	42.04	0.61

As expected, a decrease in the average pore diameter compared to native MCM-41 can be observed for the immobilized and adsorbed MCM-41 derivatives. However, the opposite is observed for the immobilized and adsorbed SBA-15 derivatives where an increase in the average pore diameter relative to the native support can be observed.

It has previously been shown by Celar *et al*. that an increase in the primary mesopore size could be observed when SBA-15 was heated to 100 °C in water for extended periods of time.[23] The TGA results obtained for our native silica showed that a large amount of water was present in the support. The presence of a significant amount of water on the native SBA-15 coupled with the high temperatures (110 °C) employed in our immobilization reactions could be the reason for the increase in the average pore size observed for the immobilized SBA-15 catalysts. The increase in the average pore size observed for the adsorbed SBA-15 catalyst **AC2**, could be ascribed to the complex blocking the smaller mesopores leaving the larger pores open for adsorption/desorption of nitrogen.

3.2.2.3. Characterization of immobilized catalysts IC1-IC6 and adsorbed catalysts AC1 and AC2 by means of powder XRD

Characterization of the immobilized and adsorbed catalysts by means powder XRD indicated that the well-ordered mesostructures of the silica was not compromised during the immobilization process.

The PXRD patterns (Figure 3.14 and Figure 3.15) for all the catalysts shows a no noticeable shift in the 2 theta degrees of the reflection peaks, however a slight decrease in the relative intensities of the reflection peaks relative to the native supports can be observed. The immobilization process may have caused minor changes in the degree of ordering of the mesostructures in the silicate materials, giving rise to the decrease in relative intensities of the reflection peaks. Overall, it can be concluded that the supports retain their respective properties of the native mesoporous MCM-41 and SBA-15 silica.

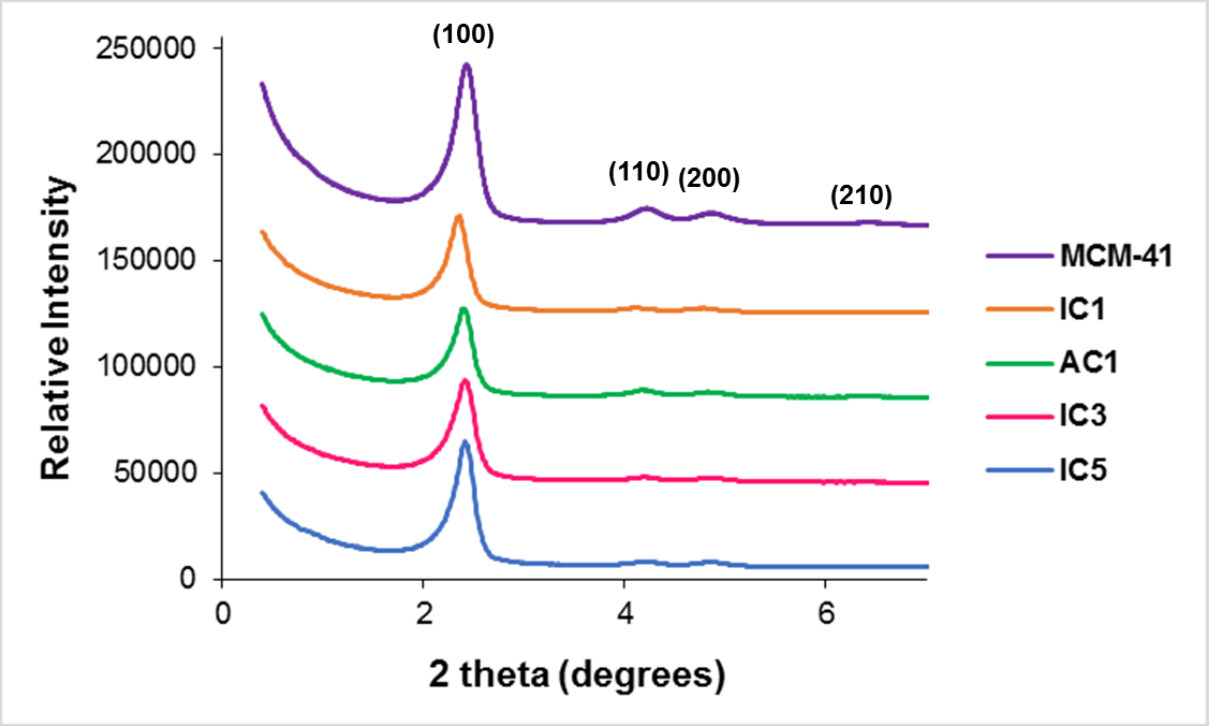

Figure 3.14: Powder XRD plots for MCM-41 immobilized and adsorbed catalysts IC1,3,5 and AC1.

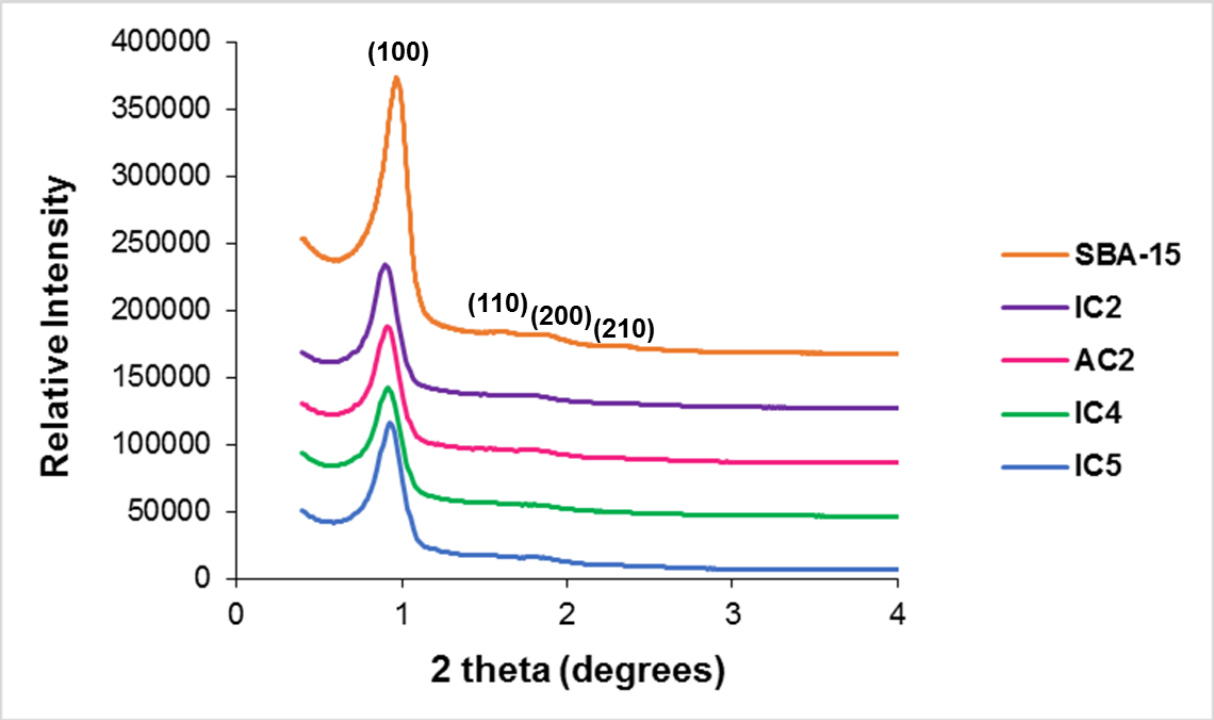

Figure 3.15: Powder XRD plots for SBA-15 immobilized and adsorbed catalysts IC2,4,6 and AC2.

3.2.2.4. Characterization of immobilized catalysts IC1-IC6 and adsorbed catalysts AC1 and AC2 by means of transmission electron microscopy (TEM) and scanning electron microscopy (SEM)

The TEM micrographs of the immobilized/adsorbed MCM-41 and SBA-15 silica are shown below in Figure 3.16 and Figure 3.17 respectively. It can be observed that no noticeable difference in the TEM micrographs of the immobilized and adsorbed catalysts could be detected compared to the native MCM-41 and SBA- 15 supports.

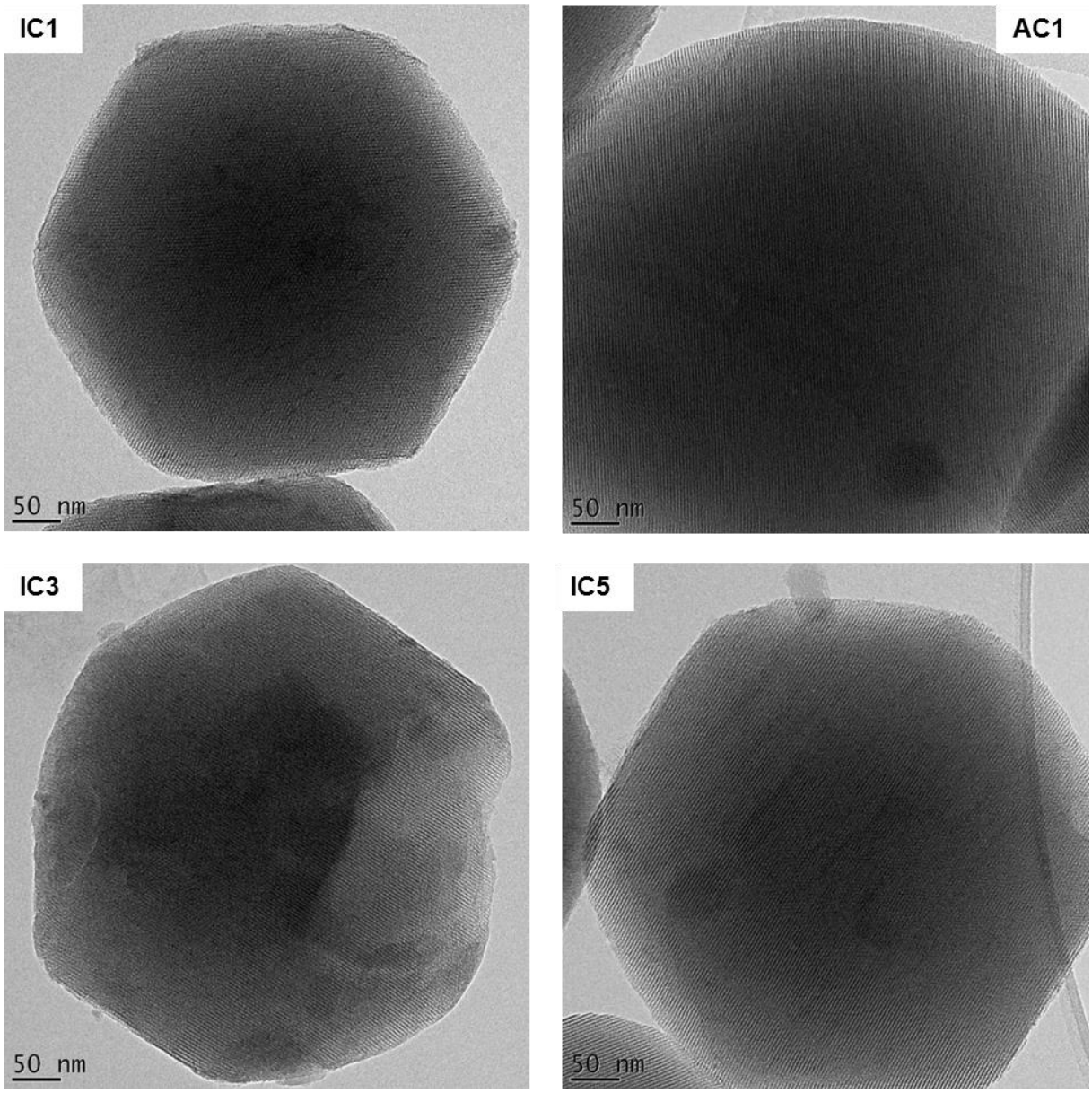

Figure 3.16: TEM micrographs of MCM-41 immobilized and adsorbed catalysts IC1,3,5 and AC1.

Energy-dispersive X-ray spectroscopy (EDS) was carried out on the MCM-41 and SBA-15 supported complexes to determine the content of the material. TEM-EDS analysis confirmed the presence of ruthenium on the surface of the heterogenized catalysts.

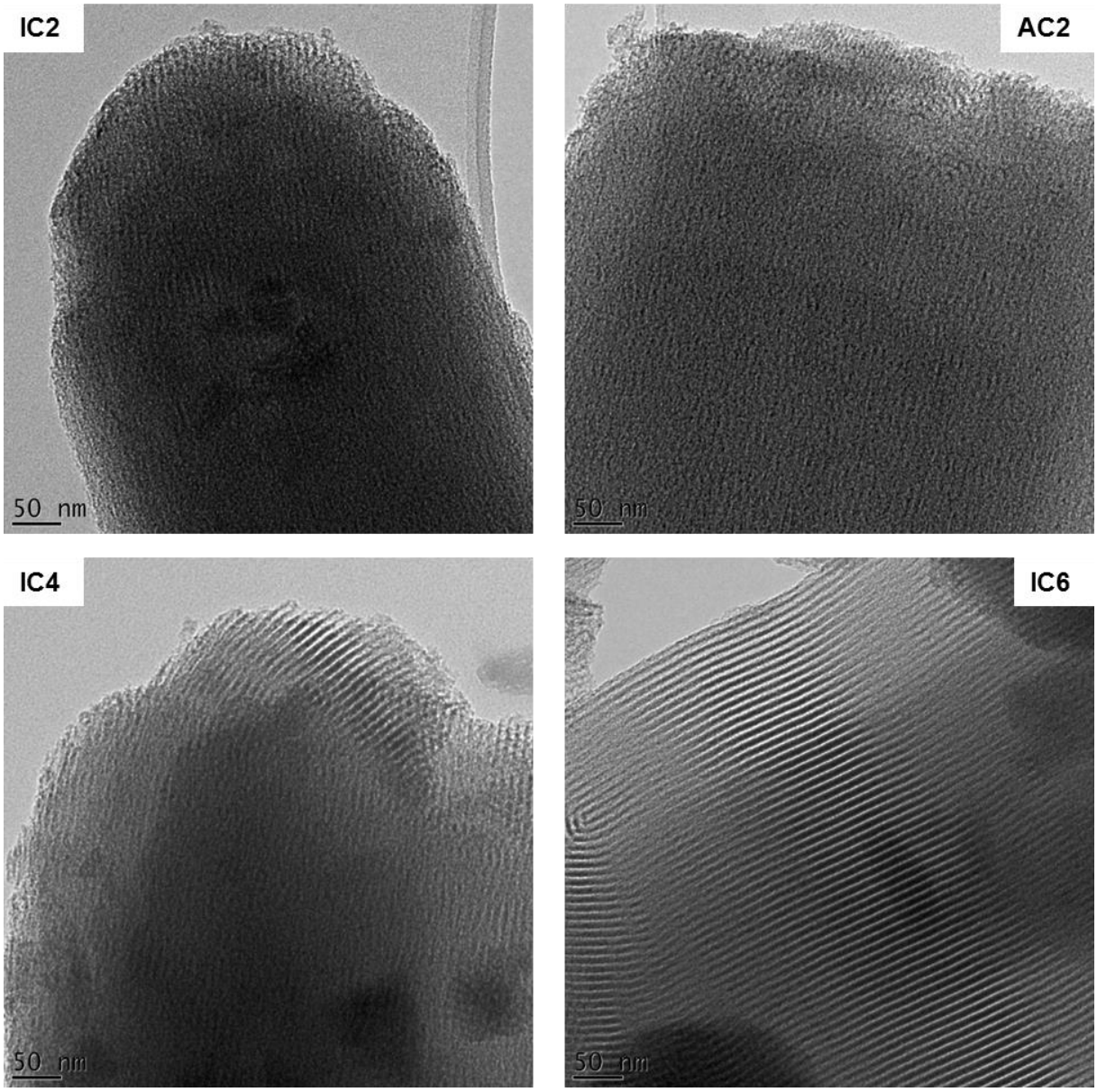

Figure 3.17: TEM micrographs of SBA-15 immobilized and adsorbed catalysts IC2,4,6 and AC2.

The morphology of the MCM-41 and SBA-15 immobilized/adsorbed catalysts was determined using scanning electron microscopy (SEM) and the images are shown in Figure 3.18 and Figure 3.19, respectively. The micrographs show no distinct difference in morphologies of the immobilized/adsorbed catalysts relative to the MCM-41 and SBA-15 native supports.

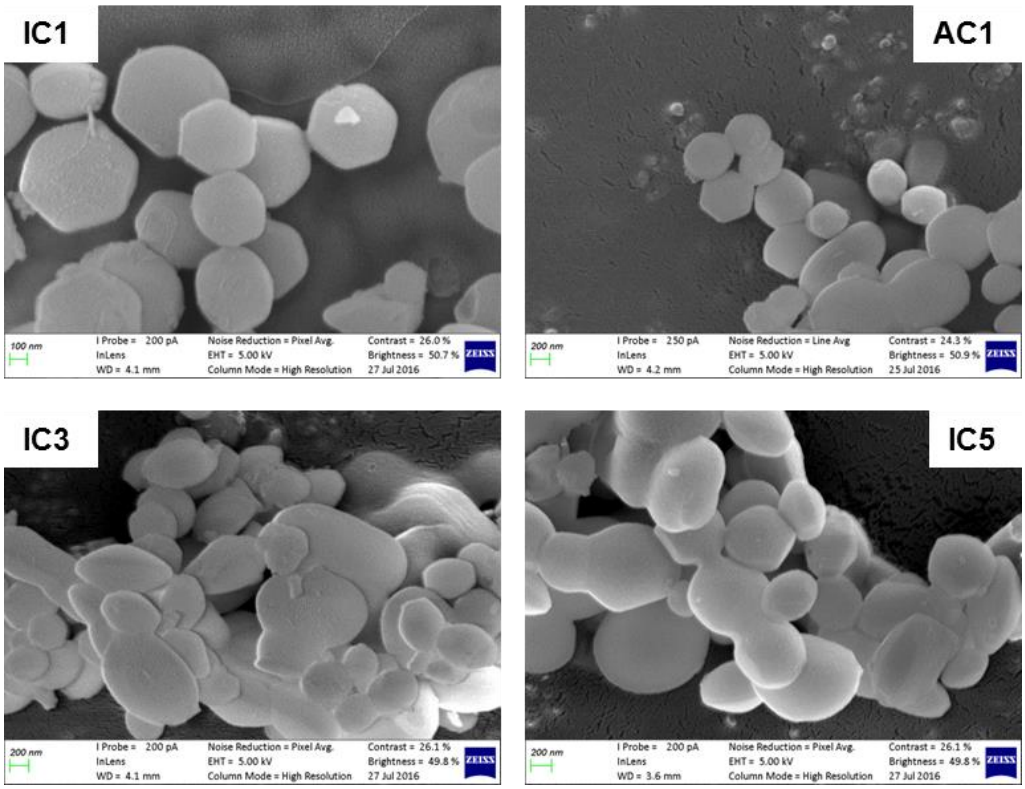

Figure 3.18: SEM micrographs of MCM-41 immobilized and adsorbed catalysts IC1,3,5 and AC1.

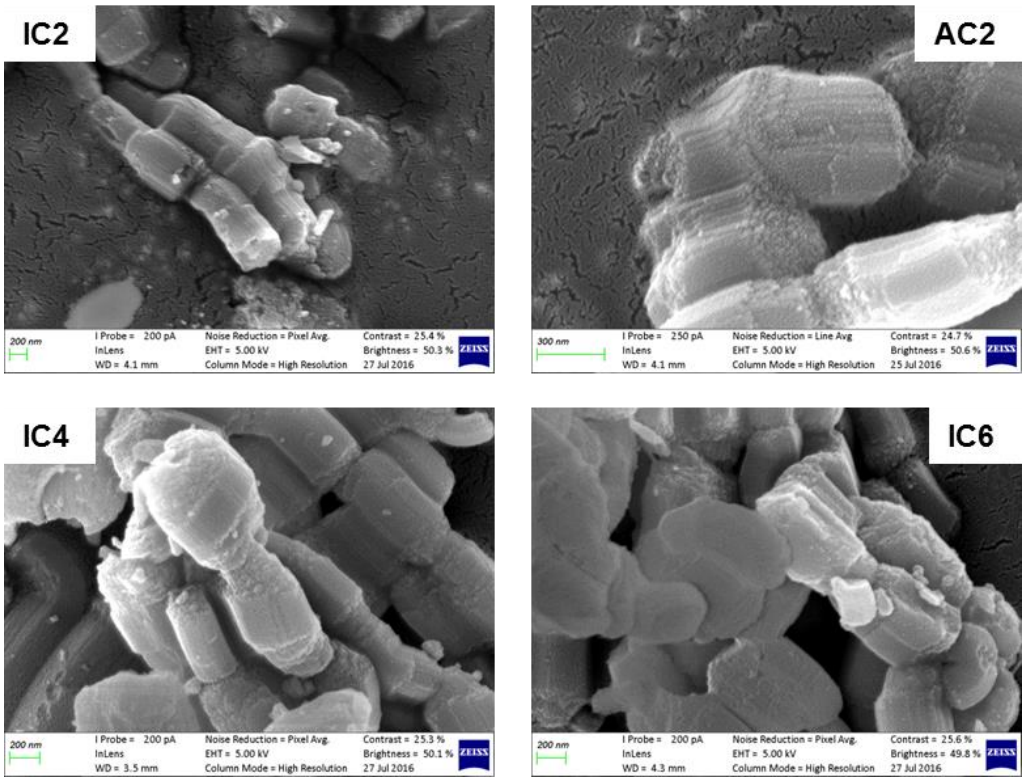

Figure 3.19: SEM micrographs of SBA-15 immobilized and adsorbed catalysts IC2,4,6 and AC2.

3.2.2.5. Characterization of immobilized catalysts IC1-IC6 and adsorbed catalysts AC1 and AC2 by means of thermal gravimetric analysis (TGA)

Thermal gravimetric analysis (TGA) was done on **IC1** (Figure 3.20) and **IC2** (Figure 3.21), where **SC1** was immobilized on MCM-41 and SBA-15, respectively. A significant weight loss can be observed just below 100 °C for both the immobilized catalysts. This 7-8 % weight loss can be ascribed to the loss of adsorbed water. Another drop in the weight of the catalysts (7-8 %) can be observed between 100 and 600 °C. This loss is due to small amounts of unreacted TEOS or templating agent that was not effectively removed during calcination (1-4 %) as well as the presence of the organometallic complex on the supports (3-7 %). This type of weight loss distribution is typical for TGA analysis of materials with a compound adsorbed or immobilized on mesoporous silica such as MCM-41 and SBA-15.[22] As such the trend in the TGA plots for **IC1** and **IC2** is representative for all the immobilized/adsorbed MCM-41 and SBA-15 catalysts, **IC3-IC6** and **AC1** and **AC2**.

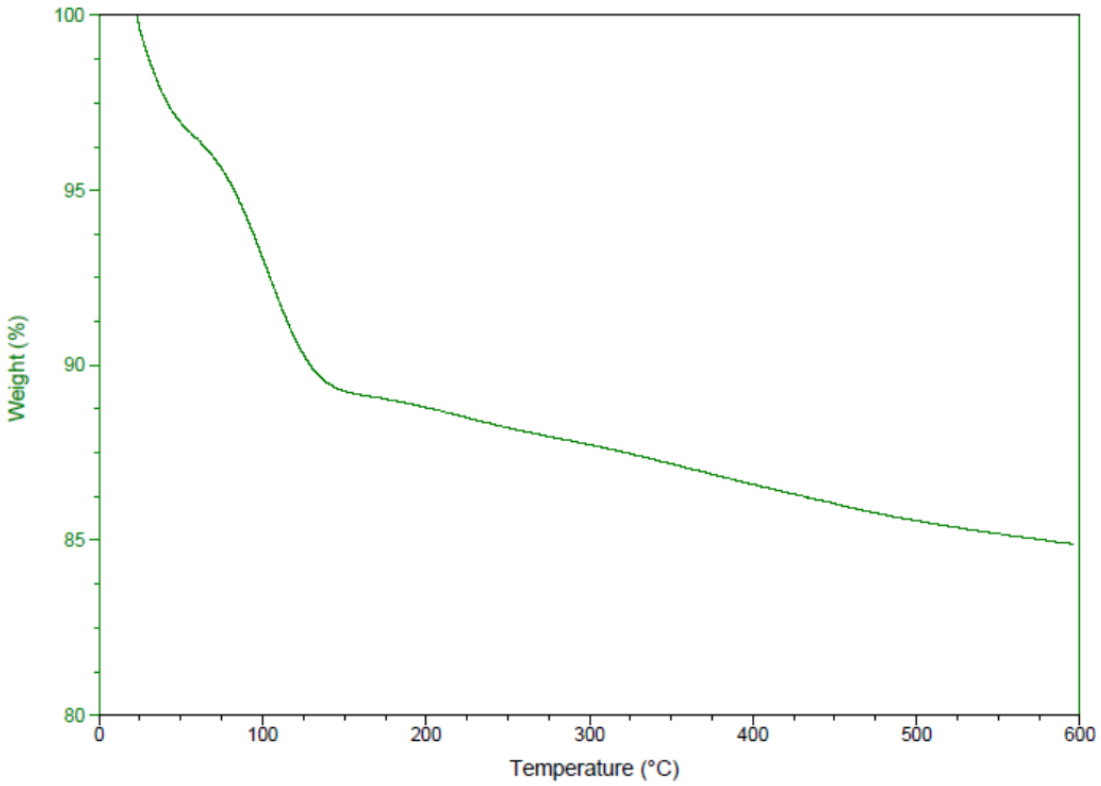

Figure 3.20: TGA analysis of IC1 (SC1 immobilized on MCM-41).

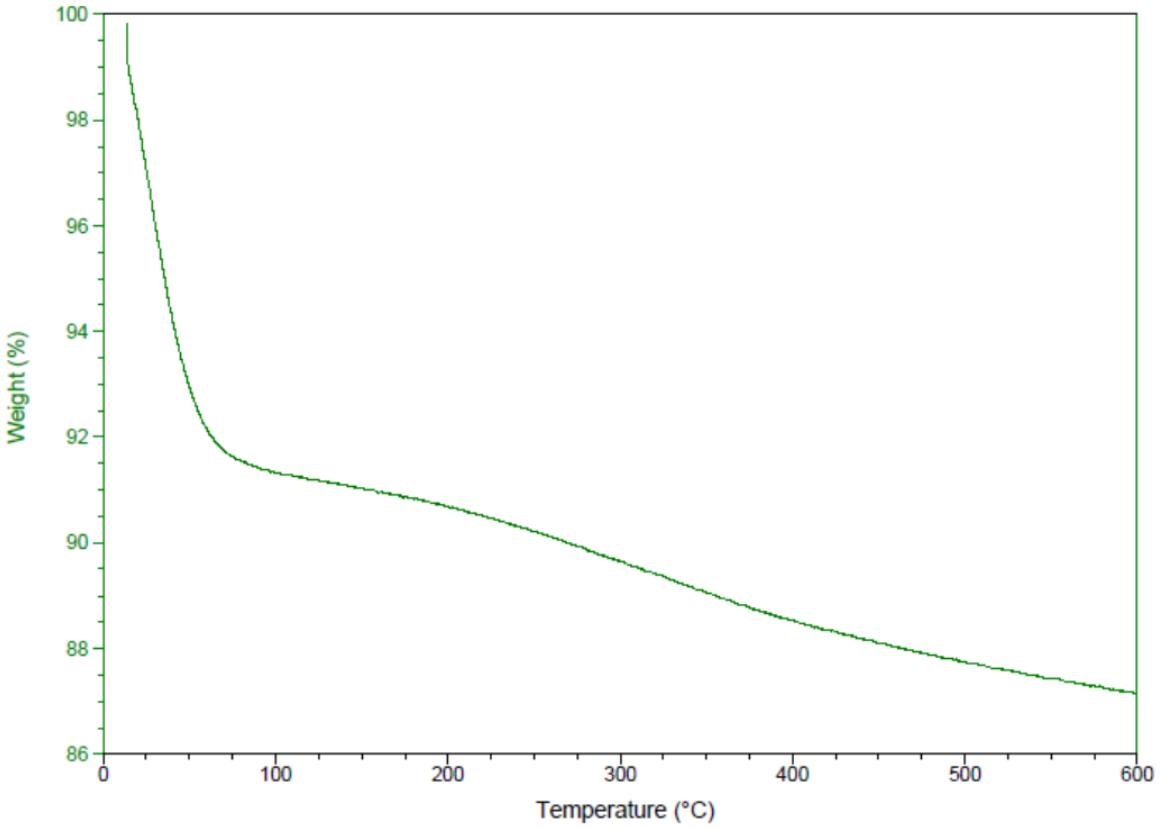

Figure 3.21: TGA analysis of IC2 (SC1 immobilized on SBA-15).

3.2.2.6. Characterization of immobilized catalysts IC1-IC6 by means of ICP-OES

ICP-OES is a crucial analysis for determining the amount of metal complex immobilized on the silica supports. This result gives an indication of the effectiveness of the immobilization process. The results obtained are summarized in Table 3.4. Overall it appears that the immobilization does not go to completion, with only between 26-49 % of the desired complex being covalently bonded to the silica. The results show that the immobilization of the siloxane functionalized complex **SL3** was most effective, with 41 % and 49 % of the introduced complex being immobilized on MCM-41 and SBA-15 respectively. The immobilization of siloxane functionalized complexes **SL1** and **SL2** was least effective, with between 22-29 % of the complexes being immobilized on the silica. ICP-OES therefore provides a means to determine metal loading on the silica for application of the immobilized complexes in catalysis.

Table 3.4: Summary of ICP-OES results for immobilized catalysts IC1-IC6[a]

Material	Ru Loading (% w/w)		Ru immobilized (%)[b]
	Theoretical	Experimental	
IC1 (MCM-41)	1.07	0.28	26.32
IC2 (SBA-15)	1.07	0.31	28.52
IC3 (MCM-41)	1.05	0.23	22.04
IC4 (SBA-15)	1.05	0.25	23.84
IC5 (MCM-41)	1.02	0.41	40.52
IC6 (SBA-15)	1.02	0.50	49.12

[a] Analyzed by ICP-OES to determine Ru loading of immobilized catalysts; mg Ru per 100 mg of silica; [b] Percentage of experimental Ru loading versus theoretical Ru loading for the immobilization.

3.3 Concluding remarks

The successful immobilization of three siloxane functionalized complexes, **SC1-SC3**, onto MCM-41 and SBA-15 to afford six immobilized catalysts **IC1-IC6** was achieved. Furthermore adsorption of the model complex, **MC1**, onto MCM-41 and SBA-15 to afford two adsorbed catalysts **AC1** and **AC2** was also successful. The native MCM-41 and SBA-15 supports as well as the immobilized and adsorbed catalysts were characterized using a range of solid state analytical techniques including infrared spectroscopy, nitrogen adsorption/desorption (BET) surface analysis, low-angle powder X-ray diffraction, transmission electron microscopy (TEM), scanning electron microscopy (SEM), thermal gravimetric analysis (TGA) and ICP-OES. The results of the characterization of the native silica corresponds well with literature data and confirms the mesoporous materials as suitable catalyst supports. The immobilization/adsorption of the complexes onto the supports was monitored by the decrease in BET surface area, the increase in weight loss relative to the native silica obtained for TGA analysis and the presence of ruthenium on the supports confirmed by TEM-EDS and ICP-OES. The quantitative result obtained from ICP-OES provides a means by which to determine catalyst loading for the application of the supported ruthenium complexes in catalytic oxidations (Chapters 4 and 5).

3.4 Experimental section

3.4.1 General remarks and instrumentation

All reactions were performed using standard Schlenk techniques under an inert atmosphere unless stated otherwise. Highly air-sensitive materials were stored in a nitrogen purged glovebox and all manipulations with these materials were carried out in the glovebox. The native silica, MCM-41[10] and SBA-15[11], were synthesized according to modified literature procedures.

IR spectra were recorded using an ATR accessory on a Nicolet Avatar 330 FT-IR spectrometer equipped with a Smart Performer ATR attachment with a ZnSe crystal. BET nitrogen adsorption/desorption analysis was done on a Micromeritics 3Flex Surface Characterization instrument (77 K). The samples were degassed at 273 K for 18 hours prior to analysis. Powder XRD analysis was done with a BRUKER AXS (Germany) D8 Advance Diffractometer. Transmission electron micrographs were collected using an FEI Tecnai G2 20 field-emission gun (FEG) TEM, operated in bright field mode at an accelerating voltage of 200 kV. Energy dispersive x-ray spectra were collected using an EDAX liquid nitrogen cooled Lithium doped Silicon detector. A Zeiss MERLIN Field Emission Scanning Electron Microscope was operated at 5kV and approximately 250pA, with the working distance from the microscope pole piece being less than 4mm during acquisition, to obtain secondary electron images. The images were collected with a Zeiss SE1 (inLens) secondary electron detector and processed using Zeiss SmartSEM software. Prior to imaging, the samples were mounted on a stub with double sided carbon tape. The samples were then coated with a thin (~10nm thick) layer of gold, using an Edwards S150A Gold Sputter Coater, in order to make the sample surface electrically conductive. A TA Instruments Q500 thermogravimetric analyser was used to acquire TGA data. ICP-OES analysis was perfomed on a Spectro Arcos ICP-OES with a Burgener T2100 and cyclonic spray chamber as nebulizer. The samples were prepared by digesting between 20-30 mg of the immobilized catalyst in concentrated nitric acid (15 ml), at 100 °C for 24 hours. The sample was then filtered and made up to a known volume and analyzed.

3.4.2 Materials

Reagents were purchased from Sigma-Aldrich and Merck and used as received; including: Cetyltrimethylammonium bromide (CTAB), tetraethyl orthosilicate (TEOS) and Poly(ethylene)-*block*-poly(propylene)-*block*-poly(ethylene). Solvents were purchased from Sigma-Aldrich and Kimix Chemicals. THF, DCM and toluene were dried using Pure Solv™ Micro solvent purification systems fitted with activated alumina columns.

3.4.3 Synthesis of native mesoporous silica, MCM-41 and SBA-15

3.4.3.1. Synthesis of MCM-41

To a mixture of distilled water (540 mL) and ammonium solution (410 mL, 25% wt) was added cetyltrimethylammonium bromide (4.0 g) as surfactant. The mixture was heated to 50 °C with stirring. Tetraethoxysilane (TEOS) (20 ml) was added after the solution had become homogeneous. The white slurry was left to stir for 2 hrs. The reaction mixture was then left to cool to room temperature. The solid was filtered off, washed with distilled water (1100 mL) and left to dry. The white solid obtained was calcined at 550 °C (temperature slowly increased) for 8 hrs. 3.363 g of MCM-41 was obtained.

3.4.3.2. Synthesis of SBA-15

Poly(ethylene)-block-poly(propylene)-block-poly(ethylene) (8.050 g) was dissolved in 60 ml of distilled water and 2 M HCl solution (360 ml) while being stirred at 35 °C. TEOS (18.2 ml) was added to this stirred solution (after everything dissolved) and was stirred at 35 °C for 20 hours. The temperature of the mixture was then increased to 80 °C and aged for 24 hours without being stirred. A solid product formed and it was filtered off and washed with 2200 ml of distilled water and dried at room temperature overnight. The white powder was then calcined at 550 °C for 8 hours. 4.834 g of SBA-15 was obtained.

3.4.4 Synthesis of immobilized and adsorbed catalysts

3.4.4.1. Synthesis of immobilized catalysts IC1-IC6

General procedure for immobilization: To a slurry of the silica (1.00 g), MCM-41 or SBA-15, in toluene (8 mL) was added a solution of the functionalised complex (0.100 g), **SC1**, dissolved in THF (2 mL). The yellow mixture was refluxed at 110 °C with stirring for 24 hrs. After the allotted time the yellow reaction mixture was left to cool to room temperature and the solid filtered off. The yellow solid was repeatedly washed with THF, DCM, and Ether. The light yellow solid was left to dry at room temperature and further dried *in-vacuo* at 40 °C.

3.4.4.2. Synthesis of adsorbed catalysts AC1 and AC2

To a slurry of MCM-41 (1.00 g) in THF (5 mL) was added a solution of MC1 (0.100 g) dissolved in DCM (5 mL). The yellow mixture was stirred at 20 °C for 2 hrs. The solvent was then removed from the mixture under reduced pressure and the light yellow solid was dried *in-vacuo* overnight.

3.5 References

1 J. Ying, C. Mehnert and M. Wong, *Angew. Chem. Int. Ed.*, 1999, **38**, 56–77.

2 S. Wang, *Microporous Mesoporous Mater.*, 2009, **117**, 1–9.

3 U. Ciesla and F. Schüth, *Microporous Mesoporous Mater.*, 1999, **27**, 131–149.

4 V. Meynen, P. Cool and E. F. Vansant, *Microporous Mesoporous Mater.*, 2009, **125**, 170–223.

5 A. Taguchi and F. Schüth, *Microporous Mesoporous Mater.*, 2005, **77**, 1–45.

6 A. Tuel, *Microporous Mesoporous Mater.*, 1999, **27**, 151–169.

7 L. X. Xu, C. H. He, M. Q. Zhu, K. J. Wu and Y. L. Lai, *Catal. Letters*, 2007, **118**, 248–253.

8 Y. Wan, F. Zhang, Y. Lu and H. Li, *J. Mol. Catal. A Chem.*, 2007, **267**, 165–172.

9 A. Bleloch, B. F. G. Johnson, S. V. Ley, A. J. Price, D. S. Shephard and A. W. Thomas, *Chem. Commun.*, 1999, **18**, 1907–1908.

10 Q. Cai, W.-Y. Lin, F.-S. Xiao, W.-Q. Pang, X.-H. Chen and B.-S. Zou, *Microporous Mesoporous Mater.*, 1999, **32**, 1–15.

11 D. Zhao, Q. Huo, J. Feng, B. F. Chmelka and G. D. Stucky, *J. Am. Chem. Soc.*, 1998, **120**, 6024–6036.

12 M. Sieves, M.- Sepiolite and M. Yang, *Chem. Anal.*, 2007, **961**, 957–961.

13 M. V. Landau, S. P. Varkey, M. Herskowitz, O. Regev, S. Pevzner, T. Sen and Z. Luz, *Microporous Mesoporous Mater.*, 1999, **33**, 149–163.

14 P. B. Balbuenat and K.E. Gubbins, *Langmuir*, 1993, **9**, 1801–1814.

15 H. Zhang, J. Sun, D. Ma, X. Bao, A. Klein-Hoffmann, G. Weinberg, D. Su and R. Schlögl, *J. Am. Chem. Soc.*, 2004, **126**, 7440–7441.

16 V. B. Fenelonov, V. N. Romannikov and A. Y. Derevyankin, *Microporous Mesoporous Mater.*, 1999, **28**, 57–72.

17 P. L. Llewellyn, Y. Grillet, F. Schuth, H. Reichert and K. K. Unger, *Microporous Mater.*, 1994, **3**, 2–6.

18 F. Di Renzo, A. Galarneau, D. Desplantier and F. Fajula, *Catal. Today*, 2001, **66**, 75–79.

19 E. C. De Oliveira, C. T. G. V. M. T. Pires and H. O. Pastore, *J. Braz. Chem. Soc.*, 2006, **17**, 16–29.

20 C. T. Kregse, M. E. Leonowicz, W. J. Roth, J. C. Vartuli and J. S. Beck, *Nature*, 1992, **359**, 710–712.

21 Q. Huo, D. I. Margolese and G. D. Stucky, *Chem. Mater.*, 1996, **8**, 1147–1160.

22 L. B. de O. Freitas, I. J. G. Bravo, W. A. de A. Macedo and E. M. B. de Sousa, *J. Sol-Gel Sci. Technol.*, 2016, **77**, 186–204.

23 E. B. Celer, M. Kruk, Y. Zuzek and M. Jaroniec, *J. Mater. Chem.*, 2006, **16**, 2824–2833.

Chapter 4: Oxidative cleavage of 1-octene

4.1 Introduction

Unsaturated hydrocarbons, namely alkenes can be converted to more valuable oxygenates via oxidative cleavage. This process is important and has been the topic of several reviews.[1–5] Oxidative cleavage of olefins is normally performed industrially using ozonolysis, with ozone as the oxidant. Ozone is relatively unstable thus posing a safety hazard to work with. In addition, working with ozone is also costly on account of the specialized equipment needed to perform the ozonolysis reaction. This process is used commercially, despite its disadvantages, due to the fact that ozone selectively cleaves alkenes into the desired aldehydes or carboxylic acids. Alternatives to ozonolysis would therefore have to be selective for the desired oxygenated product, preventing side reactions such as dihydroxylation and epoxidation. There are examples of stoichiometric transition metal based oxidation reactions using $KMnO_4$ or CrO_2Cl_2 which are known to selectively transform olefins into aldehydes or carboxylic acids. The use of these systems is however undesirable due to the toxicity of such chromium salts and the fact that the organic substrate is not very soluble in the aqueous medium required for the permanganate ion.[5]

Thus, catalytic olefin oxidations using a group 7 or 8 transition metal and an oxidant, such as IO_4^- or H_2O_2 are generally preferred.[5,6] There are catalytic systems based on Ru, Os, and W which have been studied and are known to catalyze the oxidative cleavage of various unsaturated fatty acids and alkenes. There is also research into Fe and Mn catalytic systems however these are currently limited to activated alkenes such as styrene as substrates. Alkenes can be selectively cleaved to form aldehydes using osmium based catalytic systems with $NaIO_4$ as an oxidant. A major drawback however is that Os is very toxic causing its usage to be undesirable.[5]

For this reason, it is desirable to develop ruthenium based catalysts due the versatility of one of its oxides, RuO_4, which can be used either stoichiometrically or catalytically to oxidise alkenes into aldehydes and/or carboxylic acids.[5] As discussed in Chapter 1, there has been research into several homogeneous and heterogeneous ruthenium based catalytic systems for the oxidative alkene cleavage reaction. Shoair et al. discovered that a Ru-bipy complex in the presence of $IO(OH)_5$ oxidatively cleaved both terminal and internal alkenes to yield carboxylic acids. It was also found that the incorporation of bipyridine, a bidentate nitrogen

donor ligand led to a catalyst capable of carrying out the oxidative cleavage reaction at a much lower (tenfold lower) catalyst loading than other ruthenium catalyst precursors which do not possess a nitrogen donor ligand.[7]

The purpose of this current study correlates strongly to related systems previously reported by our group in which it was shown that RuCl(arene)(N,N) complexes immobilized on mesoporous silica (MCM-41 & SBA-15) were more active in the oxidative cleavage of 1-octene than their homogeneous counterparts, with a ten-fold lower catalyst loading required.[8] It was therefore decided to further explore these types of systems using other complexes of Ru with other N,N chelating ligands. Thus we explored some of the complexes reported in Chapters 2 and 3. The oxidative cleavage of 1-octene was carried out by the model (**MC1-MC3**) and immobilized catalysts (**IC1-IC6**), which were synthesized and discussed in Chapters 2 and 3 respectively. The results of the catalytic oxidative cleavage of 1-octene using these catalyst precursors are reported in the sections to follow.

4.2 General procedure for the oxidative cleavage of 1-octene

The nature of the solvent has been shown to have a significant impact on the catalytic reaction. Thus for example it has been found that the use of acetonitrile and carbon tetrachloride plays an important role in the oxidative cleavage using these Ru complexes as precursors. The oxidation of organic compounds by RuO_4 has been known for quite a long time. Prior to the work reported by Sharpless *et al.* it was common to perform these oxidative cleavage reactions in a mixture of H_2O/CCl_4 with periodate or hypochlorite as terminal oxidant. Carbon tetrachloride has previously been found to stabilize the volatile active species, RuO_4, in solution preventing its loss via evaporation. Sharpless *et al.* found that by adding the coordinating solvent, acetonitrile, to the oxidative cleavage reaction mixture a dramatic increase in activity could be achieved. In the presence of this solvent, lower catalyst loadings and shorter reactions times could be employed. Deactivation of the catalyst could be arrested via the addition of acetonitrile, which serves the role of stabilizing the low valent RuO_4 ruthenium species, resulting in an increased activity. Furthermore, acetonitrile prevents the coordination to ruthenium of carboxylic acids produced in the reaction, this is important for the catalytic cycle as the carboxylate complexes are insoluble in the reaction mixture.[9] For systems where ruthenium trichloride is used in the catalytic oxidative cleavage of alkenes in the presence of sodium hypochlorite or sodium periodate, the reduction products NaCl or $NaIO_3$ are not soluble in the aqueous reaction conditions and these precipitates therefore cause work-up to be problematic.[7] In the case where periodic acid,

$IO(OH)_5$, is used as the terminal oxidant for oxidative cleavage of alkenes with ruthenium trichloride the reduction product HIO is very soluble in water preventing issues with regards to work-up of the reaction. Another important factor is that the solubility of RuO_2 in the reaction mixture allows for the reaction to be catalytic and $IO(OH)_5$ is a powerful oxidant capable of re-oxidizing RuO_2 back to RuO_4.[10]

The reaction conditions employed for the oxidative cleavage of 1-octene in our study are very similar to those reported by Kotze and Mapolie. The reaction conditions were not altered significantly in order to directly compare the results obtained in our system with the results reported by Kotze and Mapolie.[8] A typical reaction was conducted with 0.5 mmol of 1-octene at 24 ˚C in a biphasic solvent system of $CH_3CN/CCl_4/H_2O$ (1.25 mL, 1.25 mL and 2.5 mL respectively) with 2.5 mmol Periodic acid, $IO(OH)_5$, as the terminal oxidant (Scheme 4.1).

Heptaldehyde and heptanoic acid were the only products observed in our reaction mixtures, however side reactions leading to the formation of 1,2-epoxyoctane and 1,2-octanediol are also possible.[7]

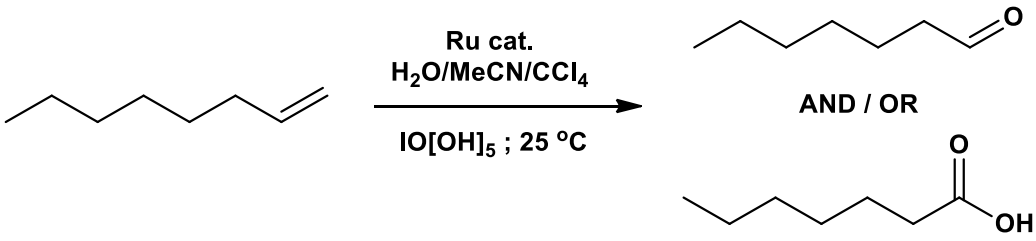

Scheme 4.1: Typical reaction conditions and products formed in the oxidative cleavage of 1-octene.

The catalysts evaluated in the oxidative cleavage of 1-octene are depicted in Figure 4.1.

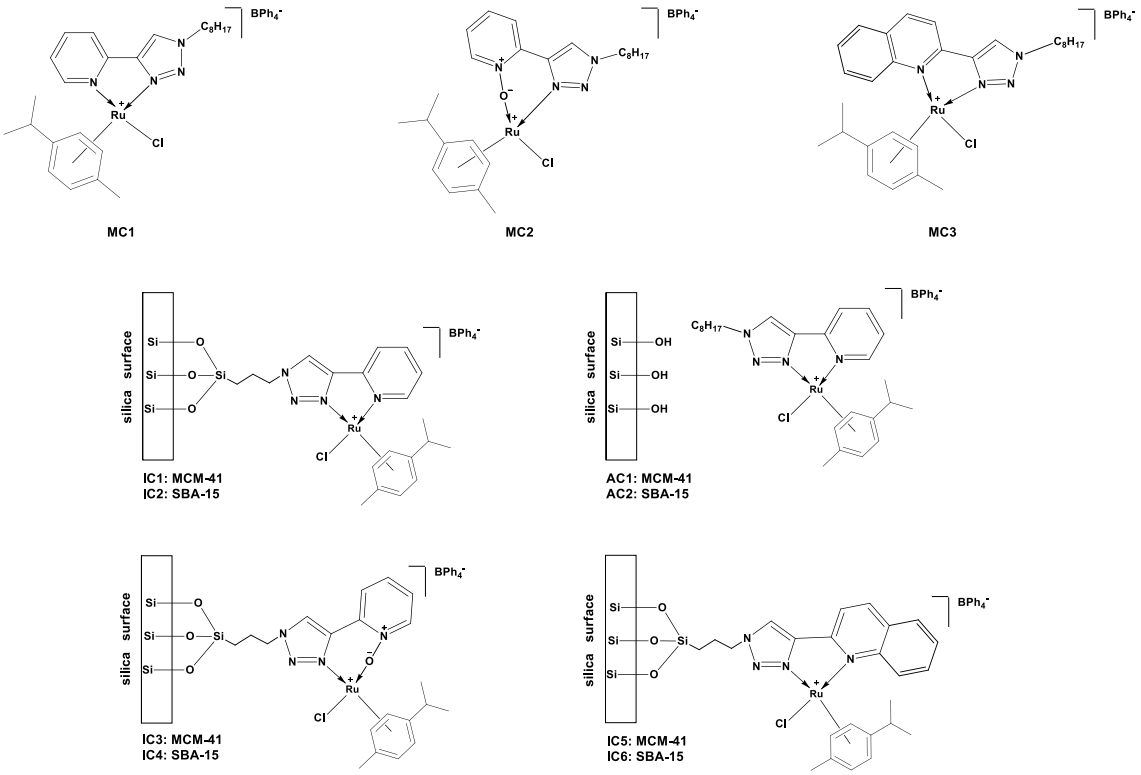

Figure 4.1: Catalyst precursors employed in the oxidative cleavage of 1-octene.

4.3 Evaluation of immobilized catalysts (IC1-6) and model catalysts (MC1-3) in the oxidative cleavage of 1-octene

The model complexes (**MC1-MC3**) and immobilized catalysts (**IC1-IC6**) were applied in the oxidative cleavage of 1-octene at a 0.1 mol% catalyst loading. The results obtained for the N,N bidendate complexes containing the pyridine triazole ligand (**IC1-IC2** and **MC1**) are shown below in Figure 4.3. It can be observed that both the MCM-41 and SBA-15 based immobilized catalysts (**IC1-IC2**) are capable of converting 100% of 1-octene to heptanoic acid after 12 hours, whereas the model complex (**MC1**) is only capable of converting 6.8 % of 1-octene to heptaldehyde over the same 12 hour period and at the same Ru loading. Possible reasons why the model complex performed worse than its immobilized counterparts was not evident at this stage in the study. When comparing **IC1** and **IC2** we see that **IC2** appears to convert the substrate slightly faster than **IC1** between a 6 and 9 hour reaction period, with 100% conversion of 1-octene being achieved after a 9 hour reaction period. The catalyst **IC1** was immobilized on MCM-41 which has an average pore diameter of 28.56 Å and the catalyst **IC2** was immobilized on SBA-15 which has an average pore diameter of 40.52 Å. The reason why **IC2** performs slightly better than **IC1** may be due to the fact that more of the pyridine triazole ruthenium complex is immobilized within the pores of the

SBA-15 in the case of **IC2** whereas for **IC1** less of the complex is immobilized within the pores of the support due to the smaller average pore diameter of MCM-41. Thus when the oxidizing species, RuO_4, is formed it is better stabilized within the pores of the SBA-15 support before it is introduced into the organic phase. The immobilized catalysts transform 1-octene mainly into heptaldehyde at shorter reaction times (3 and 6 hours) however a small amount of heptanoic acid is formed due to oxidation of the heptaldehyde at 6 hours even though 1-octene has not yet been fully converted. The immobilized catalysts (**IC1-IC2**) exhibited good selectivity for heptaldehyde during the oxidation process with majority of the aldehyde formed at shorter reaction times, however selectivity for the acid can be achieved at extended reaction times.

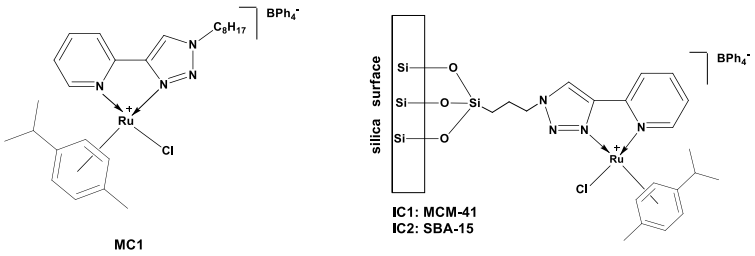

Figure 4.2: Model complex MC1 and immobilized complexes IC1 and IC2 evaluated in the oxidative cleavage of 1-octene.

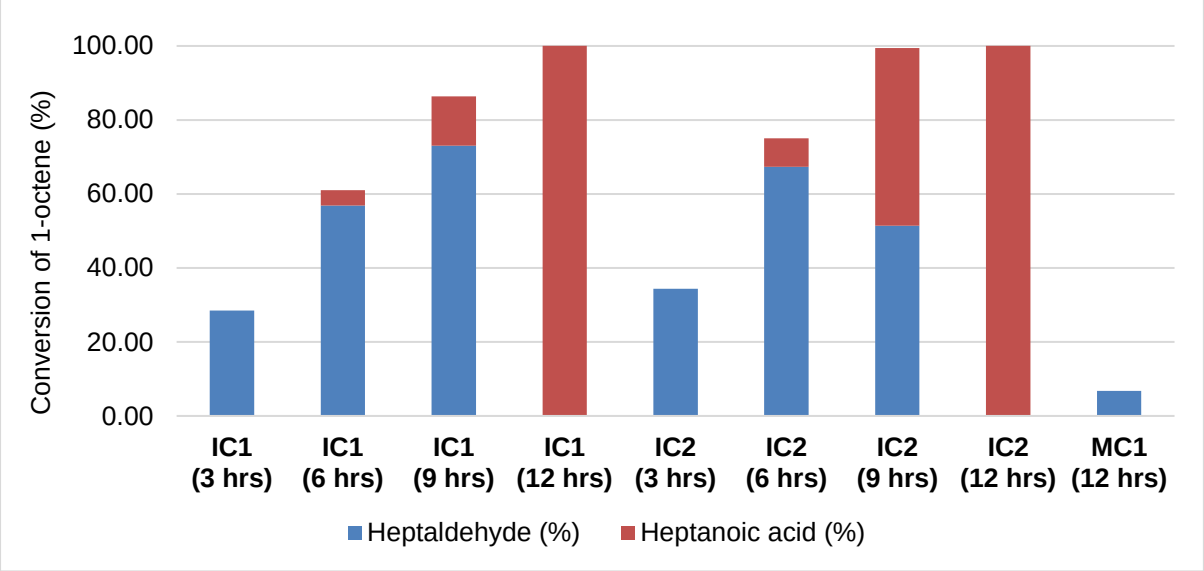

Figure 4.3: Conversion and product selectivities obtained in the oxidative cleavage with immobilized catalysts, IC1-IC2, and model catalyst, MC1.

The results obtained for the N,O bidendate complexes containing pyridine N-oxide triazole ligand (**IC3-IC4** and **MC2**) are depicted in Figure 4.5. Both the immobilized catalysts (**IC3-IC4**) and model complex (**MC2**) are capable of converting 100% of 1-octene after only 6 hours. The immobilized catalysts (**IC3-IC4**) yield heptanoic acid after the 6 hours, whereas the model complex (**MC2**) produces a mixture of the aldehyde and acid over the same time period. At a reaction time of 3 hours the immobilized catalysts yield similar results with between 47-50% conversion of 1-octene being observed. It therefore appears that the rate of the reaction is not majorly influenced by the nature of the silica support for the N,O systems. Once again we see that the selectivity exclusively for heptaldehyde using the immobilized catalysts (**IC3-IC4**) is not optimal even at short reaction times (3 hours), due to some degree of overoxidation of 1-octene to heptanoic acid.

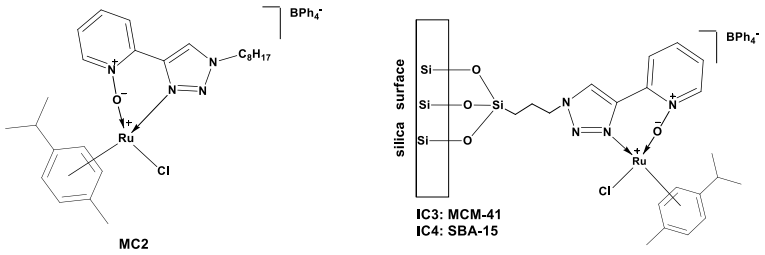

Figure 4.4: Model complex MC2 and immobilized complexes IC3 and IC4 evaluated in the oxidative cleavage of 1-octene.

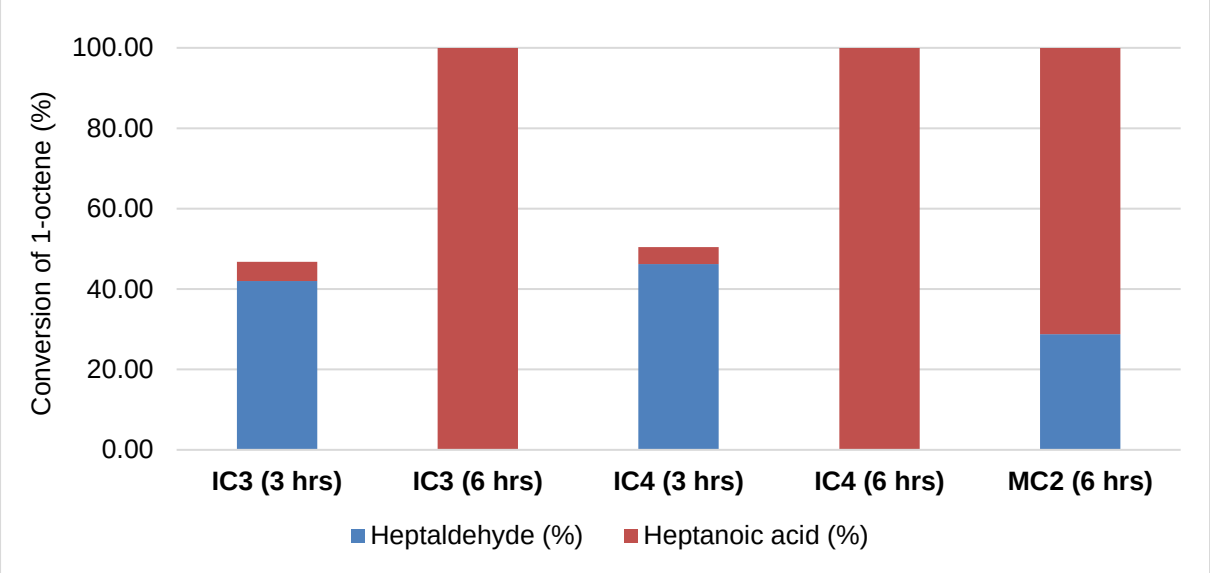

Figure 4.5: Conversion and product selectivities obtained in the oxidative cleavage with immobilized catalysts, IC3-IC4, and model catalyst, MC2.

The N,N bidendate quinoline triazole complexes (**IC5-IC6** and **MC3**) were evaluated in the oxidative cleavage of 1-octene, the results of which are shown below in Figure 4.7. The immobilized catalysts (**IC5-IC6**) convert 100% of 1-octene after a 12 hour reaction period, whereas the model complex (**MC3**) only converts about 24 % of 1-octene to heptaldehyde after 12 hours. The MCM-41 immobilized complex, **IC5** converts 100% of 1-octene mainly to heptaldehyde after 9 hours and affords only heptanoic acid after 12 hours, whereas the SBA-15 analogue, **IC6** only achieves 100% conversion of the substrate after 12 hours to afford mainly heptanoic acid with some heptaldehyde still present. The reason why **IC5** performs slightly better than **IC6** may be due to the fact that the quinoline triazole ruthenium complex is too large to fit within the pores of the support and the differences in activity may be due to surface area effects. The catalyst **IC5** was immobilized on MCM-41 which has a BET surface area of 1079 m^2/g and the catalyst **IC6** was immobilized on SBA-15 which has a BET surface area of 709 m^2/g. The larger surface area of MCM-41 may allow better stabilization of the oxidizing species, RuO_4, before it is introduced into the organic phase. Similar to all the other catalysts we see that a small amount of heptanoic acid is produced before complete consumption of 1-octene to heptaldehyde. Only at very low conversions of 20-30 % is heptaldehyde produced exclusively. The catalysts are selective for aldehyde even at reasonable conversions around 80%. This is true provided we're dealing with relatively short reaction times.

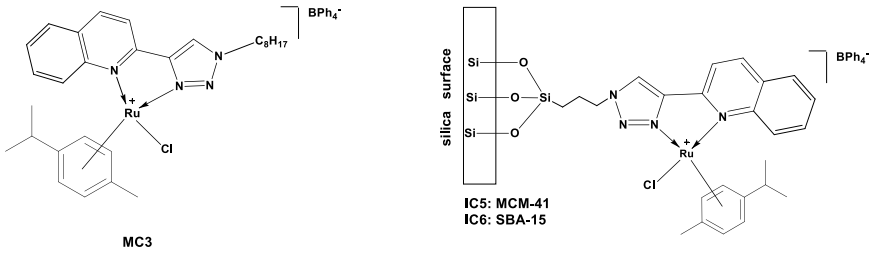

Figure 4.6: Model complex MC3 and immobilized complexes IC5 and IC6 evaluated in the oxidative cleavage of 1-octene.

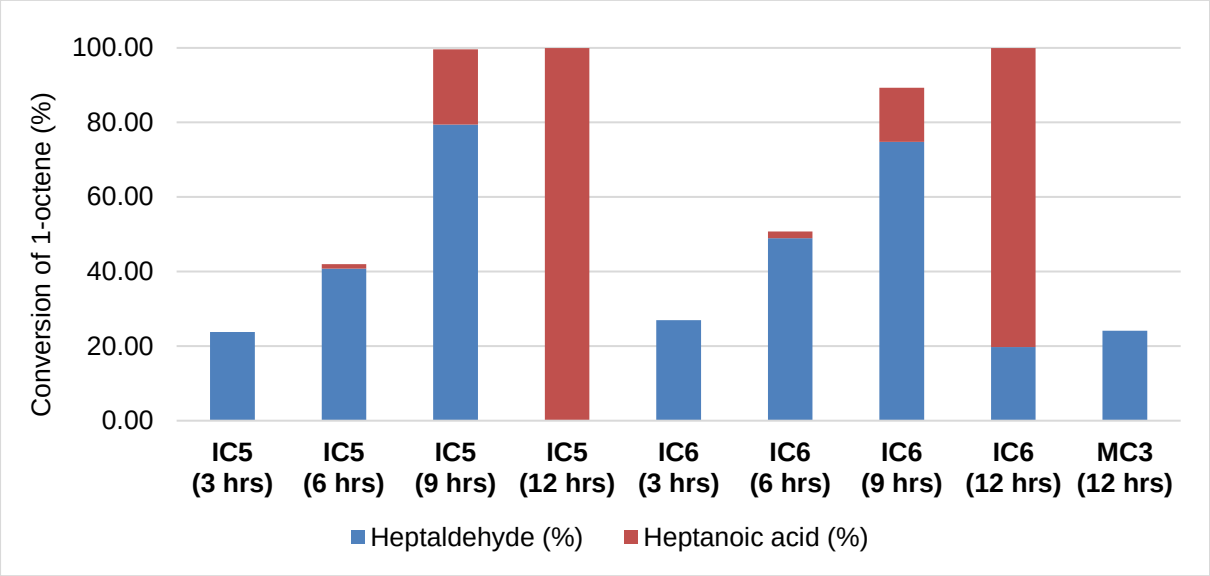

Figure 4.7: Conversion and product selectivities obtained in the oxidative cleavage with immobilized catalysts, IC5-IC6, and model catalyst, MC3.

Overall, comparison of all the catalysts show that the model catalyst **MC2** and immobilized catalysts **IC3** and **IC4** convert the substrate in a shorter time than the other catalysts, with 100% of 1-octene being converted after 6 hours as opposed to 9 or 12 hours. The model catalyst (**MC2**) bearing the pyridine N-oxide ligand shows complete conversion of 1-octene after 6 hours. This is significantly better than the performance of the N,N pyridine triazole (**MC1**) and quinolone triazole (**MC3**) model catalysts which only convert between 7-24% of 1-octene after a 12 hour reaction period. The immobilized complexes **IC1-IC2** and **IC5-IC6** perform drastically better than their model counterparts over a 12 hour reaction period. When we compare the results obtained with our pyridine-triazole and quinoline-triazole based catalysts to oxidative cleavage results reported previously in our group with pyridine-imine and quinoline-imine based catalysts, we see that the triazole based systems do not perform as well as the imine based systems. Complete conversion of 1-octene, mostly to heptanoic acid, was achieved after a 6 hour reaction period at a 0.05 mol% catalyst loading with the pyridine-imine and quinoline-imine complexes immobilized on MCM-41 and SBA-15. The pyridine-triazole and quinoline-triazole complexes immobilized on MCM-41 and SBA-15 could only achieve 100% conversion of 1-octene after a 12 hour reaction period. The triazole based systems do however still catalyse the oxidative cleavage reaction at a low catalyst loading of 0.1 mol% when compared with other ruthenium systems in the literature. In Chapter 1 we reported that known homogeneous systems based on ruthenium complexes require between 0.5-5 mol% catalyst loading for alkene oxidative cleavage reactions.

Heterogeneous systems based on ruthenium require between 1-3 mol% metal loading to perform oxidative alkene cleavage reactions.

4.4 Effect of native silica and phase transfer for immobilized catalysts

4.4.1 Evaluation of model catalysts MC1-3 at higher catalyst loadings

In experiments previously conducted by other members of our group.[11] It was noted that the immobilized catalysts performed better than their model counterparts. In order to investigate the cause of this enhanced activity, experiments were conducted where native silica was added to the reaction mixture together with a model compound as catalyst. An increase in the rate of the reaction was noted when native silica was added, however the increase was not as drastic as for the complex immobilized on mesoporous silica.[11]

In light of the above, it was decided to probe our system using a similar experiment. In order to be able to observe a significant change in conversion we needed the model catalysts to show appreciable conversion. It was decided to conduct reactions with the model compounds at a 0.5 mol% catalyst loading (previous experiments were conducted at a 0.1 mol% catalyst loading) over a 24 hour period.

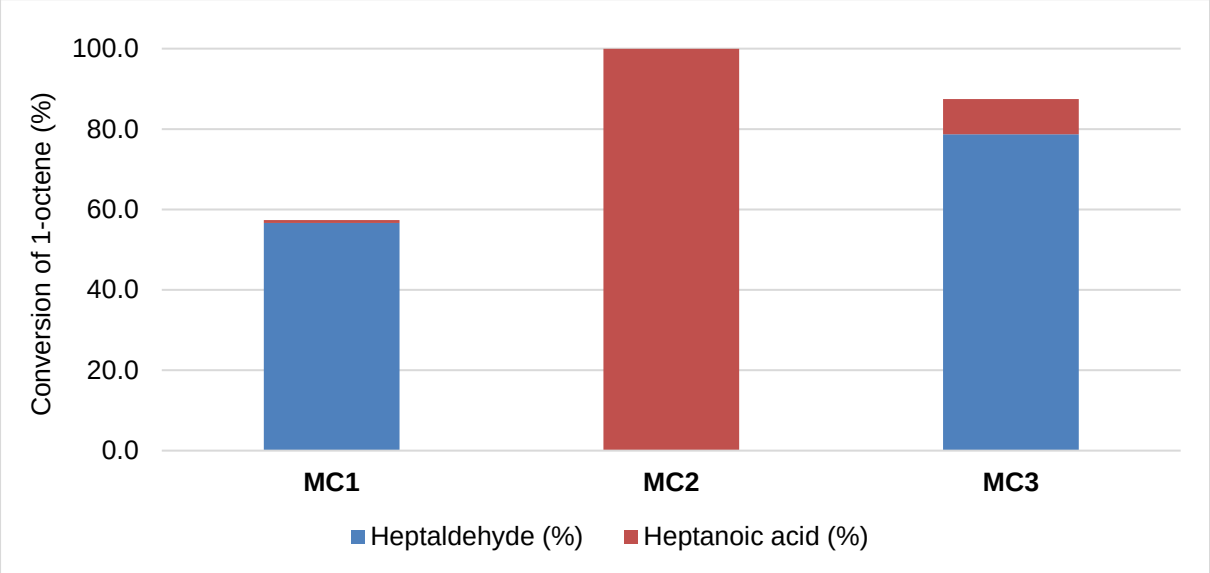

Figure 4.8: Conversions and product selectivities obtained with model complexes MC1-MC3 at a 0.5 mol% catalyst loading.

The increase in catalyst loading was necessary to obtain appreciable conversions with the N,N model complexes **MC1** and **MC3**. The results of this are shown in Figure 4.8. As expected, model complex **MC2** shows complete conversion of 1-octene to heptanoic acid over this time period. Model complexes **MC1** and **MC3** on the other hand show conversions of 58% and 87% respectively, with mainly the aldehyde product being formed. Based on these results, model complex **MC1** was selected for experiments involved in the investigation into the effect of silica.

4.4.2 Investigation into the effect of silica and phase transfer in the oxidative cleavage of 1-octene

In order to fully investigate the effect of silica in the oxidative cleavage of 1-octene it was decided to employ and compare various catalytic systems. Of the four systems evaluated, the first system utilizes model complex **MC1** under the standard reaction conditions developed for the oxidative cleavage of 1-octene. The second system involves the use of "mixed" systems, **MX1** and **MX2**, where native MCM-41 and SBA-15 respectively, are added to the reaction mixture together with the model complex **MC1**. The third system evaluates the catalytic ability of model complex, **MC1** physically adsorbed onto MCM-41 and SBA-15 giving rise to the adsorbed catalyst systems **AC1** and **AC2** respectively. The last system used, involves the oxidative cleavage of 1-octene, carried out with model complex **MC1**, in the absence of CCl_4. It should be noted that all these reactions were conducted using a reaction time of 24 hours, with a 0.5 mol% catalyst loading.

The results of the catalytic investigations using the above mentioned systems are depicted in Figure 4.9. It should be noted that when carrying out a control reaction in the absence of catalyst no product formation was observed. Additionally, reactions carried out in the absence of catalyst but in the presence of native silica and oxidant also yielded no products. Reactions carried out using only pure **MC1** as catalyst resulted in 57% conversion of the substrate. However when native silica was added to the reaction mixture already containing **MC1**, no significant change was observed in the conversion, with 59% and 55% conversion of 1-octene conversion being obtained for **MX1** and **MX2** respectively. This then seemed to indicate that the support material on its own was not directly responsible for an increase in activity of the immobilized ruthenium catalysts and that the increased activity was more likely due to the actual immobilization of the catalyst on the mesoporous silica support.

It was previously observed that when performing oxidative cleavage reactions with immobilized catalysts, **IC1-IC6**, the heterogeneous catalysts appear to have

hydrophilic-like characteristics such that the major fraction of the silica material tended to migrate to the water layer of the biphasic reaction mixture. It is well known that silica is a hydrophilic material due to the abundance of hydroxyl groups on the silica surface.[12–15] Ordered mesoporous materials are ideal for the adsorption of guest molecules due to their uniform pore sizes, large surface area and the free silanol groups on the support surface. Various chemical species can be adsorbed within the pores of the support or on the support surface. The guest molecule is retained on the support through weak hydrogen bonds between the surface silanols and the guest molecule. Mesoporous silica has therefore often been used to attempt to increase the solubility and dissolution rate of molecules that are poorly water-soluble.[14] Silica has also been used to overcome solubility issues faced in biphasic catalysis, through serving as a hydrophilic support for liquid-phase catalysts and enhancing reaction rates by increasing the liquid-liquid interfacial area between immiscible solvents.[15]

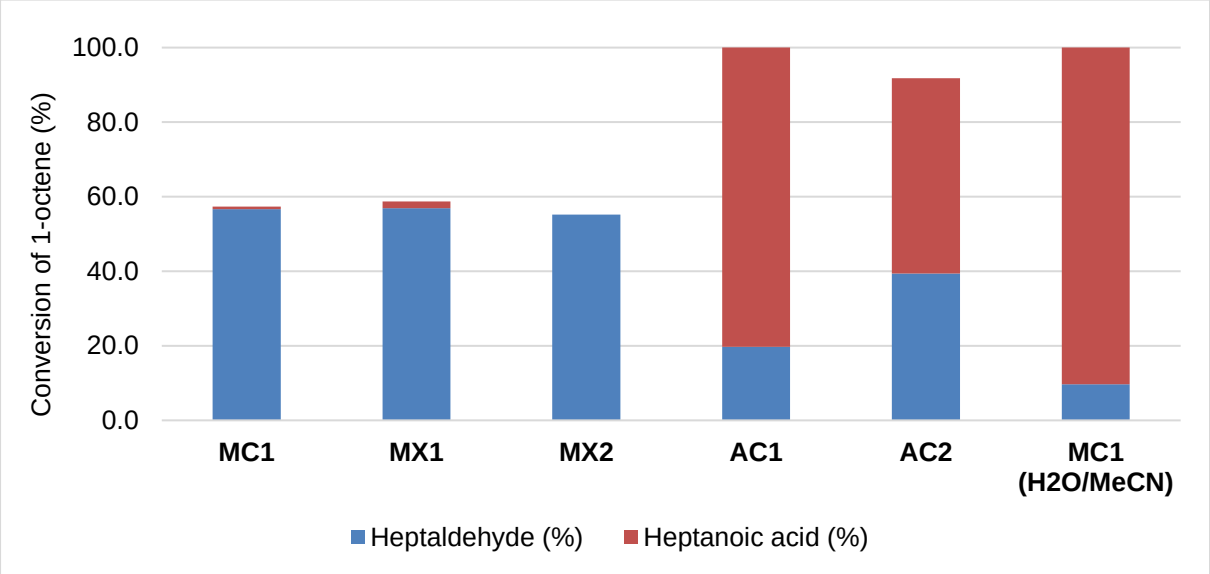

Figure 4.9: Results obtained from the investigation into the effect of silica.

After the results obtained with **MC1**, **MX1** and **MX2** in which the model catalyst was used in the presence of native silica it was then suspected that the increased activity observed for the immobilized complexes could possibly be due to the hydrophilic nature of mesoporous silica which causes the silica to migrate to the aqueous phase. In the case of the adsorbed catalysts, this allows for the transfer of the ruthenium complex, which is immobilized on the support, from the organic CCl_4/MeCN phase into the water phase in which the oxidant is dissolved. This facilitates close contact between the ruthenium pre-catalyst and the oxidant, $IO(OH)_5$, in the water layer thus promoting the formation of the active species, RuO_4. In

contrast, in the case where pure model complexes are used, the complexes are soluble in the organic phase (CCl_4/MeCN), and therefore the ruthenium pre-catalyst takes longer to come into contact with $IO(OH)_5$ in the water layer. Thus the formation of RuO_4 is essentially slowed down. Looking again at Figure 4.9 we see that the conversion of 1-octene (between 92-100%) obtained with the adsorbed catalysts, **AC1** and **AC2**, far exceeds the conversions obtained with **MC1**, **MX1** and **MX2**. Similarly to the immobilized catalysts, **IC1-IC6** which were discussed earlier, the adsorbed catalysts could also be observed in the water layer of the biphasic mixture and therefore the rate of RuO_4 formation using the former is faster.

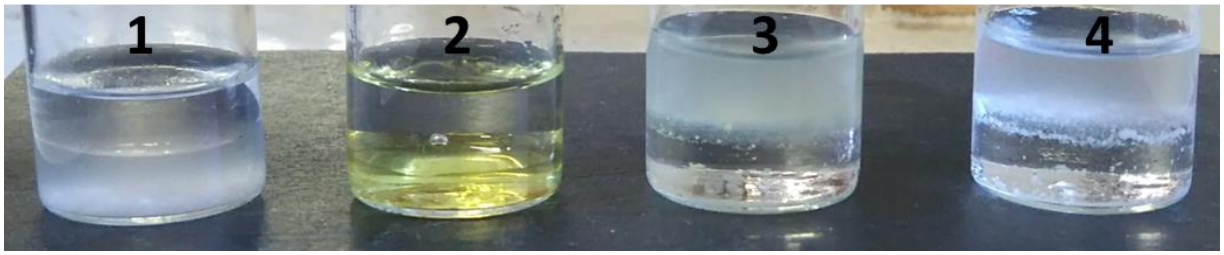

Figure 4.10: Depiction of hydrophilic silica in the aqueous phase of biphasic solvent mixtures (1 = MCM-41 + H_2O/Ether; 2 = Model complex MC1 + CCl_4/MeCN/H_2O; 3 = Immobilized complex IC1 + CCl_4/MeCN/H_2O; 4 = MCM-41 + CCl_4/MeCN/H_2O).

Figure 4.10 shows a visual depiction of the mesoporous silica preferring the aqueous phase in biphasic reaction mixtures. In mixture number **1** we see that native MCM-41 prefers the water layer to the organic ether layer on top. Mixture number **2** shows that the model complex **MC1** remains in the organic phase in a mixture of CCl_4/MeCN/H_2O whereas in mixture number **3** we see that immobilized complex IC1 prefers the aqueous layer in this same solvent mixture. And again in mixture **4** we observe that native MCM-41 prefers the aqueous phase in a CCl_4/MeCN/H_2O solvent system. The results depicted in Figure 4.9 confirms that the mesoporous silica, MCM-41 and SBA-15, serve as some sort of solid state phase transfer agent for the immobilized ruthenium complexes thereby accelerating the formation of RuO_4 and the overall reaction rate for the oxidative cleavage of 1-octene. The last system evaluated, where the reaction was carried out in the absence of CCl_4, resulted in 100% of 1-octene being converted mostly into heptanoic acid. It is to be noted that MeCN and water are miscible under these conditions. This solvent mixture therefore allows for close contact between the ruthenium complex dissolved in the MeCN and periodic acid in the water, resulting in an acceleration of the reaction. However a major drawback of this system is that the catalyst is extremely unstable as shown by rapid decomposition to Ru black. The absence of CCl_4 resulted in a significant amount of ruthenium black being formed in the reaction vessel, as CCl_4 is necessary for the stabilization of RuO_4.

4.5 Active species in the oxidative cleavage of 1-octene: RuO_4

Previous reports in the literature including work from our own group indicate that the oxidative cleavage of alkenes is mediated by RuO_4, which is formed *in-situ* during the reaction.[7,11] For all these previously reported systems, the presence of RuO_4 was confirmed using UV-Vis spectroscopy. The presence of RuO_4 is detected as two characteristic peaks between 280-340 nm and 370-420 nm, and these peaks also possess a distinctive fine structure.[8,16]

We thus set out to establish whether RuO_4 was indeed an intermediate in the catalytic systems reported in this thesis. Ruthenium tetroxide was thus generated using the general oxidative cleavage reaction conditions in the presence of $RuCl_3 \cdot xH_2O$ and the absence of substrate. After a reaction time of 1 hour RuO_4 could be detected via UV analysis of the organic layer. The spectrum obtained in Figure 4.11 shows two characteristic peaks between 280-330 nm and 360-390 nm. The characteristic fine structure of the peaks can also be observed.

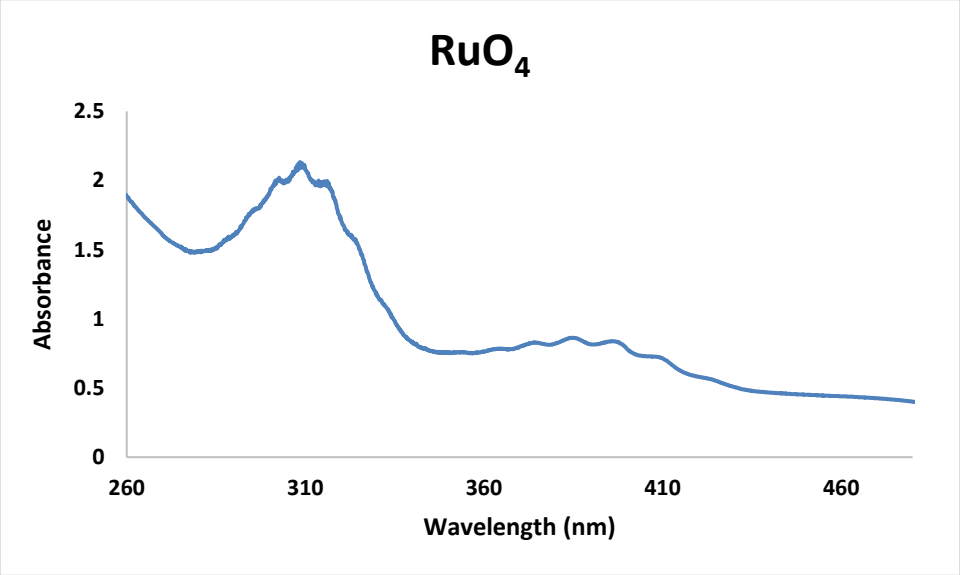

Figure 4.11: The UV-Vis spectrum indicating the formation of RuO_4 from $RuCl_3 \cdot xH_2O$.

Due to the fact that our immobilized complexes performed better than their model counterparts in the oxidative cleavage of 1-octene, it was decided to carry out the reaction with model complex, **MC2**, and immobilized complex, **IC4**. Reactions were carried out in the absence of substrate and the organic layer was sampled at different time intervals. The

times selected were 1, 3 and 5 hours given the fact that generally for the pyridine N-oxide systems studied in this thesis complete conversion of 1-octene could be observed after reaction periods of 6 hours and thus the active species, RuO_4, should form within this time frame.

The UV-Vis spectra obtained with model complex, **MC2**, are shown in Figure 4.12 below. At reaction times of 1 and 3 hours no change in the spectra are observed compared to the spectrum of **MC2** in solution. However after 5 hours the fine structure indicating the presence of RuO_4 is starting to be observed, as indicated by the arrows in the figure. It is to be noted that the absorbance of the model complex to some extent overlaps with the signal of RuO_4 causing the fine structure not to be observed with the same intensity as it is for the immobilized complex.

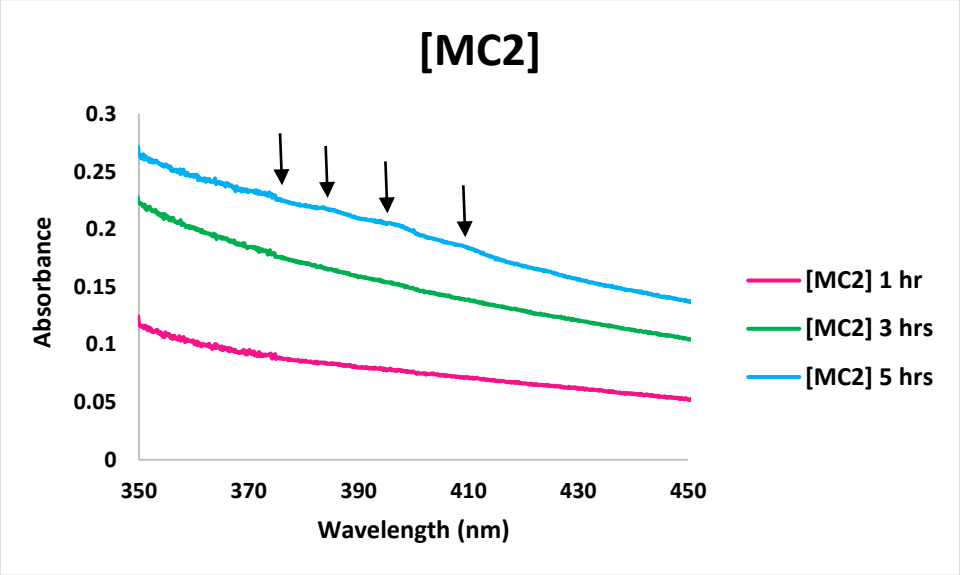

Figure 4.12: UV-Vis spectra of the organic layer of reaction mixtures using model complex, MC2, as catalyst.

The same procedure was followed using immobilized catalyst, **IC4**, and the spectra are shown in Figure 4.13. For the immobilized catalyst we distinctly observe the fine structure indicating the presence of RuO_4 after 3 and 5 hours. This then suggests that the RuO_4 active species forms faster for the immobilized system than is the case for the model system under similar reaction conditions. This explains the faster reaction rates for these immobilized catalysts.

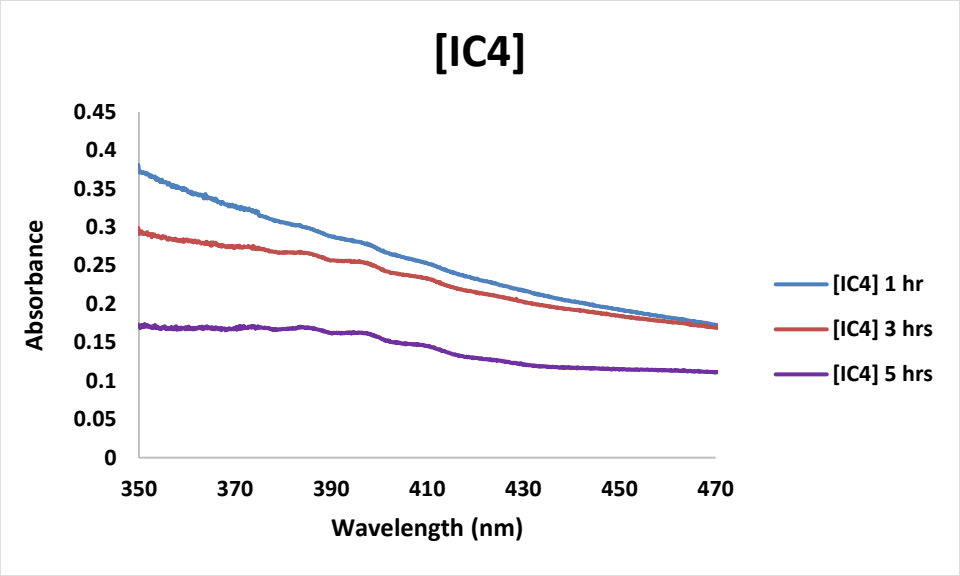

Figure 4.13: UV-Vis spectra of the organic layer of reaction mixtures using immobilized complex, IC4, as catalyst.

4.6 Possible mechanism for the oxidative cleavage of 1-octene

From experiments regarding the oxidative cleavage of 1-octene with our ruthenium catalysts, it can be seen that the results obtained are very similar to those obtained previously in our group for Ru complexes of diimine complexes. It therefore follows that the proposed mechanism for the oxidative cleavage using the triazole based complexes is similar to their diimine counterparts. A depiction of the proposed mechanism can be seen in Scheme 4.2. The first step in the cycle involves the oxidation of the ruthenium (II) complex in the presence of periodic acid to RuO_4. Although the exact means by which this transformation takes place is currently not fully understood, UV-Vis experiments confirm that the complex is indeed oxidized to the metal tetroxide. The alkene then coordinates to the RuO_4 to most likely form a ruthenium (VI) diester.[8] The existence of this metal diester as a key intermediate has not been experimentally confirmed for our system, however the existence of such a ruthenium cyclodiester has previously been detected by Albarella *et al.* in the reaction between RuO_4 and (-)-α-pinene performed in CCl_4.[17] It should be noted that to the best of our knowledge this is the only example where this type of ester has been isolated. The rearrangement of this cyclic ruthenium diester then affords the aldehyde as product in conjunction with RuO_2 which is then subsequently reoxidized in the presence of oxidant back to RuO_4. Once the aldehyde has been formed it is then oxidized to the carboxylic acid product.[8]

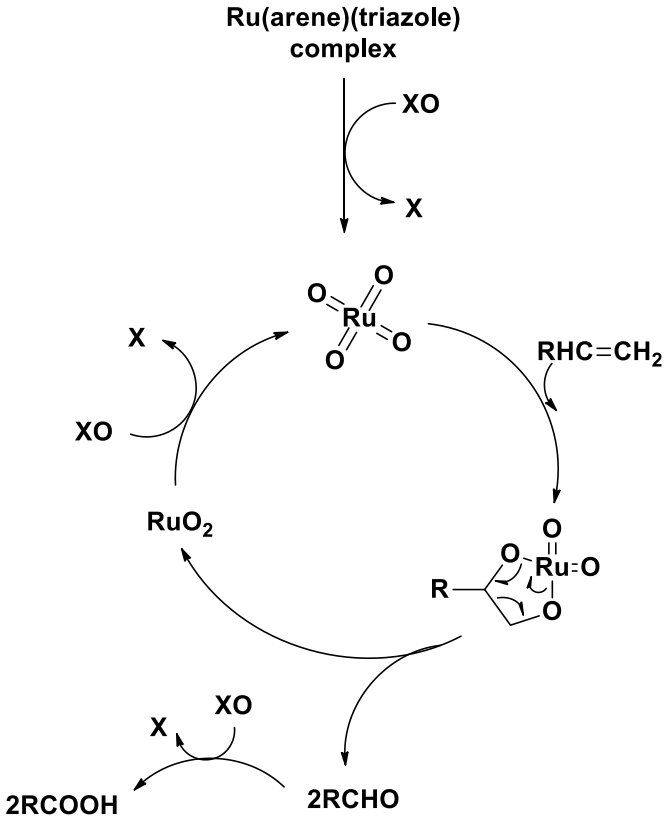

Scheme 4.2: Proposed mechanism for the oxidative cleavage of alkenes using a Ru(arene)(triazole) complex (R = C_6H_{13}; OX = oxidant).[11]

4.7 Possible reasons for the differences in activity of the ruthenium catalyst systems employed in the oxidative cleavage of 1-octene

Overall it would appear from results of the phase transfer experiments and UV-Vis analysis that the rate limiting step for the reaction is the formation of RuO_4 from the ruthenium pre-catalyst. The rate of formation of the tetroxide is largely influenced by the proximity of the ruthenium pre-catalyst and the oxidant due to the immiscible nature of the biphasic solvent mixture. Immobilization of the ruthenium complex on hydrophilic mesoporous silica therefore overcomes this barrier through transferring the ruthenium pre-catalyst from the organic phase into the water phase where the oxidant is present, allowing for a rapid formation of the active oxidizing metal species. It is also observed that both the model and immobilized N,O complexes catalyse the reaction faster than the N,N complexes. In Chapter 2 of this thesis we observed significant upfield shifts for the arene and triazole ligand protons in the N,O complexes. This suggests that there is a greater electron density on the metal centre for these complexes. This should lower the oxidation potential of the metal centre leading to the facile conversion of the Ru(II) species to Ru(VIII) as in RuO_4. Another observation is that the

complexes bearing quinoline triazole ligands performed slightly better than the complexes bearing pyridine triazole ligands. Quinoline (pK_b = 9.1) is slightly less basic than pyridine (pK_b = 8.8) which may cause the quinoline ligand to have a weaker coordination to ruthenium and thereby dissociate easier allowing the formation of RuO_4 to be faster than for the pyridine triazole containing complexes. In order to fully understand the differences in activity of the catalysts employed for the oxidative cleavage one would also have to subject these complexes to cyclic voltammetry to determine how the oxidation potentials differ for the two classes of complexes.

4.8 Concluding remarks

The model (**MC1-MC3**) and immobilized (**IC1-IC6**) ruthenium catalysts employed for the oxidative cleavage of 1-octene yielded heptaldehyde and heptanoic acid as products. The immobilized catalysts were more active than their model counterparts at a low catalyst loading of 0.1 mol%. The model and immobilized pyridine N-oxide triazole complexes were capable of converting 100% of 1-octene within 6 hours. The immobilized N,N (pyridine triazole and quinolone triazole) catalysts converted 100% of 1-octene after 12 hours, whereas their model counterparts converted between 7-24% of 1-octene after 12 hours.

The rate of formation of the tetroxide is largely influenced by the proximity of the ruthenium pre-catalyst to the oxidant due to the immiscible nature of the biphasic solvent mixture. Immobilization of the ruthenium complex on hydrophilic mesoporous silica overcomes this barrier by transferring the ruthenium pre-catalyst from the organic phase into the water phase where the oxidant is present, allowing for a rapid formation of the active oxidizing metal species. UV-Vis studies confirmed RuO_4 to be an important intermediate in the catalytic cycle in these reactions and is most likely the active species. It would also appear that the rate limiting step for the reaction is the formation of RuO_4 from the ruthenium pre-catalyst but kinetic studies are required to confirm this. Recycling of the immobilized catalysts was not attempted as it was observed that RuO_4 is formed in the reaction, which would result in the metal leaching off the support and into solution.

Overall, the catalyst systems evaluated show potential as catalysts for the oxidative cleavage of alkenes at very low catalyst loading of 0.1 mol% in relatively short reaction times.

4.9 Experimental section

4.9.1 General remarks and instrumentation

All reagents were acquired from Sigma-Aldrich or Fluka and used without any further purification. All solvents were purchased from Sigma-Aldrich or Kimix Chemicals, CCl_4 was used without further purification. Acetonitrile was purified by distillation over phosphorous pentoxide. Diethylether was purified by a Pure SolvTM Micro solvent purifier fitted with activated alumina columns.

A Radleys 12-stage carrousel parallel reactor equipped with a gas distribution system was used for the catalytic reactions. Samples were analyzed by a Varian 3900 GC fitted with a polar Cyclosil-B column (30 m, 0.250 mm diam. and 0.25 µm film) using helium as carrier gas. *p*-Xylene was used as internal standard.

4.9.2 Typical procedure for the oxidative cleavage of 1-octene

The catalyst, **ML1** (0.002 mmol), was added to a mixture of CCl_4 (1.25 mL) and MeCN (1.25 mL) in a parallel reactor tube. To the yellow mixture was added 1-octene (0.078 mL, 0.5 mmol) followed by a solution of oxidant, $IO(OH)_5$, (0.57 g, 2.5 mmol) dissolved in distilled water (2.5 mL). The biphasic reaction mixture was allowed to stir for the required time at 25 °C. The mixture was then extracted with diethyl ether (9 mL) and the organic layer dried over $MgSO_4$. The mixture was sampled (1 mL) and *p*-xylene (0.100 mL) added as internal standard for product quantification. Conversions were determined via GC.

4.9.3 UV-Vis analysis in the oxidative cleavage of 1-octene

Reactions were carried out under the general reaction conditions employed for the oxidative cleavage of 1-octene in the absence of substrate. At the appropriate time between 0.2-0.4 ml of the organic layer of the reaction was sampled and this was then diluted to a total volume of 3 ml with a 1:1 (v/v) MeCN/CCl_4 solvent mixture.

4.10 References

1 A. Rajagopalan, M. Lara and W. Kroutil, *Adv. Synth. Catal.*, 2013, 3321–3335.

2 S. N. Dhuri, K. Cho, Y. Lee, S. Y. Shin, J. H. Kim, D. Mandal, S. Shaik and W. Nam, *J. Am. Chem. Soc.*, 2015, **137**, 8623–8632.

3 T. Naota, H. Takaya and S. Murahashi, *Chem. Rev.*, 1998, **98**, 2599–2660.

4 V. Piccialli, *Molecules*, 2014, **19**, 6534–6582.

5 P. Spannring, P. C. A. Bruijnincx, B. M. Weckhuysen and R. J. M. Klein Gebbink, *Catal. Sci. Technol.*, 2014, **4**, 2182.

6 A. Haimov, H. Cohen and R. Neumann, *Interface*, 2004, 11762–11763.

7 A. G. F. Shoair and R. H. Mohamed, *Synth. Commun.*, 2006, **36**, 59–64.

8 H. Kotzé and S. Mapolie, *Appl Organometal Chem*, 2016, 1–13.

9 P. Carlsen, T. Katsuki, V. Martin and K. Sharpless, *J. Org. Chem.*, 1981, **46**, 3936–3938.

10 W. P. Griffith, A. G. Shoair and M. Suriaatmaja, *Synth. Commun.*, 2000, **30**, 3091–3095.

11 H. Kotze. Immobilized Ru(II) Catalysts for Transfer Hydrogenation and Oxidative Alkene Cleavage Reactions, Stellenbosch University, 2015, DOI: 10.1002/aoc.3643.

12 Y. Zhang, B. You, W. Hsu, C. Ren, X. Li and J. Wang, *Chem. Soc. Rev. Chem. Soc. Rev*, 2015, **44**, 315–335.

13 M. M. Van Schooneveld, E. Vucic, R. Koole, Y. Zhou, J. Stocks, D. P. Cormode, C. Y. Tang, R. E. Gordon, K. Nicolay, A. Meijerink, Z. A. Fayad and W. J. M. Mulder, *Nano Lett.*, 2008, **8**, 2517–2525.

14 V. Ambrogi, F. Famiani, L. Perioli, F. Marmottini, I. Di Cunzolo and C. Rossi, *Microporous Mesoporous Mater.*, 2006, **96**, 177–183.

15 B. M. Bhanage and M. Arai, *Catal. Rev.*, 2001, **43**, 315–344.

16 R. E. Connick and C. R. Hurley, *J. Am. Chem. Soc.*, 1952, **74**, 5012–5015.

17 L. Albarella, F. Giordano, M. Lasalvia, V. Piccialli and D. Sica, *Tetrahedron Lett.*, 1995, **36**, 5267–5270.

Chapter 5: Application of model and immobilized catalysts in the oxidation of *n*-octane

5.1 Introduction

The activation of alkanes is a desirable yet challenging process due to the inert nature of the carbon back bone, as well as the fact that the activated products are often more reactive than the alkane substrate which may lead to over oxidation of products. It is for this reason that extensive research in the fields of biocatalysis, heterogeneous and homogeneous catalysis is being carried out to develop catalytic systems capable of mediating the selective oxidation of hydrocarbon substrates.[1]

Saturated hydrocarbons, namely alkanes can be converted to more valuable oxygenates via oxidation reactions carried out by various homogeneous catalysts. These types of systems include complexes of first row metals[2] V, Mn, Fe, Co, Cu and late transition metals[3] such as Pt, Pd and Hg. Shul'pin & coworkers have done extensive research using the complexes of the group 8 metals Fe and Os as catalysts for alkane oxidation.[4] These systems include Os complexes bearing *p*-cymene ligands which have been found to be successful in the oxidation of alkanes such as *n*-octane.[5,6]

There are various multiphase catalytic systems which have been applied in the oxidation of linear alkanes, such as metal organic framework (MOF) materials[7], nanoparticles[8] and metal complexes[2] supported on inorganic supports such as mesoporous silica. An iron metal organic framework material, Fe-MOF-5, has been reported by Friedrich and co-workers and has been found to oxidize *n*-octane in the presence of hydrogen peroxide, with a substrate conversion of 10.5%.[7] An oxide, vanadium pentoxide, supported on magnesium and barium hydroxyapatite capable of oxidizing *n*-octane was reported by Friedrich *et al*.[9] There has also been research into montmorillonite supported Fe Schiff base complexes, by Bala and co-workers, capable of *n*-octane oxidation with a 7.4% conversion.[10]

Asefa *et al.* reported the synthesis of mesoporous silica-supported gold nanoparticles which were efficient in the oxidation of various alkyl-substituted benzenes and linear alkanes in the presence of *tert*-butyl hydroperoxide (TBHP).[8]

There are many catalytic systems where a metal complex is covalently anchored to the silica surface, one such example is silica supported Cu and Co Schiff base complexes reported by Ispir capable of cyclohexane oxidation with conversions as high as 91% for the copper complexes.[11] Mishra *et al.* have recently reported a recyclable rhenium complex immobilized on mesoporous silica, SBA-15, capable of oxidizing pentane (19.6% conv.) and hexane (22.6% conv.) in the presence of molecular oxygen.[2]

There are several homogeneous and heterogenous catalytic systems containing ruthenium which are capable of oxidizing alkanes. These systems were discussed extensively in Chapter 1 and provide evidence for the capability of ruthenium as an alkane oxidation catalyst.

This motivated us to explore the possibility of applying new model triazole ruthenium complexes (**MC1-MC3**) as well as their immobilized analogues (**IC1-IC6**) in the oxidation of *n*-octane. The results of the catalytic investigations are reported in the following sections.

5.2 Typical reaction conditions for the catalytic oxidation of *n*-octane

Preliminary investigations were conducted using conditions similar to those reported by Valodkar and co-workers. The authors synthesized ruthenium(III) complexes with N,O donor sites anchored on l-valine-bound styrene–divinyl benzene copolymer for the oxidation of cyclohexane in the presence of TBHP. The homogeneous complex, $Ru(L\text{-valine})_2Cl_2$, was generated *in-situ* and also evaluated in the oxidation of cyclohexane. Oxidation reactions were carried out for 24 hrs at 45 °C, with a cyclohexane:TBHP ratio of 2:5 and MeCN as solvent.[12] Several authors have used TBHP as the terminal oxidant for successful oxidation of alkanes with ruthenium catalysts.[13–16] Furthermore conducting the oxidation in the presence of air has proven to be beneficial for some alkane oxidation reactions using ruthenium catalysts.[14,16]

For the purpose of this study, *n*-octane oxidation reactions were initially carried out in air for 17 hrs at 60 °C, with an octane:TBHP ratio of 2:5 and MeCN as solvent (Scheme 5.1). Once the reaction was completed, the mixture was quenched on ice and subsequently sampled for GC analysis. Solvents other than MeCN were not tested as this solvent has been used successfully for several alkane oxidation reactions found in literature.[5,6,12,16] Another factor is the fact that the model complexes, **MC1-MC3**, employed as catalysts in our octane oxidation reactions have been found to be soluble and stable in MeCN for extended periods of time.

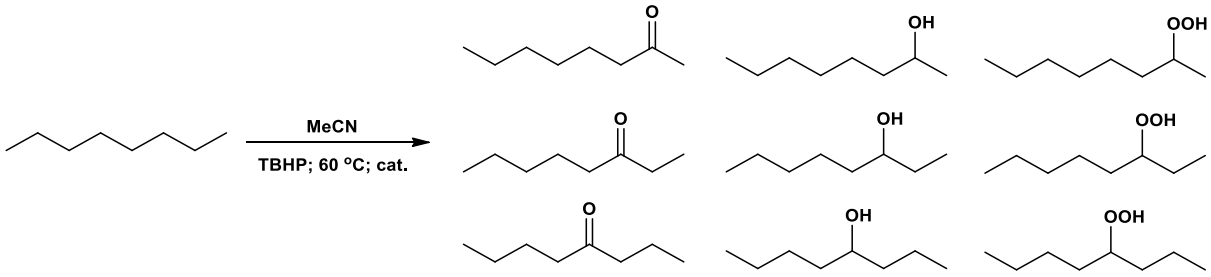

Scheme 5.1: Typical reaction conditions and products formed in the oxidation of *n*-octane.

It is to be noted that product yields reported throughout the following sections are based solely on the production of 2-, 3- and 4-octanone/octanol/octyl hydroperoxide (Scheme 5.1). Other peaks could be observed in the GC chromatograms which could not be identified and therefore not quantified. Other potential products evaluated as GC standards include 1-octanol, octanal and octanoic acid however none of these compounds were observed as products in the oxidation of *n*-octane.

The structures of the catalysts employed for this study include the model complexes (**MC1-MC3**) and immobilized complexes (**IC1-IC6**) depicted in Figure 5.1.

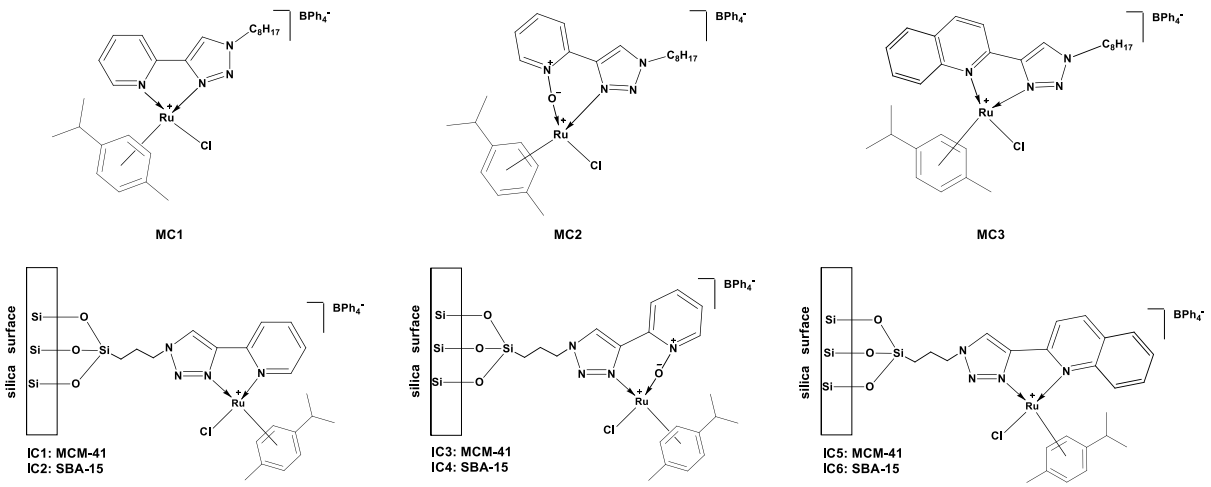

Figure 5.1: Catalysts employed for the oxidation of *n*-octane.

5.3 Optimization of reaction parameters in the oxidation of *n*-octane

The reaction parameters were optimized using model catalyst, **MC1**. The main finding are summarized below.

5.3.1 Effect of catalyst loading

The first parameter that was varied in the oxidation of *n*-octane was that of the catalyst loading. On account of the fact that ruthenium is a relatively expensive metal it is desirable to obtain good turnover numbers at low catalyst loading. The results using the model complex **MC1** are shown in Figure 5.2. For these experiments the catalyst was tested at 0.1 mol%, 0.01 mol% and 0.001 mol%. From the results obtained it can be observed that the yield of oxygenated products (specifically 2-, 3- and 4-octanone) decreases as the catalyst loading decreases.

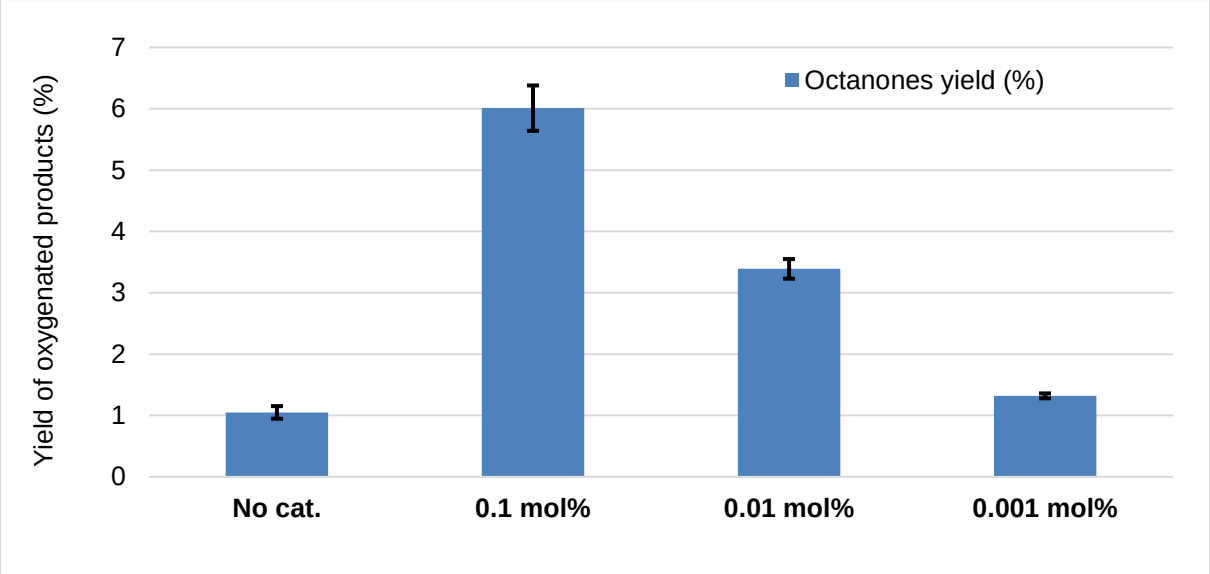

Figure 5.2: Product yield and selectivities obtained in the absence of catalyst and at different loadings of catalyst MC1 in the oxidation of *n*-octane. Reaction conditions: octane:TBHP (2:5); MeCN (solvent); 60 °C; 17 hrs.

From the product yields observed at different catalyst loadings the respective turnover over numbers (TON) can be calculated. The TON is calculated as the mmol of oxygenates formed divided by the mmol of catalyst employed. The TON's at the different loadings are reported in Table 5.1. It is to be noted that the TON's were calculated using the product yields obtained after correcting for the mmol of products formed in the absence of catalyst (approximately 1.05 % octanones). It can be observed that the TON increases as the catalyst loading decreases. The most noticeable increase is from a TON of 43 at 0.1 mol% catalyst to a TON of 184 at a 0.01 mol% catalyst loading.

On decreasing from 0.01 mol% to 0.001 mol% we observe that the TON almost doubles, however the yield of octanones obtained at a 0.001 mol% loading is very close to that obtained in the absence of catalyst.

Table 5.1: Product yields and Turnover Numbers (TON) obtained at different loadings of catalyst MC1 in the oxidation of *n*-octane.[a]

Catalyst loading (mol %)	Yield of products (%)[b]	TON[c]
0.1	6.01	43
0.01	3.39	184
0.001	1.32	341

[a] Reaction conditions: octane:TBHP (2:5); MeCN (solvent); 60 °C; 17 hrs. [b] Yields based on 2-, 3- and 4-octanone. [c] TON = mmol products/mmol catalyst; TON calculated after subtraction of product yield formed in the absence of catalyst (1.05 % consisting of 2-, 3- and 4-octanone)

For this reason a 0.01 mol% catalyst loading was chosen as the optimum loading due to the fact that it yields a higher TON compared to 0.1 mol% catalyst, as well as the fact that there is a distinct difference of about 2.34 % in the product yield compared to a loading of 0.001 mol% which yields products in a similar percentage range to that obtained in the absence of catalyst.

5.3.2 Effect of reduction with Triphenylphosphine

Shul'pin published a review regarding alkane oxidation in which he discussed a method for reducing alkyl hydroperoxides produced in alkane oxidation reactions. The reason for doing this is because alkyl hydroperoxides cannot be accurately quantified via GC due to the fact that they decompose during GC analysis. In the method developed by Shul'pin an excess of solid triphenylphosphine is added to reaction mixtures 10-20 minutes before analysis. The triphenyl phosphine reacts with alkyl hydroperoxides and reduces them to their corresponding alcohols. If the alkyl hydroperoxides are not reduced before GC analysis they will decompose to the corresponding ketones or alcohols in the GC injector. The decomposition products ratio (ketone:alcohol) for the alkyl peroxides in the GC injector, depends on various factors including the type of material of the injector, type of column, the stationary phase, etc. Comparison of the GC chromatogram obtained before and after reduction allows one to determine the actual amount of alkyl hydroperoxide products present in the reaction mixture.

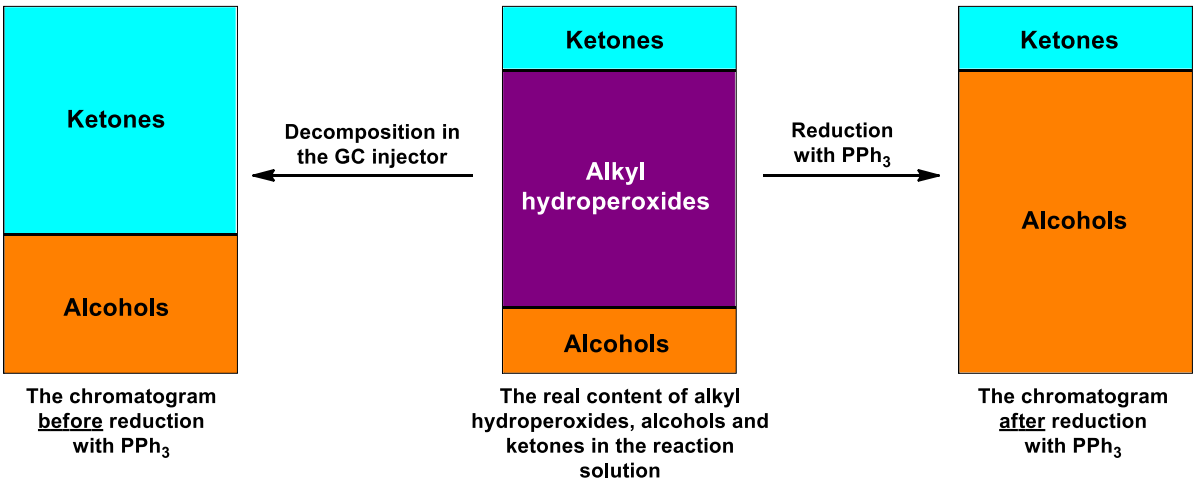

Scheme 5.2: The GC analysis of the mixture obtained in alkane oxidation before and after reduction with triphenyl phosphine. Method for determining the real concentration of alkyl hydroperoxides produced from the oxidation.[17]

As illustrated in Scheme 5.2 we observe that the chromatogram obtained before reduction gives a better indication of the true amount of alcohol products present, whereas the chromatogram obtained after reduction indicates the true amount of ketones present. The difference between ketone and alcohol products before and after reduction can therefore be attributed to the presence of alkyl hydroperoxide products.[17]

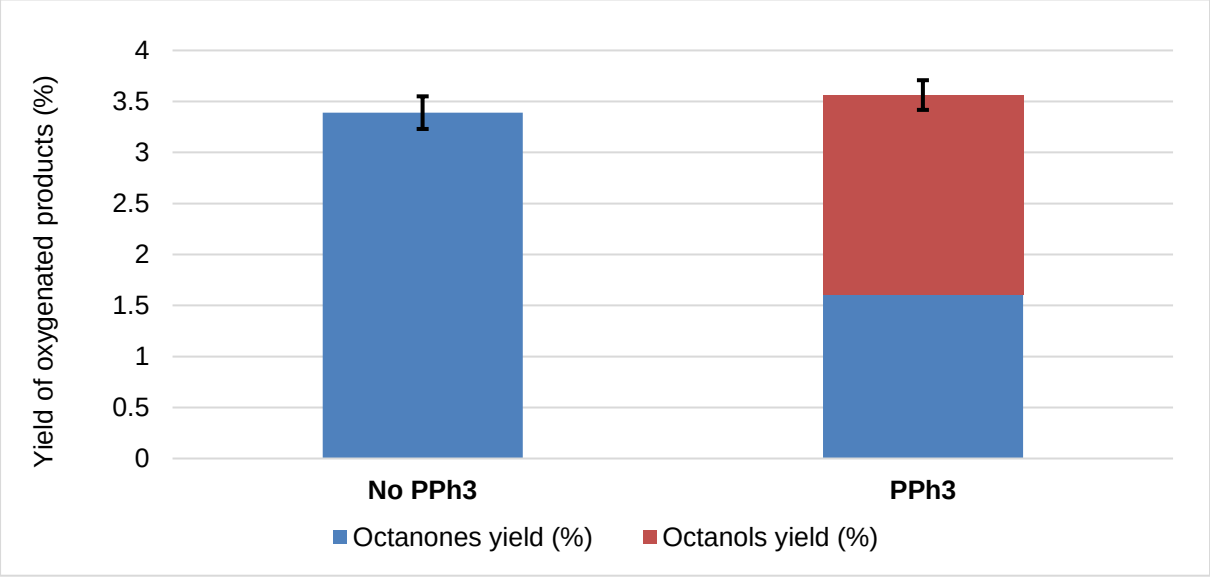

Figure 5.3: Product yield and selectivities obtained for catalyst MC1 in the oxidation of *n*-octane before and after reduction with triphenylphosphine. Reaction conditions: 0.01 mol% cat.; octane:TBHP (2:5); MeCN (solvent); 60 °C; 17 hrs.

In light of this information, it was decided to apply the above method involving reduction with excess triphenylphosphine to our reaction mixtures after octane oxidation with **MC1**. The results presented in Figure 5.3 show that only 2-, 3- and 4-octanone are present before reduction, whereas 2-, 3- and 4-octanone and 2-, 3- and 4-octanol can be observed after the reduction. This result indicates that no octanols are produced in our reaction mixtures, but rather only 2-, 3- and 4-octanone and 2-, 3- and 4-octyl hydroperoxide. It was decided from this point forward to reduce all samples with excess triphenylphosphine prior to GC analysis.

5.3.3 Effect of temperature

The next parameter that was varied in the oxidation of *n*-octane was the reaction temperature. Reactions were carried out in the absence of catalyst, as well as in the presence of catalyst **MC1** at different temperatures. Figure 5.4 shows a distinct increase in conversion with a corresponding increase in temperature, with no significant effect on the selectivity for octanones and octanols at the different temperatures. It can be observed that the best product yield, after taking into account the percentage of products produced in the absence of catalyst, is observed at a reaction temperature of 70 °C. Higher temperatures were not tested as temperatures above 70 °C approach the boiling point of MeCN. It was therefore decided to conduct reactions at 70 °C from this point forward.

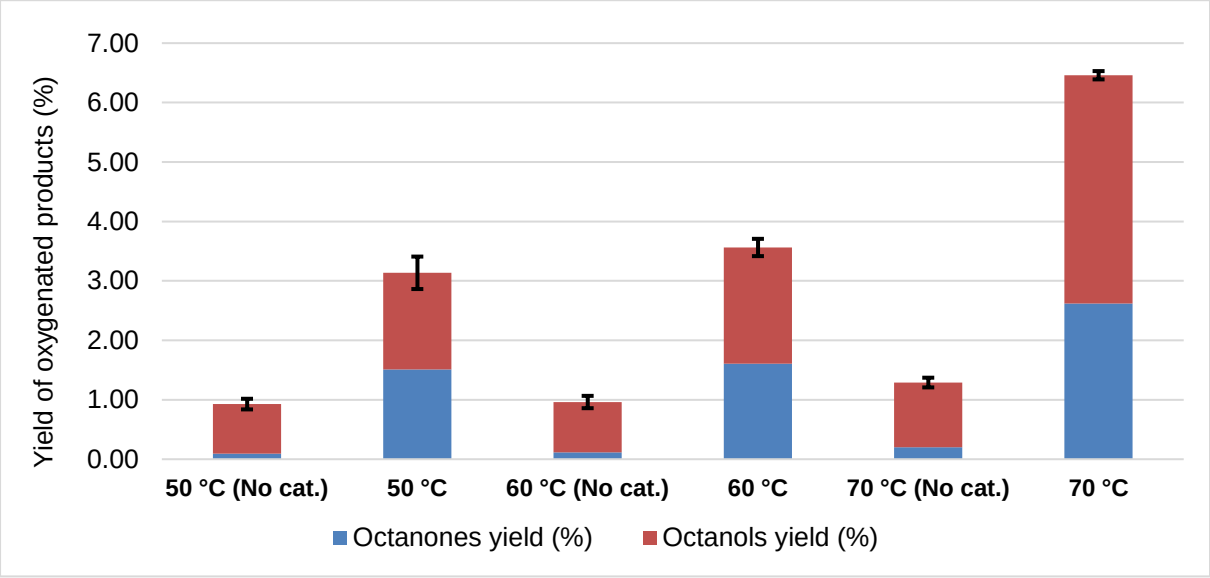

Figure 5.4: Product yield and selectivities obtained in the oxidation of *n*-octane at different temperatures in the absence of catalyst and with catalyst MC1. Reaction conditions: 0.01 mol% cat.; octane:TBHP (2:5); MeCN (solvent); 60 °C; 17 hrs.

5.3.4 Effect of oxidant concentration

The last parameter varied in the optimization of *n*-octane oxidation was that of the oxidant loading. In order to determine the contribution of the catalyst in the oxidation, the reactions were carried out in the absence of catalyst as well as with the catalyst **MC1** at different loadings of TBHP relative to octane (Figure 5.5).

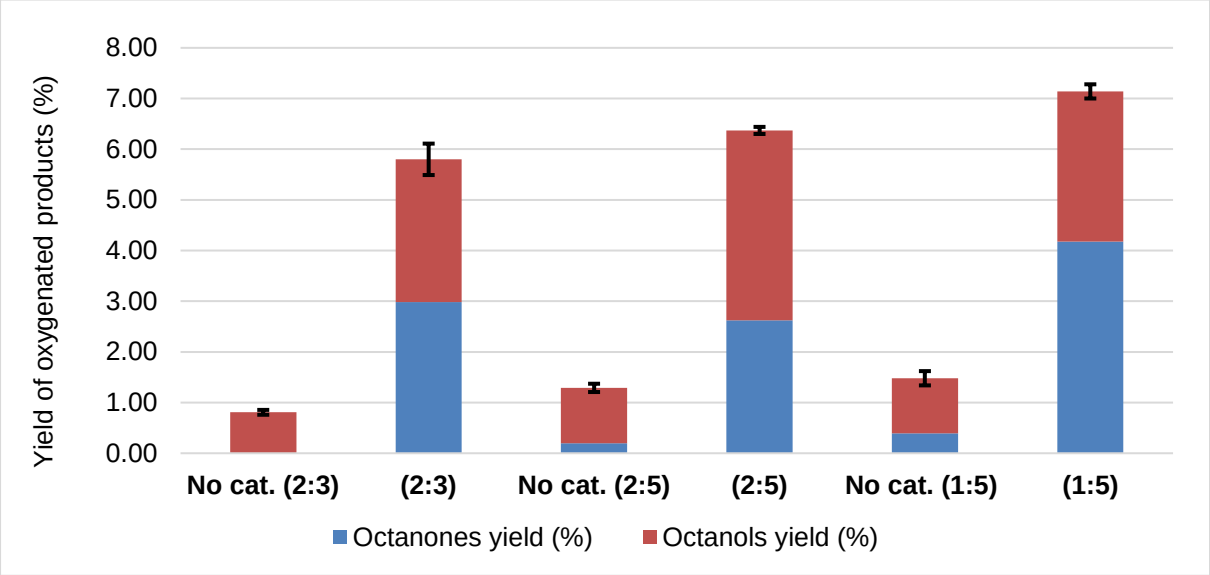

Figure 5.5: Product yield and selectivities obtained in the oxidation of *n*-octane at different oxidant loadings in the absence of catalyst and with catalyst MC1. Reaction conditions: 0.01 mol% cat.; MeCN (solvent); 70 °C; 17 hrs.

As shown in Figure 5.5 an increase in conversion is observed with a corresponding increase in TBHP concentrations, both in the absence of catalyst as well as in the presence of catalyst **MC1**. There appear to be some selectivity differences, with a slight preference for octanones at higher TBHP concentrations. It can be observed that the best product yield, after taking into account the percentage of products produced in the absence of catalyst, is observed at a 1:5 (octane:TBHP) loading. It was therefore decided to conduct reactions at this higher TBHP loading from this point forward. Higher TBHP concentrations were not investigated due to concerns regarding temperature control at higher reaction volumes.

5.4 Comparison of model catalysts (MC1-MC3) and immobilized catalysts (IC1-IC6) in the oxidation of *n*-octane

The model (**MC1-MC3**) and immobilized (**IC1-IC6**) catalysts were applied in the oxidation of *n*-octane. The results obtained for model catalysts, **MC1-MC3**, are shown below in Figure 5.6.

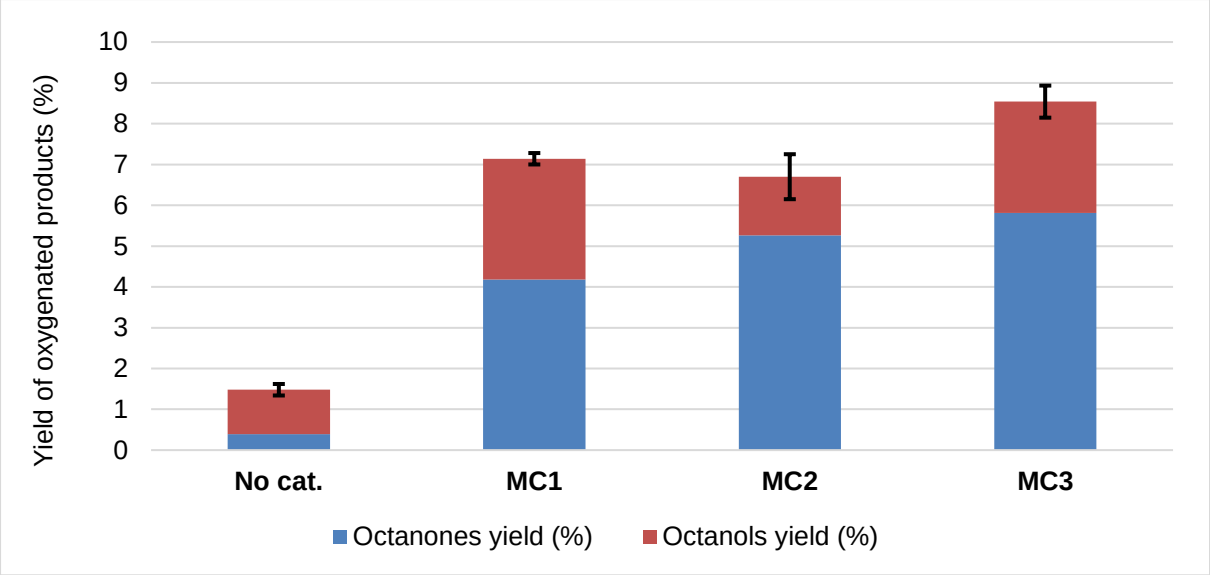

Figure 5.6: Product yield and selectivities obtained in the absence of catalyst and for model catalysts in the oxidation of *n*-octane. Reaction conditions: 0.01 mol% cat.; octane:TBHP (1:5); MeCN (solvent); 70 °C; 17 hrs.

All the model complexes tested catalyze the oxidation of *n*-octane, with the highest product yield observed for **MC3**. It can be observed that oxidation with **MC2** produces predominantly octanones, while **MC1** yields the largest relative percentage of octanols (reduced from octyl hydroperoxides). It is to be noted that throughout this chapter, reference to the yield of octanols is actually referring to the production of octyl hydroperoxides in the reaction mixture which are then reduced by triphenyl phosphine into the corresponding alcohols.

As can be seen below in Figure 5.7, the immobilized complexes (**IC1-IC6**) were also capable of catalyzing the oxidation of *n*-octane. The highest conversion was observed for **IC5** and **IC6** after 17 hrs with a 0.01 mol% catalyst loading. The native silica, MCM-41 and SBA-15, yield oxygenated products in the absence of ruthenium. The product yield observed for the native silica is about 4% more than the yield observed in the absence of any catalyst (No cat., Figure 5.6). No significant selectivity differences can be observed for **IC1-IC4**, whereas **IC5-IC6** show slight preference for the production of octanones.

No major differences in the product yield can be observed for complexes (bearing the same ligand scaffolds) immobilized on MCM-41 or SBA-15.

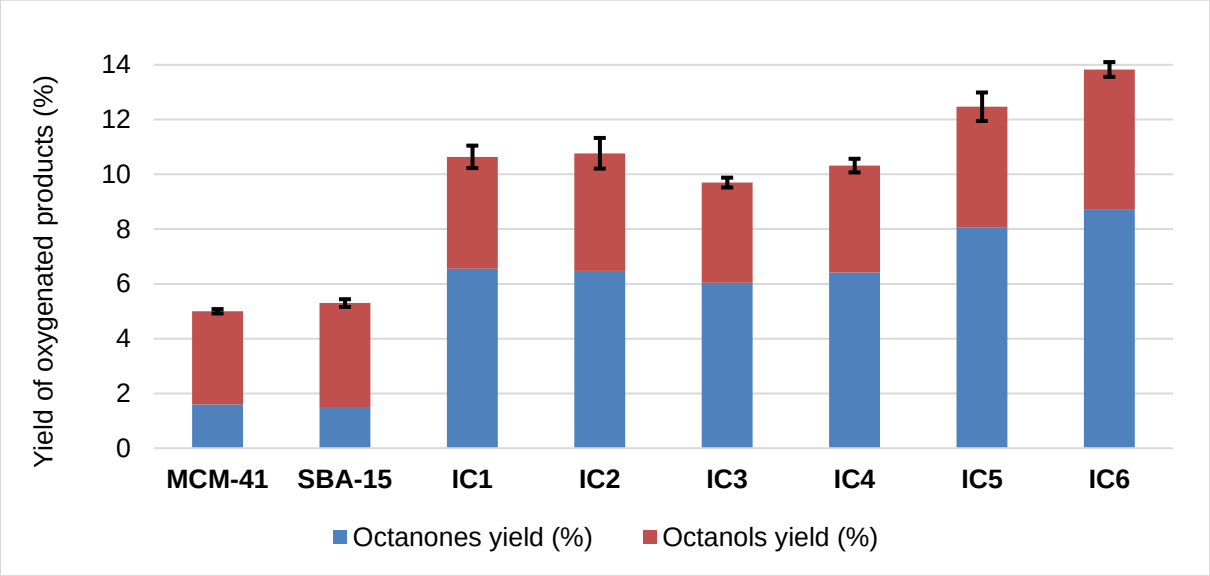

Figure 5.7: Product yield and selectivities obtained for native silica and immobilized catalysts in the oxidation of n-octane. Reaction conditions: 0.01 mol% cat.; octane:TBHP (1:5); MeCN (solvent); 70 °C; 17 hrs.

Overall, comparison of all the catalysts show that the immobilized catalysts **IC5** and **IC6** show the greatest 'net' yield of products (approximately 7.5 % and 8.5 % respectively). A general trend can be observed that the catalysts bearing the quinolone triazole ligand (**MC3**, **IC5** and **IC6**) provide the highest product yield, followed by the catalysts with the pyridine triazole ligand (**MC1**, **IC1** and **IC2**) and the pyridine N-oxide complexes (**MC2**, **IC3** and **IC4**) show the lowest product yield.

5.5 Effect of oxidant: TBHP vs H_2O_2

The oxidation of *n*-octane was carried out using **IC5** in the presence of hydrogen peroxide in order to compare the immobilized catalysts performance with a different peroxide as oxidant. As can be seen in Figure 5.8 only a small amount of *n*-octane is converted into oxygenated products (0.53 %). A dramatic drop in product yield is observed compared to the yield obtained with TBHP (12.5 %). It is to be noted that no octanols or octanones could be observed for the oxidation of *n*-octane with H_2O_2 in the absence of ruthenium catalyst, **IC5**. Another observation is that octanols, specifically 2-, 3- and 4-octanol, are selectively

produced in the presence of H_2O_2 whereas oxidation with TBHP yields a mixture of octanols and octanones (with a preference for the ketone product).

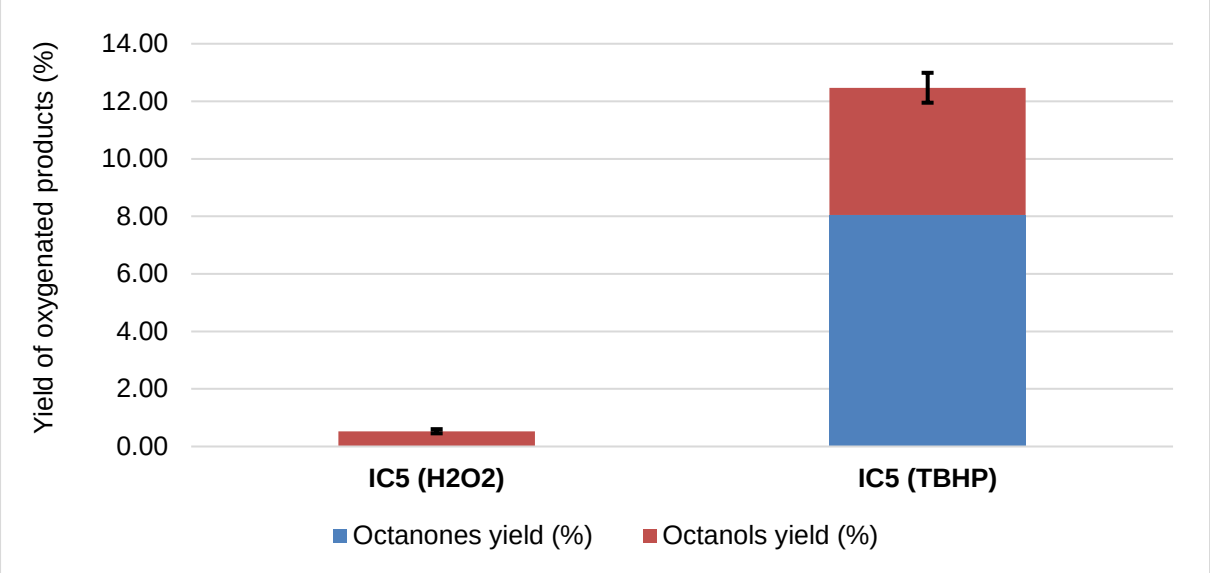

Figure 5.8: Product yield and selectivities obtained for immobilized catalyst IC5 in the oxidation of n-octane with different oxidants. Reaction conditions: 0.01 mol% cat.; octane:TBHP (1:5); MeCN (solvent); 70 °C; 17 hrs.

5.6 Oxidation of *n*-octane using IC5: Activity over time

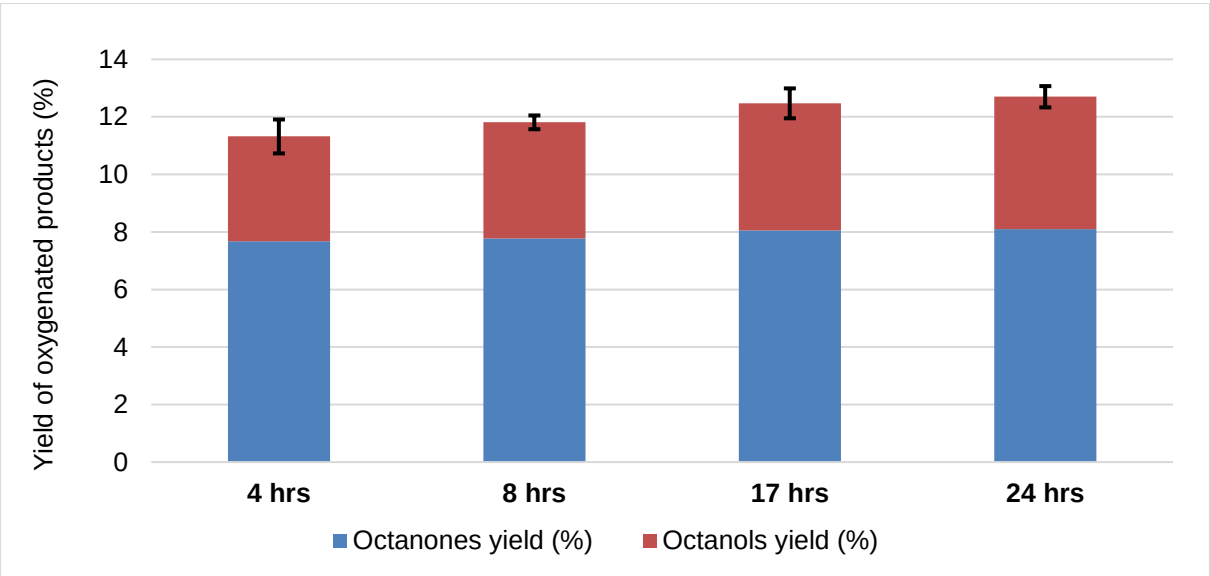

Figure 5.9: Product yield and selectivities obtained over time for immobilized catalyst IC5 in the oxidation of n-octane. Reaction conditions: 0.01 mol% cat.; octane:TBHP (1:5); MeCN (solvent); 70 °C.

The product yield obtained with immobilized catalyst, **IC5**, in the oxidation of *n*-octane over a 24 hour period was evaluated. It can be observed in Figure 5.9 that no significant increase in product yield is obtained between reaction times of 4, 8, 17 or 24 hours respectively. There does not appear to be a significant increase in activity between the time periods evaluated.

In order to determine whether or not the complex was possibly causing decomposition of TBHP in the early stages of the oxidation reaction, it was decided to divide the total TBHP loading into three portions and to add the three aliquots at different time intervals (specifically 0, 4 & 20 hours) over a 24 hour reaction period (Figure 5.10). Alas, the product yield obtained after the 24 hours was no different to the yield obtained when TBHP was added all at once at the start of the reaction. It can therefore be assumed that our complex does not decompose the TBHP to a significant extent, so as to be the cause of low activity at extended reaction times (within a 24 hour window).

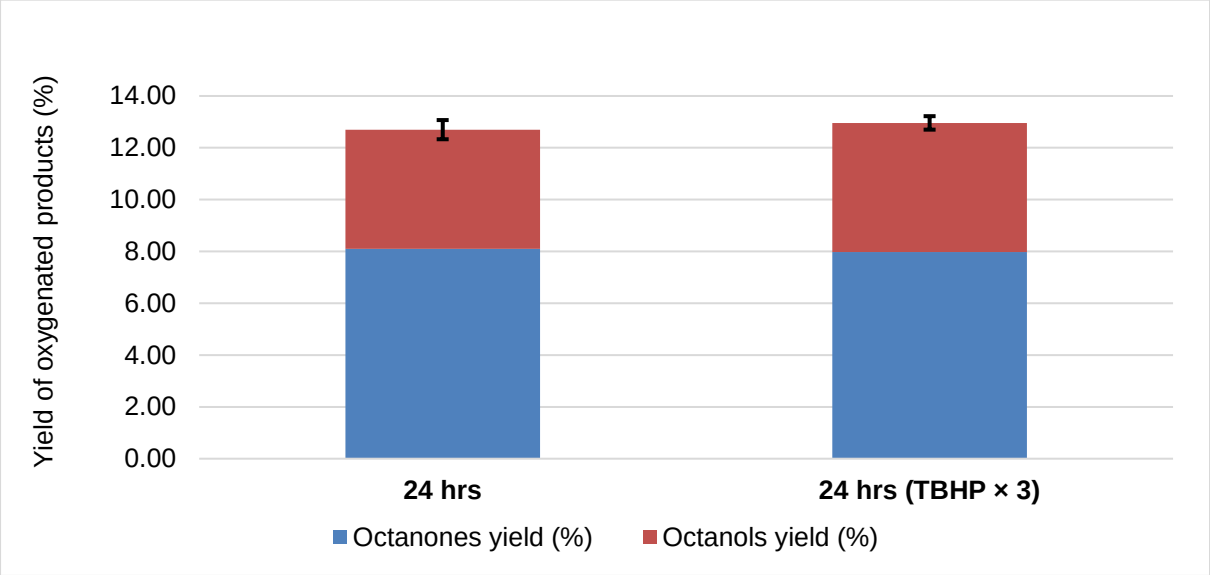

Figure 5.10: Product yield and selectivities obtained when TBHP is introduced in different ways in the oxidation of n-octane with immobilized catalyst IC5. Reaction conditions: 0.01 mol% cat.; octane:TBHP (1:5); MeCN (solvent); 70 °C.

5.7 Recyclability of immobilized catalysts in the oxidation of *n*-octane

The recyclability of catalysts **IC3-5** in the oxidation of *n*-octane was evaluated. These catalysts were selected in order to determine whether complexes immobilized on both MCM-41 and SBA-15 could be recycled (**IC3** and **IC4**) and also to determine whether complexes bearing N,N and N,O triazole ligands (**IC3** and **IC5**) could be recycled. From the results we see that all the catalysts could be recycled once with no drop in product yield (Figure 5.11).

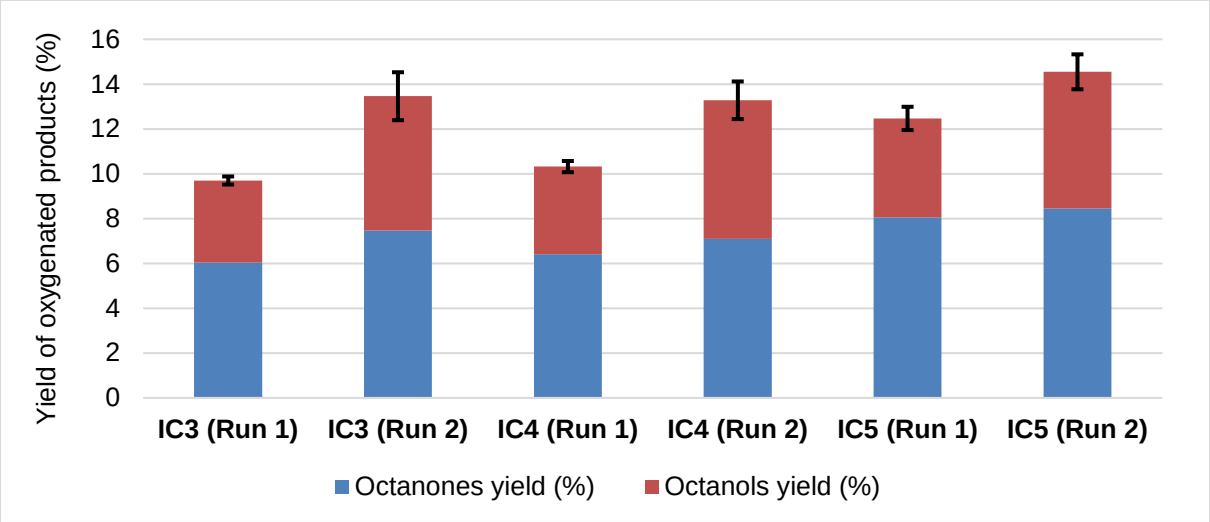

Figure 5.11: Product yield and selectivities obtained after one recycle (Run 2) of immobilized catalysts IC3-5 in the oxidation of n-octane. Reaction conditions: 0.01 mol% cat.; octane:TBHP (1:5); MeCN (solvent); 70 °C; 17 hrs.

The recycling process involves centrifuging the reaction mixture, followed by rinsing of the catalyst. The mixture is then centrifuged again, the supernatant decanted and the catalyst left to dry. This immobilized catalyst is then used as the catalyst for a new alkane oxidation reaction, where fresh substrate and oxidant are added. From the results in Figure 5.11, we see that **IC3** showed a significant increase in product yield after being recycled once (Run 2). It was therefore decided to recycle this catalyst for a second time.

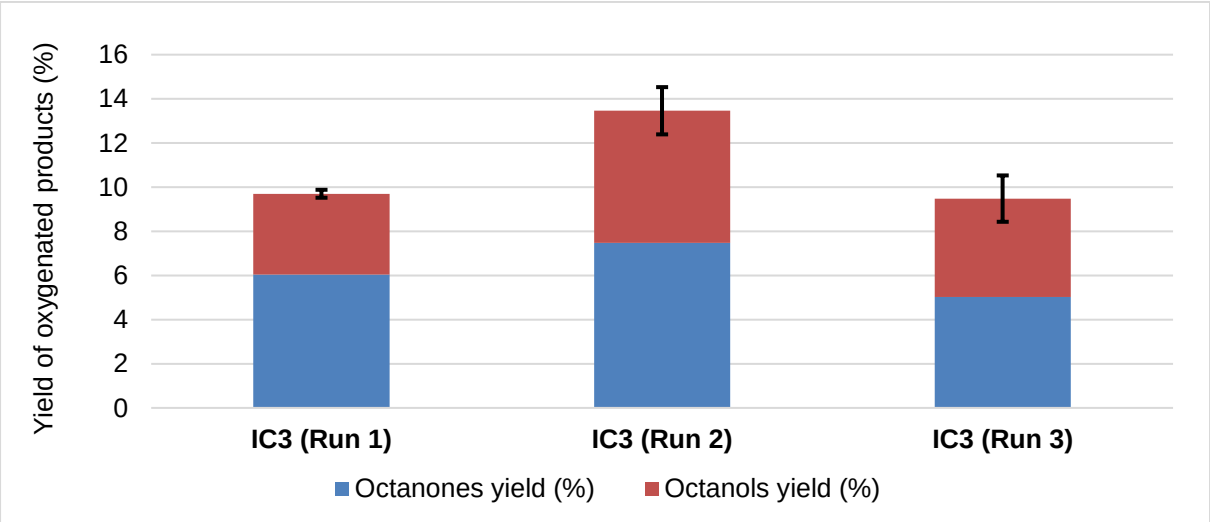

Figure 5.12: Product yield and selectivities obtained after two recycles (Run 2 & 3) of immobilized catalyst IC3 in the oxidation of n-octane. Reaction conditions: 0.01 mol% cat.; octane:TBHP (1:5); MeCN (solvent); 70 °C; 17 hrs.

We can see from the results in Figure 5.12 that the product yield decreases after the second recycling of **IC3** (Run 3 compared to Run 2). However, the product yield obtained after the second recycle is comparable to that obtained after the first reaction with **IC3** (Run 3 compared to Run 1). The fact that Run 2 affords a larger product yield than Run 1, would seem to indicate that there is perhaps an induction period during the first run to transform the catalyst precursor into the active catalyst. This species may then deactivate slightly over time, explaining the slight decrease in yield for Run 3 compared to Run 2. In order to get a comprehensive understanding of this, further experiments would need to be conducted.

5.8 Possible mechanism for the oxidation of *n*-octane

As discussed in Chapter 1, various researchers have attempted to study the mechanism for ruthenium catalysed alkane oxidation in the presence of TBHP. A common approach is the addition of a radical trapping agent during the oxidation reaction. Inhibition of the oxidation reaction in the presence of the radical trapping agent, supports the hypothesis that the oxidation is effected by ruthenium mediated decomposition of TBHP via a radical chain mechanism.

Kojima and co-workers developed a system using $[Ru^{II}Cl(L)]_2(ClO_4)_2$ dimers, where L=tris(2-pyridylmethyl)amine & tris(5-methyl-2-pyridylmethyl)amine, for catalytic alkane oxidation at 40 °C, with TBHP. In their system cyclohexane was oxidized to a mixture of cyclohexanol, cyclohexanone and *t*-butyl cyclohexyl peroxide. Addition of the radical trapping agent, 2,6-di-*tert*-butyl-4-methylphenol (BHT), at the start of the reaction resulted in the inhibition of the oxidation reaction. The authors determined that the oxidation is mediated by alkoxo (RO·) and alkylperoxo (ROO·) radicals generated via Haber–Weiss-type electron-transfer reactions. A ruthenium(II) species is responsible for the formation of the alkoxo and alkylperoxo radicals (Scheme 5.3, Equations 1 & 2). This then initiates a series of radical chain reactions (Scheme 5.3, Equations 3-8) which led to the oxidation of the alkane substrate.[16]

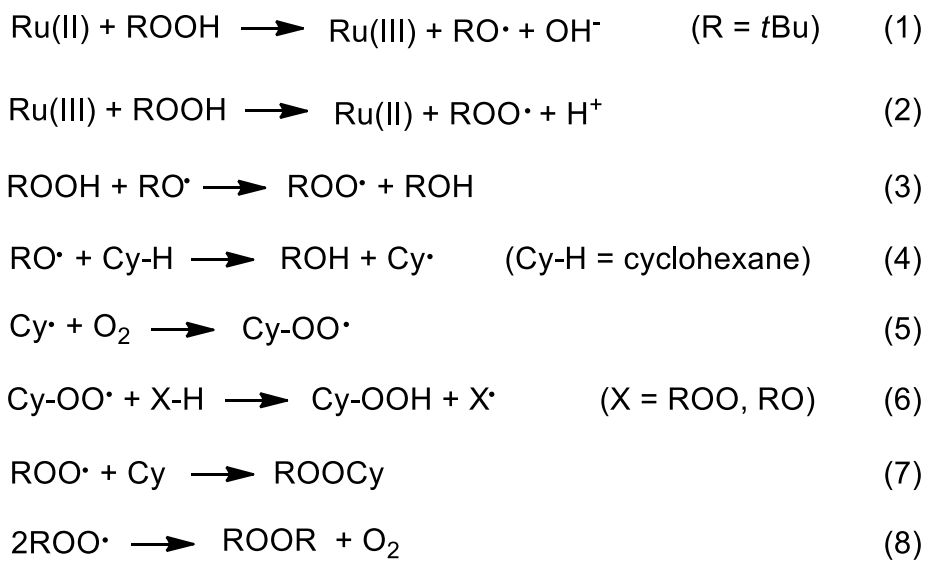

Scheme 5.3: Radical reactions initiated by ruthenium during alkane oxidation in the presence of TBHP.[16]

These researchers observed that the cyclohexanol:cyclohexanone ratio decreased over time, which therefore, implies that the cyclohexanol initially produced in the reaction is subsequently oxidized further to form cyclohexanone.[16] In our system this however does not appear to be the case as oxidation with **IC5** over time did not alter the octanol:octanone ratio. Whilst some mechanistic aspects of our system may be similar to that proposed by Kojima and co-workers, it would appear that two different processes governing the formation of octanones and octanols might exist in our system. It is thus unlikely that our catalytic system involves the over oxidation of alcohols to form the analogous ketones. The formation of ketones appear more likely to occur via a more direct route. This is akin to what was proposed by Patin and co-workers. The authors employed $RuCl_3 \cdot 3H_2O$, in a biphasic mixture of the substrate (as the organic layer) and water, with TBHP as terminal oxidant for the catalytic oxidation of cycloalkanes to their corresponding alcohols and ketones. It is proposed that the oxidation is carried out by a colloidal ruthenium species which is formed *in situ* during the reaction. It was initially thought that the oxidation proceeds via a radical chain mechanism initiated by the Haber-Weiss decomposition of TBHP. This resembles the Kojima mechanism discussed above. However, after the addition of the radical scavenger, dimethyl sulphide, it was observed that the oxidation was retarded but some oxidation still occurred. This provided evidence that a second oxidation pathway exists and it was proposed that this was most likely due to the presence of a high valent ruthenium oxo species (Scheme 5.4, Equations 6 & 7).[14]

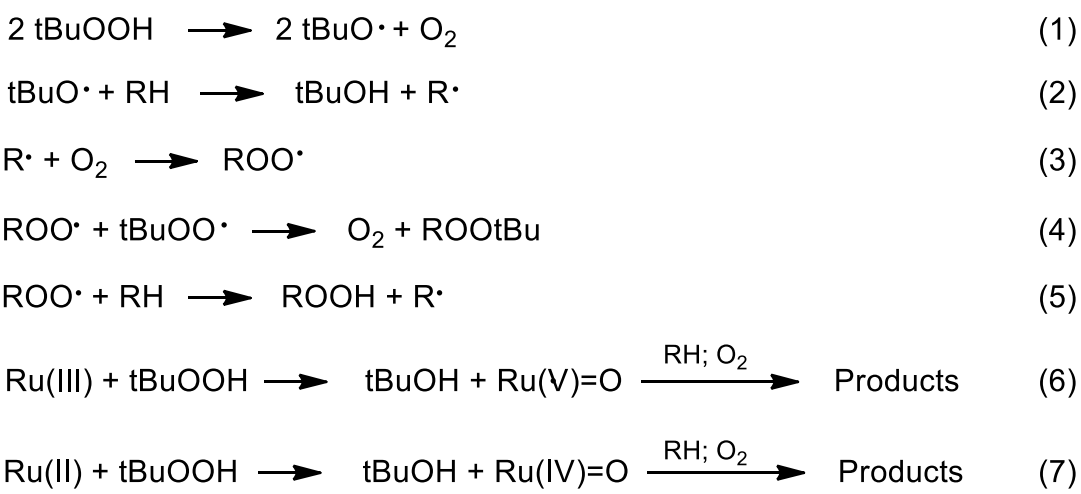

Scheme 5.4: Radical reactions and formation of oxo ruthenium species for alkane oxidation with TBHP (R = cyclooctyl). [14]

It is thus possible that a combination of the two oxidation pathways proposed by Patin and co-workers are operative in our oxidation system. Alternatively the octane oxidation reactions studied in this thesis may however follow a pathway which does not include radical chain reactions at all.

One such system was studied by Murali and co-workers who synthesised the Ru (III) complexes, $[Ru(ntb)Cl_2]Cl$ and $[Ru(ntb)Cl_2]ClO_4$ (ntb = tris-(benzimidazol-2-ylmethyl)amine), which were capable of cyclohexane hydroxylation in the presence of TBHP. The addition of BHT as radical trapping agent to the reaction did not inhibit the oxidation and no BHT oxidation products were observed. This thus confirmed that a radical mechanism was not operative in the system but rather a mechanistic pathway involving the formation of a ruthenium peroxide species $[Cl(ntb)Ru–O–O–tBu]^+$ which reacts with the C-H alkane bond directly. This is followed by heterolytic cleavage of the O–O bond to give rise to a $[Cl(ntb)Ru–O–R]^+$ species. This intermediate then reacts with H^+ and Cl^- to regenerate the catalyst and produce the alcohol product (Scheme 5.5).[18]

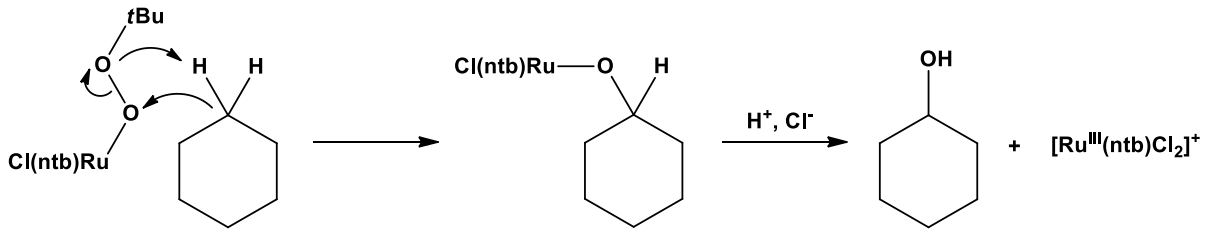

Scheme 5.5: Proposed mechanistic pathway for the catalytic oxidation of alkanes.[18]

If this mechanism was operative in our case then we should have seen alcohols as the main products, which is not the case. This particular mechanism is thus not the main reaction pathway for our catalyst system. It is also clear from surveying the literature that pinpointing the actual mechanism for the alkane oxidation reaction is a fairly complex exercise. At this stage, attempts at elucidating the mechanism for *n*-octane oxidation using the ruthenium complexes reported in this thesis is largely speculative. Also given the time constraints, such investigation into a detailed understanding of the behaviour of these catalysts from a mechanistic view was deemed beyond the scope of this thesis. If such a study should indeed be embarked on in the future, the following should be addressed. Firstly, complete identification of all components of the product stream is necessary. Secondly, a systematic study of the effect of radical trapping agents would need to be conducted to establish whether a radical pathway is operative using our catalyst system. Finally, a detailed kinetic study is required to get further insight into the mechanism of the reaction as well as the nature of the active species.

5.9 Concluding remarks

In conclusion the ruthenium model complexes (**MC1-MC3**) and their immobilized counterparts (**IC1-IC6**) catalyse the oxidation of *n*-octane, to afford octanones and octanols. A low catalyst loading of 0.01 mol% is required for these oxidation reactions. Reduction of reaction mixtures with an excess of triphenyl phosphine allowed for the estimation of the selectivity for octyl hydroperoxides in the reaction. The highest product yield (13.8 %) was achieved with immobilized catalyst **IC6** after 17 hrs. The oxidation was not very effective when attempting to employ hydrogen peroxide as terminal oxidant with less than 1% conversion observed. It was also found that the immobilized catalysts **IC4** and **IC5** could be reused once with no significant drop in product yield, while **IC3** could be recycled twice during which very little drop in product yield was observed. The catalysts evaluated in this thesis show great potential for use in alkane oxidation, however a more detailed study is required before the full potential can be fully exploited.

5.10 Experimental section

5.10.1 General remarks and instrumentation

All reagents were acquired from Sigma-Aldrich or Fluka and used without any further purification. All solvents were purchased from Sigma-Aldrich or Kimix Chemicals. Acetonitrile was purified by distillation over phosphorous pentoxide.

A Radleys 12-stage carrousel parallel reactor equipped with a gas distribution system was used for the catalytic reactions. Products were analyzed on a Varian 3900 gas chromatograph containing a Cyclosil-β column (30 m x 0.25 mm x 0.25 µm). Valeric acid was used as internal standard.

5.10.2 Typical procedure for *n*-octane oxidation

The general procedure for the catalytic oxidation of octane is illustrated using model catalyst, **MC1** as an example.

To the catalyst, **MC1** (0.01 mol%), dissolved in MeCN (3 mL) was added octane (1 mL, 6.15 mmol) followed by a solution of oxidant (3.72 ml, 30.8 mmol, 80% TBHP in di-*tert*-butyl peroxide/water 3:2 solution) in a parallel reactor tube. The reaction mixture was heated to the required temperature and allowed to stir for 17 hrs. Within the first 20 minutes of the reaction, a production of gas from the reaction mixture was observed and the vessel was then vented several times during this initial time period. The mixture was then quenched on ice and EtOAc (9 ml) was added, followed by an excess of PPh_3 on ice (to reduce possible alkyl peroxides into alcohols). The mixture was sampled (1 mL) and valeric acid (0.100 mL) added as internal standard for product quantification. Conversions were determined via gas chromatography.

5.10.3 Typical procedure for catalyst recycling experiments

The reaction mixture is centrifuged for 20 minutes at 4000 rpm after completion of the reaction. The supernatant is then decanted and a mixture of ethyl acetate and MeCN (1:3, v/v) is added to the silica and this is then shaken vigorously. The mixture is then centrifuged again for 20 minutes at 4000 rpm and the supernatant is then decanted. The silica is then left to dry and used as the catalyst for the next oxidation reaction following the typical procedure for *n*-octane oxidation.

5.11 References

1 J. A. Labinger, *J. Mol. Catal. A Chem.*, 2004, **220**, 27–35.

2 G. S. Mishra, K. Machado and A. Kumar, *J. Ind. Eng. Chem.*, 2014, **20**, 2228–2235.

3 S. S. Stahl, J. A. Labinger and J. E. Bercaw, *Angew. Chemie - Int. Ed.*, 1998, **37**, 2180–2192.

4 V. R. Landaeta and R. E. Rodríguez-Lugo, *Inorg. Chim. Acta*, 2015, 1–27.

5 M. M. Vinogradov, Y. N. Kozlov, D. S. Nesterov, L. S. Shul'pina, A. J. L. Pombeiro and G. B. Shul'pin, *Catal. Sci. Technol.*, 2014, **4**, 3214–3226.

6 M. M. Vinogradov, L. S. Shul'pina, Y. N. Kozlov, A. R. Kudinov, N. S. Ikonnikov and G. B. Shul'pin, *J. Organomet. Chem.*, 2015, **784**, 52–61.

7 M. N. Cele, H. B. Friedrich and M. D. Bala, *Catal. Commun.*, 2014, **57**, 99–102.

8 A. V. Biradar and T. Asefa, *Appl. Catal. A Gen.*, 2012, **435**–**436**, 19–26.

9 V. D. B. C. Dasireddy, S. Singh and H. B. Friedrich, *"Applied Catal. A, Gen.*, 2013, **456**, 105–117.

10 E. Kadwa, M. D. Bala and H. B. Friedrich, *Appl. Clay Sci.*, 2014, **95**, 340–347.

11 E. Ispir, *Phosphorus. Sulfur. Silicon Relat. Elem.*, 2014, **189**, 1644–1655.

12 V. B. Valodkar, G. L. Tembe, M. Ravindranathan and H. S. Rama, *J. Mol. Catal. A Chem.*, 2004, **223**, 31–38.

13 A. J. Bailey, W. P. Griffith and P. D. Savage, *J. Chem. Soc. Dalton Trans.*, 1995, 3537–3542.

14 F. Launay, A. Roucoux and H. Patin, *Tetrahedron Lett.*, 1998, **39**, 1353–1356.

15 K. J. Balkus, M. Eissa and R. Levado, *J. Am. Chem. Soc.*, 1995, **117**, 10753–10754.

16 T. Kojima, H. Matsuo and Y. Matsuda, *Inorganica Chim. Acta*, 2000, **300**, 661–667.

17 G. B. Shul'pin, *J. Mol. Catal. A Chem.*, 2002, **189**, 39–66.

18 M. Murali, R. Mayilmurugan and M. Palaniandavar, *Eur. J. Inorg. Chem.*, 2009, **2009**, 3238–3249.

Chapter 6: Project summary and future prospects

6.1 Project summary

This study set out to synthesize some novel ruthenium complexes bearing arene and triazole ligands. Model and siloxane functionalized ligands, **ML1-ML3** and **SL1-SL3**, were successfully synthesized. The ligands **SL1-SL3** were designed in such a way as to allow the incorporation of a siloxane functionality into their structure. The reaction of these ligands with the ruthenium arene dimer, $[RuCl_2(p\text{-cymene})]_2$, in the presence of sodium tetraphenylborate afforded the model and siloxane functionalized cationic complexes **MC1-MC3** and **SC1-SC3** as stable yellow to dark golden yellow solids. The siloxane functionality is sometimes susceptible to partial hydrolysis and subsequent self-condensation in refluxing reaction mixtures containing traces of water. Thus the synthesis of compounds bearing this functionality is sometimes problematic. The incorporation and preservation of the siloxane functionality was therefore crucial for subsequent immobilization of these complexes onto mesoporous silica to generate catalysts that are potentially recyclable. IR and ^{1}H NMR spectroscopy were utilized throughout the synthetic process to validate that the siloxane functionality remained intact during the synthesis of the relevant ligands and complexes reported. For the siloxane functionalized ligand **SL2** it was observed that the siloxane functionality decomposed over time even in an inert atmosphere. The ligand was however stable within a two week period, during which proton NMR and IR analysis could be carried out and complexation of the ligand to the ruthenium precursor was successfully achieved. Complexation of the N,N' and N,O ligands could be confirmed using ^{1}H NMR spectroscopy.

The mesoporous silica MCM-41 and SBA-15 were synthesized according to literature procedures. The three siloxane functionalized complexes, **SC1-SC3**, were then successfully immobilized onto MCM-41 and SBA-15 to afford six immobilized catalysts, **IC1-IC6**. The model complex, **MC1**, was physically adsorbed onto MCM-41 and SBA-15 yielding two adsorbed catalysts, specifically **AC1** and **AC2**. The native MCM-41 and SBA-15 supports as well as all the mesoporous silica based catalysts were characterized using a range of solid state analytical techniques which confirmed that the mesoporous materials were suitable to be used as heterogeneous catalysts. The solid state characterization techniques include infrared spectroscopy, nitrogen adsorption/desorption (BET) surface analysis, low-angle

powder X-ray diffraction, transmission electron microscopy (TEM), scanning electron microscopy (SEM), thermal gravimetric analysis (TGA) and ICP-OES. The decrease in BET surface area, the increase in weight loss relative to the native silica obtained for TGA analysis and the presence of ruthenium on the supports confirmed by TEM-EDS and ICP-OES confirmed that the ruthenium complexes were immobilized/adsorbed onto the silica supports. ICP-OES analysis provided a quantitative means by which to determine catalyst loading for the subsequent application of the supported ruthenium complexes in the catalytic oxidation of hydrocarbons.

The model (**MC1-MC3**), immobilized (**IC1-IC6**) and adsorbed (**AC1-AC2**) ruthenium catalysts were capable of catalyzing the oxidative cleavage of 1-octene to afford heptaldehyde and/or heptanoic acid as products in high yields. At shorter reaction times the reaction was selective for heptaldehyde, but at extended reaction times over-oxidation of heptaldehyde selectively afforded heptanoic acid. The general trend observed was that the immobilized catalysts were more active than their model counterparts at a catalyst loading of 0.1 mol%. This trend was more apparent for the N,N (pyridine-triazole and quinoline-triazole) catalysts where the immobilized catalysts converted 100% of 1-octene after 12 hours, whereas their model counterparts only converted between 7-24% of 1-octene after 12 hours. The catalysts based on N,O (pyridine N-oxide triazole) complexes were more active than the catalysts based on N,N complexes, with 100% of 1-octene being converted after a 6 hour period for both the model (**MC2**) and immobilized (**IC3** and **IC4**) systems. The immobilized N,O catalysts (**IC3** and **IC4**) performed slightly better than their model analogue (**MC2**).

An investigation into the role of the mesoporous silica in the oxidative cleavage reaction was carried out in order to gain further insight into why the immobilized complexes performed better than their model counterparts in the catalytic oxidative alkene cleavage. It was found that the rate of formation of the proposed active catalyst RuO_4 in the biphasic solvent mixture is largely influenced by the proximity of the ruthenium pre-catalyst and the water soluble oxidant. For the model catalysts the pre-catalyst is dissolved in the organic phase while the oxidant is soluble in the aqueous phase. Therefore the ruthenium precursor will only come into contact with the oxidant via vigorous stirring of the biphasic mixture which means that the rate of formation of RuO_4 is relatively slow in this case. However, when the ruthenium complex is immobilized on mesoporous silica the hydrophilic nature of the support leads to the relatively easy transfer of the complex to the aqueous phase where the oxidant is present. This facilitates the formation of the active species RuO_4. This is the most likely explanation why the immobilized catalysts show enhanced activity when compared to their model counterparts. RuO_4 has been proposed as the most likely the active species in the

oxidative cleavage reactions. UV-Vis studies of catalyst precursors in the presence of the oxidant confirms the presence of RuO_4 as an intermediate in the reaction mixtures. These experiments also provided further evidence that the active species forms faster in the case of the immobilized catalysts when compared to what is the case for the homogeneous model complexes.

The ruthenium model complexes (**MC1-MC3**) and their immobilized counterparts (**IC1-IC6**) were found to be also active as catalysts precursors for the oxidation of *n*-octane to form octanones and octanols. Reduction of reaction mixtures with an excess of triphenyl phosphine, after completion of the reaction, allowed for the estimation of the selectivity for octyl hydroperoxides in the oxidation. The immobilized catalyst **IC6** afforded the highest yield of products, specifically 13.8 %, after 17 hrs at a low catalyst loading of 0.01 mol%. Hydrogen peroxide was found unsuitable as a terminal oxidant for these alkane oxidation reactions, with less than 1% conversion observed when this oxidant was employed. Recycling studies showed that the immobilized catalysts **IC4** and **IC5** could be recycled once with no drop in product yield being observed. The immobilized catalyst **IC3** could be recycled twice, and during these two recycling reactions little to no drop in product yield was observed.

The model and immobilized catalysts evaluated in this thesis are therefore effective as hydrocarbon oxidation catalysts, in both the oxidative cleavage of alkenes and the oxidation of alkanes.

6.2 Future prospects

The work performed as part of this thesis can be regarded as an exploratory exercise into the feasibility of employing these immobilized catalysts in these hydrocarbon oxidation reactions. Although the results obtained are promising further research is required to fully understand these catalytic systems. Some of the suggested experiments to be considered are outlined below.

For the oxidative cleavage reactions with ruthenium based catalysts it would be useful to confirm the presence of all possible intermediates in the catalytic cycle. Through this type of mechanistic study one could thus determine what the actual active oxidizing species is and how the oxidative cleavage occurs. From our studies it appears that the formation of RuO_4 from the ruthenium pre-catalyst is a rate limiting step for the reaction, however kinetic studies are required to confirm this. The role the support plays in the reactions and its ability to possibly stabilize RuO_4 before it is introduced to the organic phase would need to be investigated in order to fully understand support effects in the oxidative cleavage reaction. The differences in activity for the N,N (pyridine triazole and quinoline triazole) complexes and the N,O (pyridine N-oxide triazole) complexes would need to be investigated through assessing how the oxidation potentials differ for the two classes of complexes and whether differences in the oxidation potentials affect the conversion of the Ru(II) species to Ru(VIII) in the RuO_4 intermediate.

In the case of the oxidation of *n*-octane there are several factors that will need to be investigated in order to evaluate mechanistic aspects of the reaction. The complete identification of all components of the product stream is necessary, followed by a systematic study of the effect of radical trapping agents in the oxidation to establish whether a radical pathway is operative using our catalyst systems. The last step would be to conduct a detailed kinetic study to get further insight into the mechanism of the reaction as well as the nature of the active species.